POLISH ACADEMY OF SCIENCES – WROCŁAW BRANCH

WROCŁAW UNIVERSITY OF TECHNOLOGY

ISSN 1644-9665
INDEX 375667

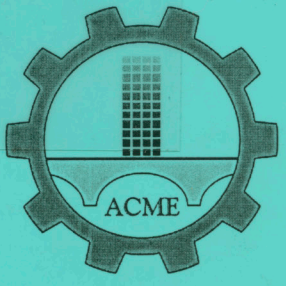

ARCHIVES OF CIVIL AND MECHANICAL ENGINEERING

Quarterly
Vol. IV, No. 2

WROCŁAW 2004

ADVISORY COMMITTEE

EDITORIAL BOARD

[1] The Faculty of Civil Engineering, Wrocław University of Technology
Wybrzeże Wyspiańskiego 27, 50-370 Wrocław, Poland
Tel. +48 71 320 22 46, Fax. +48 71 320 35 45, Email: mosty@pwr.wroc.pl

[2] The Faculty of Mechanical Engineering, Wrocław University of Technology
ul. Łukasiewicza 3/5, 50-371 Wrocław, Poland
Tel. +48 71 320 21 73, Fax. +48 71 320 34 22, Email: gronosta@itma.pwr.wroc.pl

POLISH ACADEMY OF SCIENCES – WROCŁAW BRANCH
WROCŁAW UNIVERSITY OF TECHNOLOGY

ARCHIVES OF CIVIL AND MECHANICAL ENGINEERING

Quarterly
Vol. IV, No. 2

WROCŁAW 2004

EDITOR IN CHIEF

JERZY GRONOSTAJSKI

EDITORIAL LAYOUT AND PROOF-READING

EWA SOBESTO, SEBASTIAN ŁAWRUSEWICZ

SECRETARY

TERESA RYGLOWSKA

Publisher: Committee of Civil and Mechanical Engineering
of Polish Academy of Sciences – Wrocław Branch,
Faculty of Civil Engineering and Faculty of Mechanical Engineering
of Wrocław University of Technology

OFICYNA WYDAWNICZA POLITECHNIKI WROCŁAWSKIEJ
Wybrzeże Wyspiańskiego 27, 50-370 Wrocław

ISSN 1644-9665

Drukarnia Oficyny Wydawniczej Politechniki Wrocławskiej. Zam. nr 469/2004.

Contents

Spis treści

ARCHIVES OF CIVIL AND MECHANICAL ENGINEERING

Vol. IV 2004 No. 2

Measurement system of "crash-test" experiments

J. GRONOSTAJSKI, Z. GRONOSTAJSKI, A. NIECHAJOWICZ, S. POLAK,
M. STRUŚ, A. TOBOTA, P. WIEWIÓRSKI, P. ZAJĄC
Wrocław University of Technology, Wybrzeże Wyspiańskiego 27, 50-370 Wrocław

In the paper, the measurement system of "crash-test" experiments was presented. The prototype system based on two laser transmitters (red light) with special detectors with electronic system was used as the sensor. The system became an option of much more expensive accelerometers. The advantage of the method presented is its simplicity as well as the possibility of high acceleration recording due to contactless measuring method. Drop hammer software making it possible to observe results right after testing was used. This enables real time correction of an experiment leading to the best solutions. The method developed was used for testing the energy absorption by the car body elements, depending on their geometry as well as filling.

Keywords: *measuring system, crash-test, laser, energy absorption*

1. Introduction

The main goal of passive safety is to minimize a threat to life or health of persons involved in a road accident. The passengers having the accident are first of all in the danger of overloads resulting from the energy conservation law. A decrease of overloads is obtained by such vehicle design that enables an appropriate absorption and dissipation of collision energy [1]. This aim is achieved due to the so-called deformation zones being made from the elements of different energy absorption characteristics. Such a diversity may be created by the use of the elements of different stiffness absorbing collision energy [1, 2].

At the Engineering Forming Department at Wrocław University of Technology research into the effect of specimens crushing in "crash-test" type experiments has been carried out for several years [3, 4, 5]. Special emphasis was given to testing and analyzing the energy absorption by elements of different construction and profiles. The specimens tested represented the elements of stringers and strengthening parts of vehicles that have been produced all over the world. One- and multilayer, empty or filled with plastics of different density specimens were used for the tests. Based on the analysis of specimens behaviour while straining, the energy absorbed by the elements tested was assessed [4].

For dynamic testing the modern test stand that makes it possible to record and process data in a very short time is necessary. In the computer-aided system, such a type of tests that allow us to design new constructions improving the safety of vehicles are presented [5].

2. The test stand

The main parts of the test stand (Figure 1) are as follows:

- automated drop hammer with a ram of a weight ranging from 58.5 kg to 206 kg, depending on the number of bobs,
- computerized data recording system [6] connected with appropriate sensors and devices recording signal during sample deformation,
- software visualizing the tests results obtained.

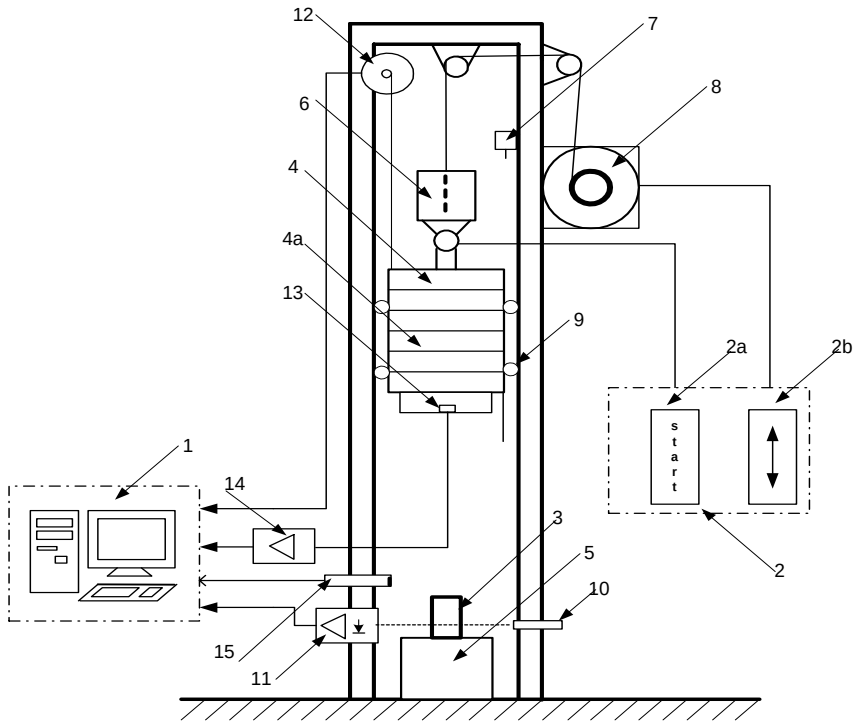

Fig. 1. The test stand scheme: 1 – data acquisition system, 2 – manual control of the ram displacement, 2a – ram release, 2b – ram position setting, 3 – specimen, 4 – ram, 4a – hammer bobs, 5 – anvil, 6 – electromagnet, 7 – limit switch, 8 – electric motor, 9 – rolling bearings, 10 – laser transmitter, 11 – exalted receiver, 12 – rate generator, 13 – piezoelectric sensor, 14 – piezoelectric sensor amplifier, 15 – distance release sensor

The ram was dropped from a height of 1.95 m, which was the distance from the working surface of the ram (4) to the upper surface of the specimen (5). The specimens (3) of the height equal to 200 mm were placed on the anvil. The ram (4) was raised by driving system (8) until it came into contact with limit switch (7). Using ram release (2) the electromagnet (6) was switched on and the ram-holding jaws were

opened releasing the ram. In order to diminish the friction force between rolls guiding and rolling bearing (9) that could decrease the ram velocity, the guide poles were lubricant coated. At a proper height the distance release sensor (15) sends a signal to the data acquisition system.

The system was recording data from: rate generator (12), piezoelectric accelerometer (13, 14) and optical detector (10, 11). The samples were deformed very quickly, therefore sensor and measuring system had to satisfy very stringent requirements.

Comparing a behaviour and energy absorption of each sample the usability of different geometry and technical characteristics of the real elements in car body construction was determined.

The aim of the experiment was to record and determine the parameters describing the specimen deformation process. Basic parameters of the process were as follows:

- displacement measured from the moment when the ram touched the specimen until the end of the motion – $s(t)$;
- correlation between ram velocity and the time of the specimen deformation – $v(t)$;
- correlation between ram velocity and the displacement of specimen deformation – $v(s)$;
- correlation between ram acceleration and the time of specimen deformation – $a(t)$;
- correlation between ram acceleration and the displacement of specimen deformation – $a(s)$;
- correlation between kinetic energy of ram and the time of specimen deformation – $E(t)$;
- correlation between kinetic energy of ram and the rate of specimen deformation – $E(s)$;
- correlation between impact force of ram and the time specimen deformation – $F(t)$;
- correlation between impact force of ram and the rate of specimen deformation – $F(s)$.

2.1. Measuring system

To record the parameters of ram motion, when crashing the specimen, appropriate sensors and measuring techniques were used. We adopted three independent measuring systems which consisted of:

- The rate generator that enabled measurement of the ram velocity.
- The accelerometer that measured the ram acceleration from the moment of specimen deformation. Accelerometer was equipped with "piezo"-type sensor and piezoelectric sensor amplifier from PCB company. The signal from that sensor represented instantaneous value of acceleration. The data obtained were additionally filtered.

• Optical detector [7] that consisted of two laser transmitters operating at the wavelength of 630 nm (red beam), optical matrix with gaps and striae put on alternately and measuring device for laser signals recording.

Optical detector was designed by the team involved in the research presented. In Figure 2, the measuring system that was used for evaluating the ram motion parameters is depicted. Its most important part was data-processing card E1364 from National Instruments Company of processing speed of 5μs (200 kHz).

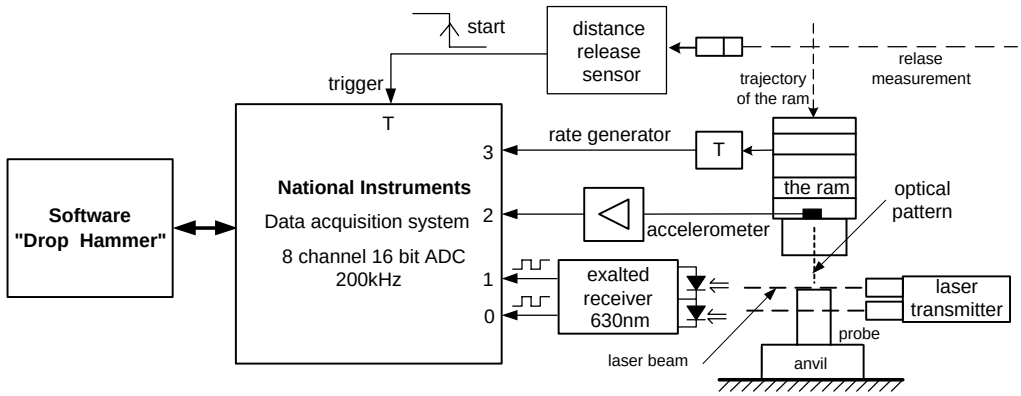

Fig. 2. The system used for measuring the ram motion parameters

The following devices were connected to the data processing card: rate generator, accelerometer, optical detector and distance release sensor as trigger.

The system of data processing actuated recording when high state appeared. This happened when falling ram was close to the distance-release sensor. Special program, in which such parameters as recording time, the number of used channels, sampling frequency etc. could be changed, was responsible for data recording.

2.2. Selection of an appropriate measuring system

At the beginning the drop hammer was equipped only with the rate generator. It was mounted at a constant height of about 2.3 meters and connected to the ram with strongly tensed cable. The ram motion produced a tension proportional to the velocity of the falling ram. While analyzing experimental results, a signal from the generator was amplified twice. Sudden changes of ram velocity during deformation (Figure 3) obtained from the measurement of generator voltage were unbelievable. Therefore, it was necessary to use other measuring device to verify the data obtained from the rate generator. For that purpose the drop hammer was fitted out with additional sensor – piezoelectric accelerometer. The sensor was placed in a bottom of the ram following the instruction [8]. After testing and comparing the results it was noticed that signals from both sensors showed different contact time as well as different time of the end of

the process. Accelerometer signalled a contact time approximately 4 ms earlier. This was justified by the construction of the rate generator that was equipped with revoluting elements of high interia. Additionally the cable tension causing a slight ram tilting could also have an influence.

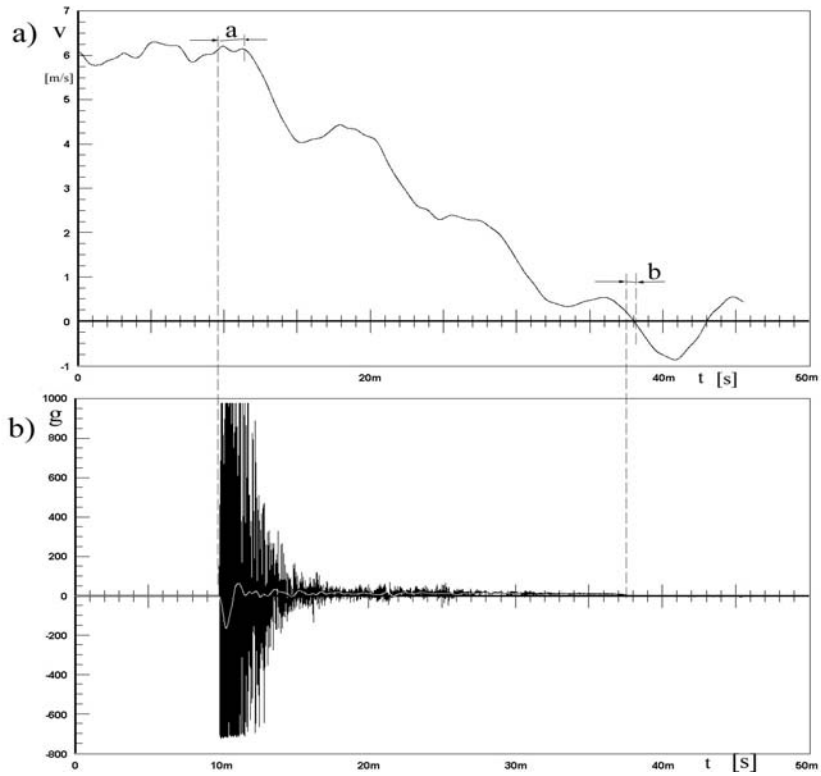

Fig. 3. Comparison of signals from rate generator (a) and piezoelectric sensor (b)

The accelerometer used was for slightly smaller acceleration values than those occurring during specimen deformation. The signal faded at the value of 1000 g which caused difficulties with filtration. It was difficult to choose optimal filtration method.

Because of these reasons it was decided to design a new measuring system based on experience from the use of the rate generator and piezoelectric sensor. The construction of optical detector was changed several times. At the beginning it was constructed with a use of one laser transmitter, matrix of 0.5 mm resolution and complex optical system. Further its construction was changed; its precision and reliability were increased. Software processing of data from detector was created. The whole was an efficient experiment servicing system that enabled immediate analysis of experimental data.

2.3. Optical detector

The system presented was designed for measuring and recording the quantities necessary for dynamic analysis of specimen deformation with a use of the drop hammer. As measuring sensor a prototype system based on two laser transmitters with special photodiodes and electronic control was used. Due to the use of two lasers the method could be an alternative to much more expensive measuring methods. Two separated slotted lines for both laser transmitters made it possible to determine exactly: dynamic parameters of the ram, the ram trajectory, the time of contact between the ram and specimen, the ram from the specimen bounce moment, the specimen strain rate and the parameters listed above.

The advantages of this measuring method are simplicity of operating and the possibility of high values of acceleration recording due to non-contact measuring. Additionally software (designed with a use of C language) allowing immediate analysis of experimental data was created. It enabled correction of real experimental time leading to optimal solutions.

The system of optical detector consisted of two independent laser transmitters (630 nm) of laser beam diameter equal to 0.3 mm, optical matrix and electronic detectors (Figure 4).

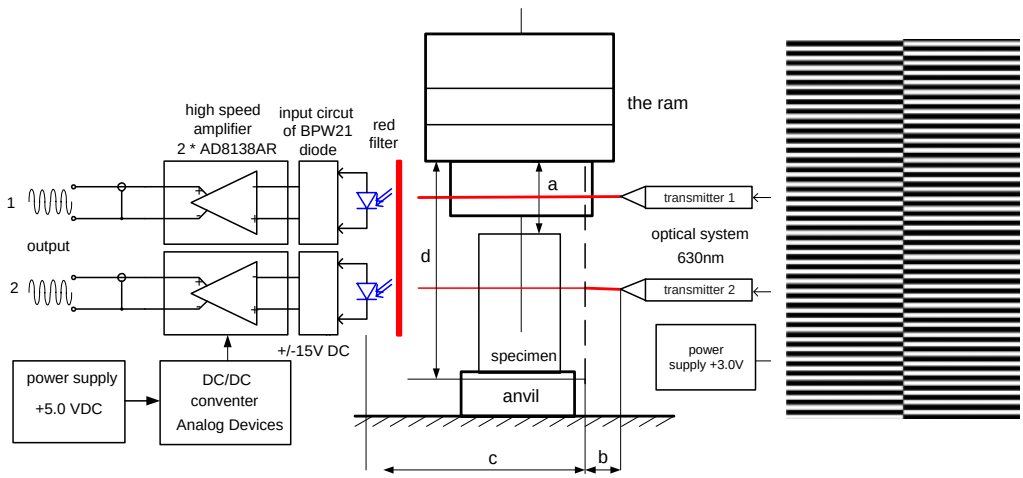

Fig. 4. The system of optical detector based on two laser transmitters and optical matrix pattern

The system functioning was based on photocell principle. The matrix consisted of gaps and striae put on alternately, it was manufactured with a use of exposure technology which resulted in high precision of pattern equal to 4000 dpi. The striae for particular laser transmitters were shifted with respect to each other so in one time the signal from only one transmitter was transmitted through the matrix.

Resolution of a device depends on a width of striae and gaps. In the device used, the width of both was the same, i.e. 0.4 mm. The width of laser beam could not be greater than this dimension because the output signal from the detector would not have appropriate measurement properties. If the laser beam hits the striae, it is stopped and voltage of photodiode is equal to the voltage of background. If the laser beam hits the gap, it is registered by the photodiode in which voltage appears. This voltage should be as high as possible so that photodiode amplifier would have low amplification at wide band of transmitted frequency and phase shift close to zero. It was possible to obtain 0.3 mm width of laser beam without interference rings at the distance of several centimeters without use of optical elements due to precisely sticked metal collimator of 0.3 mm diameter (Figure 5).

When a falling ram with optical matrix mounted in a clamping ring appeared near laser beam its movement began to be recorded as impulses forming sinusoid (Figure 6).

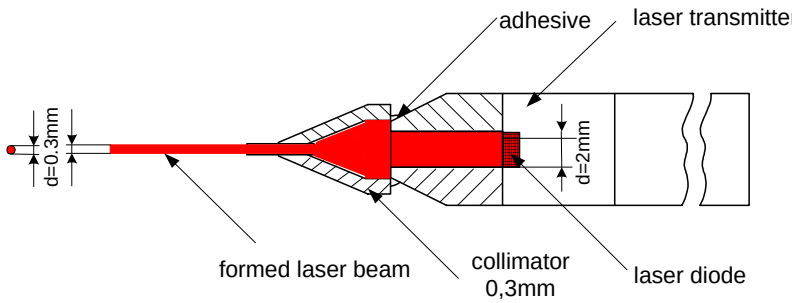

Fig. 5. Beam width reduction in laser transmitter

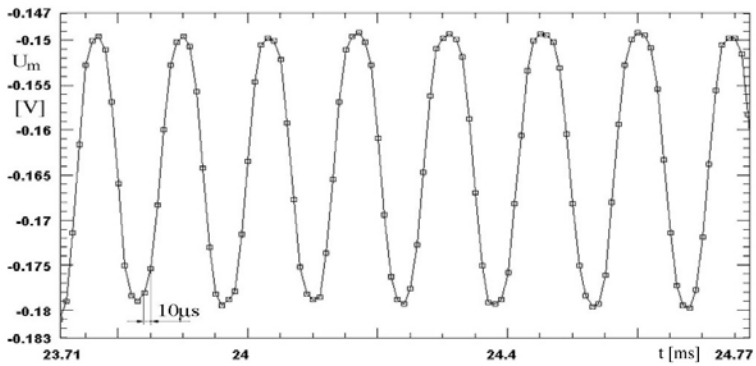

Fig. 6. "Sinusoidal" curve from optical detector

Two lasers and appropriate matrix pattern made it possible to determine direction of the ram movement which was a crucial issue when the ram bounced from the specimen.

3. Computational methods

Presently measuring systems besides typically mechanical, electronic devices must also include software enabling direct verification of tests. Modifications of software computation algorithms caused by frequent construction changes were made by researchers working on that project that ensured the best solutions.

3.1. Data processing

For data processing "drop hammer" software was used. Basic parameters necessary to analyze the ram motion during dynamic loading were previously presented. The method for determining them being based on the analysis of the signal from the optical detector is presented below. The curve previously named as "sinusoidal" (Figure 6), in fact, was not exactly pure sine. Its further periods changed, depending on the ram velocity changes.

Theoretical free velocity of ram that hits the specimen can be calculated from the energy conservation law:

$$E_p = E_k\,, \tag{1}$$

$$v = \sqrt{2gh}\,, \tag{2}$$

where:

E_p – potential energy,

E_k – kinetic energy,

g – acceleration of gravity; 9.81 m/s^2,

h – the height from which the ram was falling; 1.95 m.

Because of the rolling resistance of the rolls guiding the ram in a slideway, a real velocity was not equal to a theoretical free falling velocity. It ranged from 6.16 to 6.24 m/s.

As was already mentioned, the matrix resolution was 0.4 mm, hence the gap between two next striae was 0.8 mm. At a velocity of 6.2 m/s the frequency of the signal from optical detector was:

$$F = 6.2\,\frac{[\mathrm{m}]}{[\mathrm{s}]} \cdot \frac{1}{0.0008}\,\frac{1}{[\mathrm{s}]} = 7750\ [\mathrm{Hz}]\,. \tag{3}$$

Due to the data processing the card signals in two channels were recorded, the sampling frequency was 100 kHz per channel. That caused that when the ram was hitting the specimen (at maximal velocity) for one period of the signal, there were 13 measuring points. While the ram was sinking in a specimen, the number of measuring points per one cycle of striae–gap–striae was increasing (velocity was increasing).

The first computational algorithm was based on FFT (Fast Fourier Transform) [6]. Reading the frequency value for the highest peak (Figure 7) it was possible to get the ram velocity in a chosen moment. Adjusting parameters properly – a number of points and the so-called windows (i.e. hanging), it was possible to obtain results. The method of spectral analysis enabled us to obtain an average velocity, depending on the number of points. Taking the above into consideration we could conclude that the method based on FFT was rather slow and it would be difficult to choose it as a proper solution.

Another method of getting information about the ram velocity is the method of characteristic points presented in Figure 8. In that method, the following parameters were investigated:

- an average signal value during specimen deformation (FFT(0)),
- maximal values of next cycles (laser beam was pointing at the striae),
- minimal values of next cycles (laser beam was pointing at the gap).

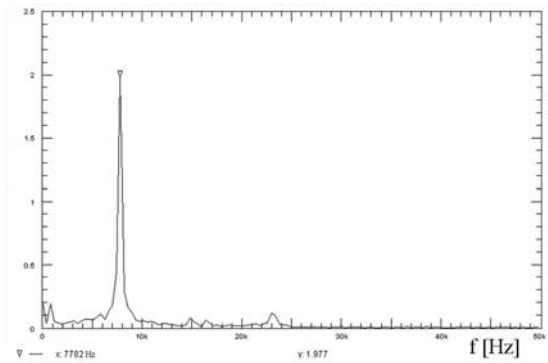

Fig. 7. FFT signal spectrum when the ram hits the specimen

Computation algorithm was based then on finding out the points corresponding to these parameters in a signal. Each point was represented by some time value t_n and some ram displacement value s_n. Thus the analysis could be based on the change of those points position in time. 3- and 5-points methods could be adopted as it was presented in Figure 8. Defining the set of time $t = \{t_0 \ldots t_n\}$, depending on the method, at the same distance between two adjacent striae equal to 0.8 mm (with one stria an average value was obtained two times so the distance between two adjacent gaps was 0.4 mm) it was possible to determine the set of positions of the ram $s = \{s_0 \ldots s_n\}$. Making up the set of positions s and the set of t the correlation between displacement and time was obtained.

As was already noticed, when the ram hit the specimen one cycle had only 13 measuring points; during identification of characteristic points this could cause errors δ_1, δ_2 (Figure 9). An appropriate calculation of an average value and identification of

characteristic points had an influence on the method accuracy which was testified by the ram velocity versus time characteristic ($v(t)$).

Having displacement s and time t set it was possible to determine consecutive differences (increments) from the following equation:

$$v_m = \frac{s_{m+1} - s_m}{t_{m+1} - t_m} = \frac{\Delta s_m}{\Delta t_m} . \tag{4}$$

This way the set of time-dependent consecutive instant velocities v of ram was obtained. Setting properly the sets of velocity v_m and displacement s_{m+1} the correlation between ram velocity and its position $v(s)$ was established. The errors in $v(t)$ calculating arise from the time-dependent position of characteristic points being identified.

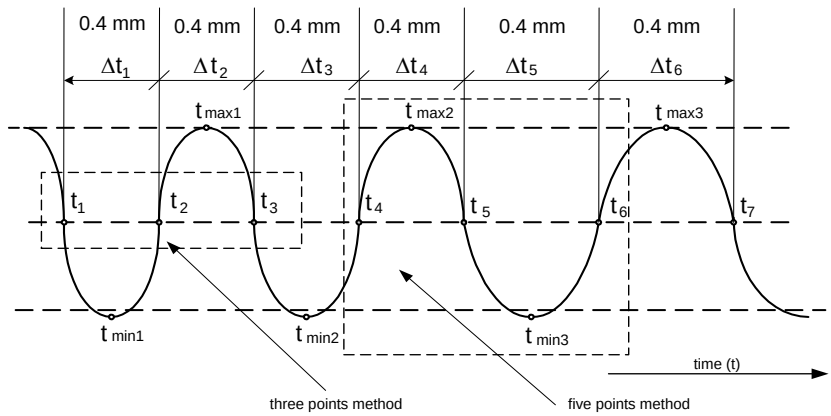

Fig. 8. Localization of zero-crossing in the methods used

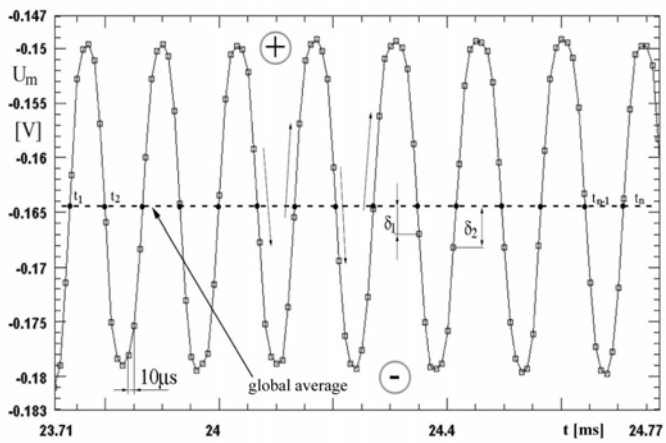

Fig. 9. Errors occurring during identification of characteristic points in sampled signal

In Figure 9, a part of signal recorded during specimen deformation was presented. It could be noticed that not many points were exactly equal to the average value of the signal. If the cycle had 13 points – 130 μs, error could be even as great as 20 μs (15%) and, which was more important, the error was not constant. Errors doubled while evaluating the ram acceleration values. It was necessary to propose the way to avoid the error arising from the signal sampling frequency. This can be done by the so-called re-sampling. The phenomenon tested lasted for about 30 ms, which gave 3000 measuring points at the sampling frequency of 100 kHz. As a result of re-sampling it was possible to obtain even 300000 measuring points due to a decrease of time from 10 μs to 0.1 μs between the adjacent points. Characteristic points in a signal were found more precisely. The fault of that method was slowing calculations down due to re-sampling.

The method of linear interpolation of equation was much faster and accurate because no preliminary re-sampling was necessary. In Figure 9, some of measuring points were over the average value (marked as "+") and some of them were below it ("–"). In that method, the points after which the sign was changed from "+" to "–" and from "–" to "+" were specified. Based on these two points of different signs straight-line equation was derived as follows:

$$(u-u_1)\cdot(t_2-t_1)=(t-t_1)\cdot(u_2-u_1)\,, \tag{5}$$

where u – photodetector voltage, t – time, (t_1, u_1), (t_2, u_2) – coordinates of the points. The time t_m for hypothetical point at which the voltage value u should be equal to u_m was evaluated. That time could be calculated directly after calculating the straight-line equation. The accuracy of that method was the best, hence that algorithm was used in the software.

3.2. Evaluating acceleration and the force of specimen deformation caused by the ram

Previously the specimen deformation versus time ($s(t)$) and the velocity versus time ($v(t)$) as well as the ram velocity versus displacement ($v(s)$) were presented. In order to gather all the parameters describing the specimen deformation, it was necessary to evaluate the ram acceleration. Acceleration values were obtained from the calculation of the next velocity Δv increments in the time Δt:

$$a_m=\frac{v_{m+1}-v_m}{t_{m+1}-t_m}=\frac{\Delta v_m}{\Delta t_m}\,. \tag{6}$$

When the set of acceleration values a_m is combined with the set of displacement values s_{m+2} the correlation between the ram acceleration and its position $a(s)$ can be calculated.

To calculate the kinetic energy of the ram the set of the ram velocity values $v(t)=\{v_0 \ldots v_n\}$ was evaluated and successively the set of kinetic energy values E_k was calculated from the following equation:

$$E_k = \frac{mv^2}{2}, \tag{7}$$

where m stands for the ram mass.

Correlating properly the set of kinetic energy E_k with the set of displacement s the correlation between kinetic energy and the specimen deformation $E_k(s)$ was obtained.

In order to calculate the force exerted by the ram on the specimen, the set of the next time-dependent acceleration values $a(t)=\{a_0 \ldots a_n\}$ was necessary. This force is given by the following equation:

$$F = m\big(g + a(t)\big), \tag{8}$$

where g is acceleration of gravity.

The correlation between the force exerted by the ram and the specimen deformation $F(s)$ was obtained by a proper correlating the set F with the set of displacement s.

4. Drop hammer software

The software was developed to evaluate dynamic parameters of the ram during its collision with the specimen and the specimen deformation. It was designed with a use of C language. This software has the advantage of being quick at data processing and simple. It enabled us to evaluate all the quantities necessary for the description of specimen deformation.

To analyze the signals obtained from the optical detector it was necessary to choose the file with data. Basic parameters of the data recording process such as date, time of recording, sampling frequency, pretrigger, channels to which recorded signals were connected were recorded in that file. The name of that file was identical to the specimen mark tested. The file extension should be "*.dat"; however, the program may load also other file types.

The structure of file is presented in the Table.

The program reads two columns of numbers representing recorded signals from two lasers. It is based on an algorithm using linear interpolation equation in order to calculate the ram motion parameters.

"Drop hammer" program enables us to observe the results right after the test and to make corrections during experiments which makes it possible to find the best test conditions. After loading the file, processing of different relations was obtained. The window from the software with some examples of courses is presented in Figure 10.

Table. The structure of the file

Date: 05-29-2003	Time: 11.13.04
Acquisition time	100 [msec]
Samping rate	100000 [pts/sec]
Sampling interval	0.01 [msec]
Number of samples	10000
Pretrigger	5 [msec]: sample number: 500
Channels	
Channel 1-transducer none	Channel 2-transducer none
0.228424	0.227966
0.228577	0.227509

Graphs from the program may be printed or can be saved as graphic files. In such a form they may be processed with different types of software. Data can be also exported to "Microsoft Excel" to create own graphs for further analysis.

The software has also the advantage of incorporating package for digital data filtration. This is especially important when the sensor used is a piezoelectric accelerometer. The software makes it possible to create an advanced FIR-type filter. In the window, attenuation diagram as well as phase characteristics of the filter are presented. After saving coefficients it is possible to load them into the program and to filter a chosen signal.

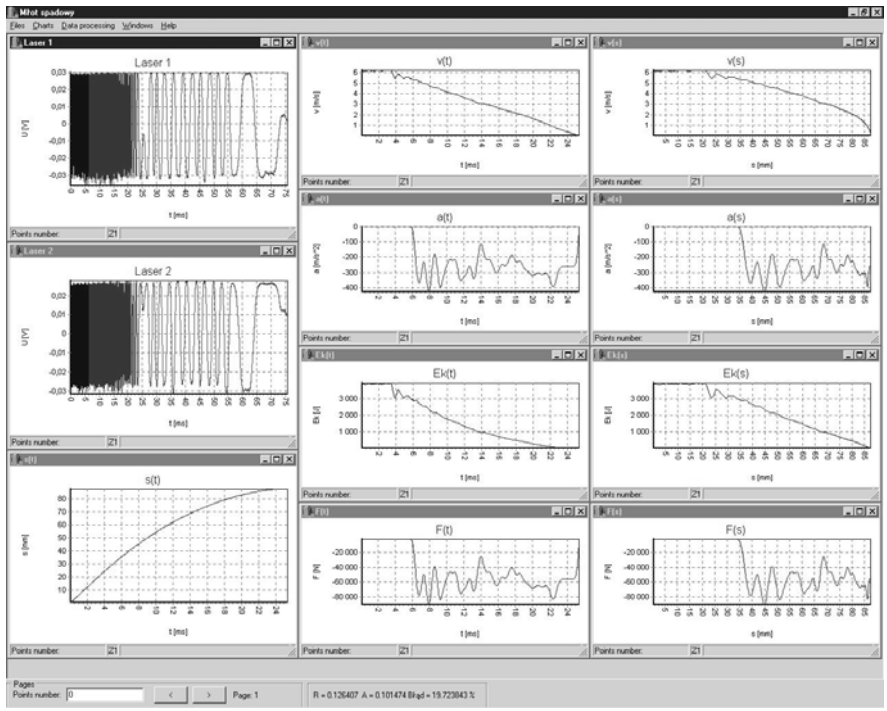

Fig. 10. Drop hammer software – window with some exemplary courses

In Figure 11, the window from the program with digital filter is presented. Filtering may be improved by the so-called signal windowing making characteristics more steep at a smaller number of coefficients. In Figure 12, the signal from the test with piezosensor is presented. In Figure 13, frequency and phase characteristics of the FIR filter designed are shown.

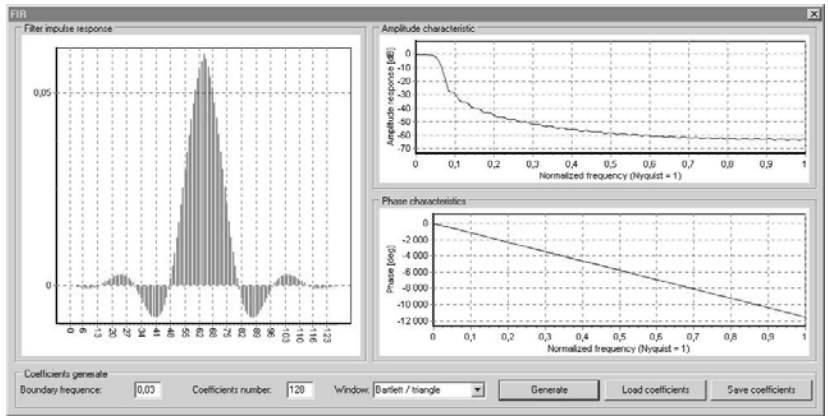

Fig. 11. The window of the FIR-type digital filter

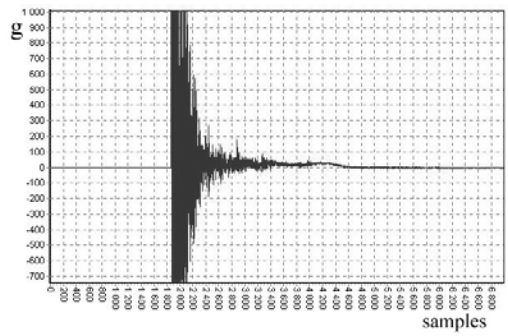

Fig. 12. The signal before filtration

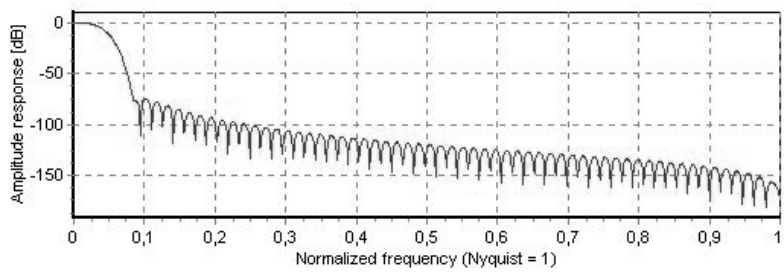

Fig. 13. FIR-filter characteristic ($f_c = 0.02\,f_g$, $n = 128$)

In Figure 14, filtered signal from Figure 12 is presented.

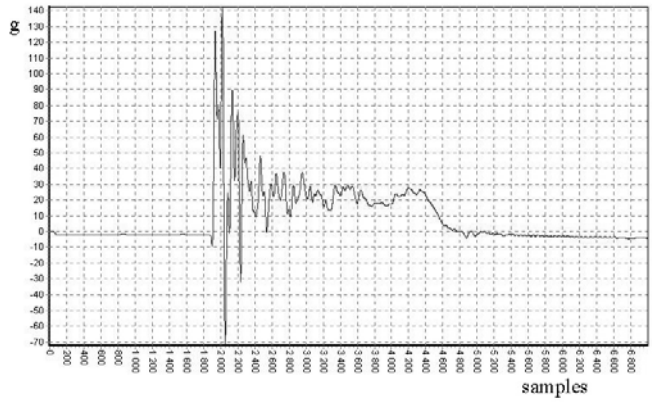

Fig. 14. Recorded acceleration signal $a(t)$ (f_p = 100 kHz)

The program is totally automatized. In "Preferences" menu (Figure 15) it is possible to set such parameters as the ram mass, time of the analysis beginning, etc. It is also possible to present graphs as points as well as to scale properly the graph.

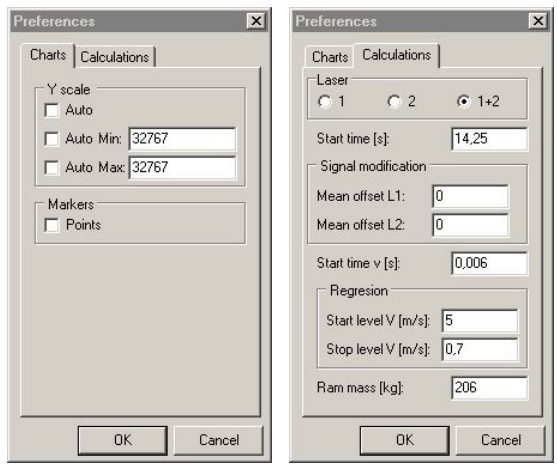

Fig. 15. The window of "preferences"

The results obtained for tubes filled with plastic foam of the density equal to 74.2 kg/m^3 are presented as an example of the software possibilities. In Figure 16, the signal recorded from optical detector is presented. In blue, the moment before the contact between the ram and the sample is reached; in red, the specimen deformation occurs; and in green, rebound and vibrations of the ram are presented.

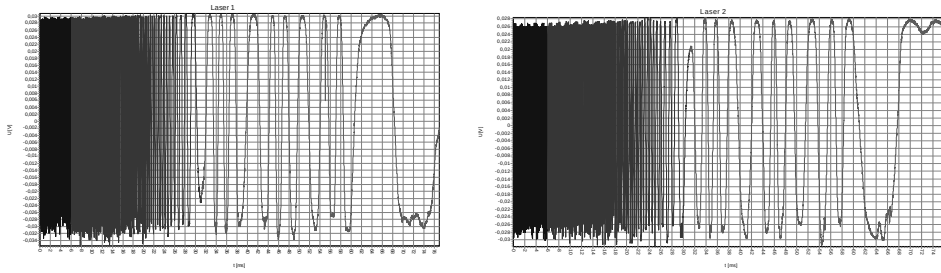

Fig. 16. Signals from optical detector

4.1. Results of verification

In Figure 17–25, basic parameters of the specimen deformation are presented. Song [8] proposed certain empirical relationship describing velocity changes in time as it should be in reality in the case of the specimen deformation. Based on that it was possible to verify calculations comparing them to the ram velocity obtained in the experiment.

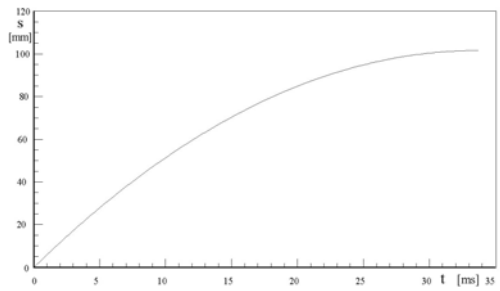

Fig. 17. The ram displacement versus time

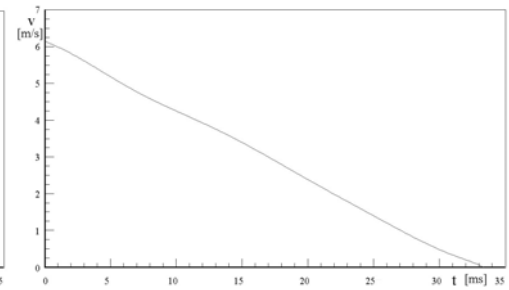

Fig. 18. The ram velocity during the specimen deformation

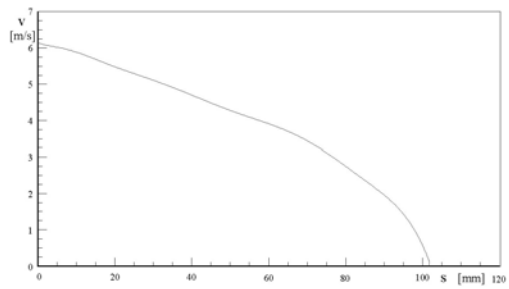

Fig. 19. Correlation between the ram velocity and its displacement

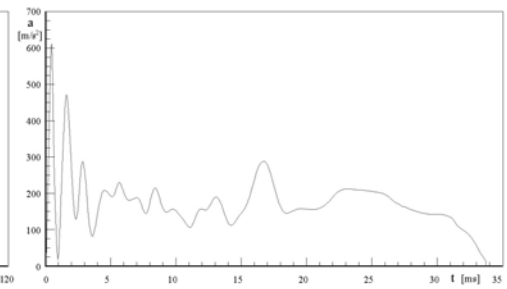

Fig. 20. The ram acceleration versus time

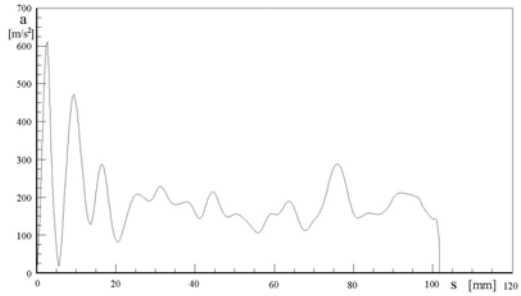

Fig. 21. Correlation between the ram acceleration and its displacement

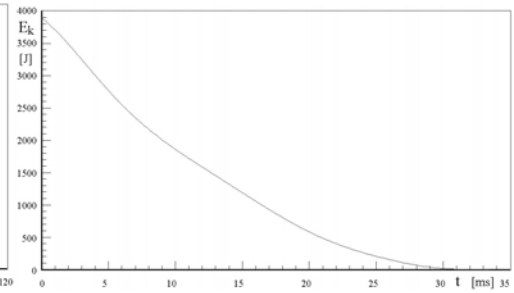

Fig. 22. Changes of the ram kinetic energy in time

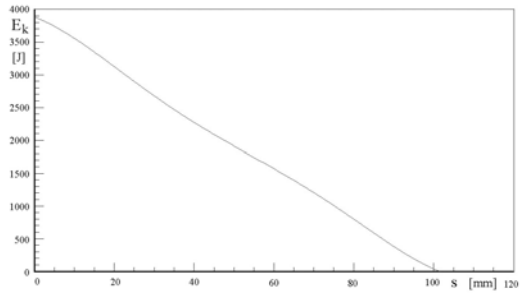

Fig. 23. The ram kinetic energy versus its displacement

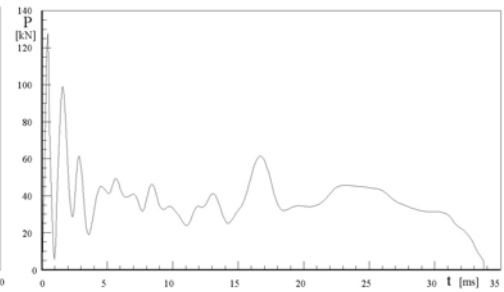

Fig. 24. The force exerted by the ram versus time

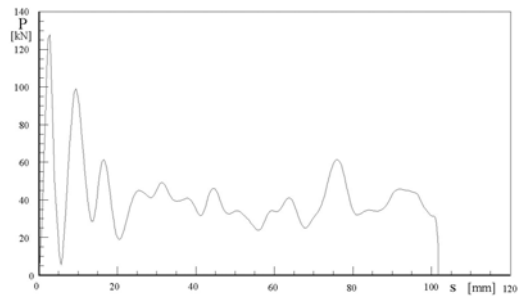

Fig. 25. The force exerted by the ram versus its displacement

From (9) it resulted that the velocity change in time should be linear:

$$v = v_0 \cdot (1 - \frac{t}{\Delta t}), \tag{9}$$

where:

v_0 – velocity at the moment the ram comes into contact with the specimen,

t – time value for a point of coordinates (s, t),

Δt – the time of the specimen deformation until a re-bound occurs or the ram stops.

From (4) it results that the velocity change in time should be linear. This allows us to verify the calculations by comparing them to the ram velocity obtained from the experiment. The algorithm converting the signal from optical detector is based on the principle of next discrete difference quotients done in the set of time values $t=\{t_0 \ldots t_n\}$ and the set of the ram displacement values $s=\{s_0 \ldots s_n\}$. This means that an incorrect evaluation of velocity is responsible for errors in all parameters. Comparison of the velocity values evaluated from the experiment with the values calculated from (4) makes the evaluation of an approximate measuring error possible.

5. The energy absorbed by the tube specimens

Based on the presented measuring system equipped with optical detector, the energy absorbed by the elements of car body, depending on their geometry and filling, was investigated. The tests showed that the shapes of the elements as well as the filling density had a profound influence on the energy absorption.

6. Summary

Computer-aided measurement system of "crash-test" experiments with a use of the drop hammer was designed. The prototype system based on two laser transmitters (red light) with special detectors with electronic system was used as the sensor. The system became an option of much more expensive accelerometers. The advantage of the method presented is its simplicity as well as the possibility of high acceleration recording due to contactless measuring method.

Drop hammer software making it possible to observe results right after testing was used. This enables real time correction of an experiment leading to the best solutions.

The method developed was used for testing the energy absorption by the car body elements, depending on their geometry as well as filling.

The system presented is still to be developed. It is foreseen that in the future thanks to the software described and the programs based on FEM analysis it will be possible to design the so-called "intelligent" stringers and the car body strengthening elements that, depending on external factors, would ensure safety for passengers of cars.

References

[1] Wicher J.: *Zagadnienia bezpieczeństwa samochodów*, Oficyna Wydawnicza Politechniki Warszawskiej, Warszawa, 1997.

[2] Zieliński A.: *Konstrukcje nadwozi samochodów osobowych i pochodnych*, Wydawnictwo Komunikacji i Łączności, Warszawa, 1998.

[3] Tobota A.: *Wpływ prędkości i odkształceń na własności anizotropowe blach stalowych stosowanych w przemyśle motoryzacyjnym*, Raport ITMiA PWr, seria SPR nr 26/2001.
[4] Jura M., Drozdowski M.: *Pochłanianie energii przez elementy nadwozia w zależności od ich kształtu i wypełnienia podczas zderzeń pojazdów*, MSc dissertation, Politechnika Wrocławska, 2003.
[5] Tobota A., Olchowik W., Domański M., Wiewiórski P.: *System pomiarowy do badania procesu zgniatania próbki w eksperymencie typu „Crash-Test"*, V Konferencja Diagnostyka Techniczna Urządzeń i Systemów, Ustroń, 2003.
[6] Gajda J., Szyper M.: *Modelowanie i badania symulacyjne systemów pomiarowych*, Wydawnictwo Jartek s.c., Kraków, 2002.
[7] Klepaczko J.: *Czujnik ektensometryczny z fotodiodą do badań statycznych dynamicznych*, Pomiary, Automatyka, Kontrola, 1970, No. 11, pp. 466–469.
[8] Song H.W., Wan Z.M., Xie Z.M., Du X.W.: *Axial impact behavior and energy absorption efficiency of composite wrapped metal tubes*, Int. J. Impact Eng., 2000, Vol. 24, pp. 385–401.

System pomiarowy do badań *crash testu*

Przedstawiono system do pomiarów, rejestracji i przetwarzania wyników badań dynamicznego spęczania próbek w tzw. *crash-teście*. Opracowano oryginalny system pomiarowy wykorzystujący dwa nadajniki laserowe na światło czerwone, specjalne detektory oraz układy elektroniczne. System ten zastępuje znacznie droższy piezokwarcowy czujnik przyśpieszeń i czujnik prędkości w postaci prądnicy tachometrycznej. Przedstawiona metoda charakteryzuje się wieloma zaletami, między innymi: prostotą i możliwością rejestrowania bardzo dużych przyśpieszeń dzięki bezstykowej metodzie pomiarów.

System ten został zastosowany do analizy zachowania się próbek wykonanych z blachy o różnych profilach, jedno- i dwuściennych, pustych i wypełnionych tworzywami sztucznymi o różnej gęstości podczas dynamicznego spęczania na młocie spadowym. W czasie spęczania, które zachodziło w ciągu kilku ms, można było uzyskać przebiegi siły spęczania, prędkości spęczania i przyśpieszenia spęczania w czasie bądź w funkcji drogi odkształcania spęczanej próbki. Opracowane oprogramowanie umożliwia obserwowanie wyników próby natychmiast po jej zakończeniu i szybką korektę eksperymentu, co pozwala szybko uzyskiwać dobre rozwiązania.

W efekcie końcowym określano przebiegi energii absorbowanej przez próbki w funkcji drogi odkształcania. Przeprowadzone badania wykazały, że najistotniejszy wpływ na energię absorbowaną wywiera kształt przekroju poprzecznego próbek i gęstość wypełnienia. Najbardziej korzystne rozwiązania, to jest takie, które zapewniały najmniejsze przeciążenie użytkowników pojazdów samochodowych, powinny znaleźć zastosowanie w budowie elementów karoserii samochodowych zapewniających możliwie dobre bezpieczeństwo bierne.

ARCHIVES OF CIVIL AND MECHANICAL ENGINEERING

Vol. IV 2004 No. 2

Simulation research in impulse compacting of moulding sands

W. KOLLEK, T. MIKULCZYŃSKI, D. NOWAK, Z. SAMSONOWICZ
Wroclaw University of Technology, Wybrzeże Wyspiańskiego 27, 50-370 Wroclaw, Poland

The paper presents a mathematical model of impulse compacting of moulding sands developed at the Institute of Machine Engineering and Automation of Wrocław University of Technology. The model presented consists of a system of differential equations that describe the impulse head dynamics and the process of moulding sand deformation. This deformation is described by a viscoelastic rheological model accepted on the grounds of rheological properties of moulding sand determined using the time-conversion method. Moreover, the results of simulation testing of the impulse compacting are presented in the paper. Based on the results of analysis it has been found that the model developed fully describes the process of impulse compacting of moulding sands. Thus, it can be used for designing and optimizing the impulse machine heads and for designing the process of moulding sand compacting.

Keywords: *moulding sand, impulse compacting, mathematical model, simulation research*

1. Introduction

Sand casting due to its numerous advantages is a basic method of casting production. Among the methods used for compacting classic moulding sands, squeezing is of a major importance. In practice, various forms of squeezing are applied: plate squeezing, squeezing with multi-piston head or with core shooter. Recently, more and more stringent quality requirements for manufactured castings have resulted in rapid development of new, dynamic squeezing methods, including impulse compacting and dynamic squeezing. An important property of the new squeezing methods is very short compacting time, of the order of a few to a dozen milliseconds.

An advantage of the new methods of moulding sand compacting is a high quality of the manufactured casting moulds. Very good results of compacting are obtained, such as high compacting degree, high uniformity of compacting degree in the mould, higher dimensional accuracy of moulds, good surface quality and greater accuracy of representation of complex shapes of patterns.

To obtain optimum results of compacting, it is necessary to know the properties of the mathematical model of impulse compacting and the results of simulation testing of this model. The simulation tests can be treated as preparation for designing and optimizing dynamic heads of moulding machines and the process of impulse compacting of moulding sands.

The phenomena that occur during compacting of moulding sands are very complex. So far, no mathematical model has been developed to describe fully the process of im-

pulse compacting of moulding sands, although attempts have been made by many researches in the world, e.g., by G.M. Orlov, J. Bast and K. Smyksy [1–3].

The research in a new impulse head with self-acting pneumatic valve and in the process of impulse compacting of moulding sands has been carried out at the Laboratory of Automation Principles of the Institute of Machine Engineering and Automation of Wrocław University of Technology for a few years [4–6]. This resulted in developing a mathematical model of the process of impulse compacting of moulding sands. In this paper, there are presented some selected simulation tests on the model developed which fully describes the process of impulse compacting of moulding sands.

2. Mathematical model of the process of impulse compacting of moulding sands

The layout of the process of impulse compacting of moulding sands is shown in Figure 1. This process runs in the following way: After switching over the valve (4), the pressure p_3 drops rapidly resulting in the movement of the piston (3) and opening of the accumulator outlet. Rapid opening of the outlet (5) generates a shock wave of compressed air in the workspace over the moulding sand. The air jet is responsible for deformation and compaction of the sand.

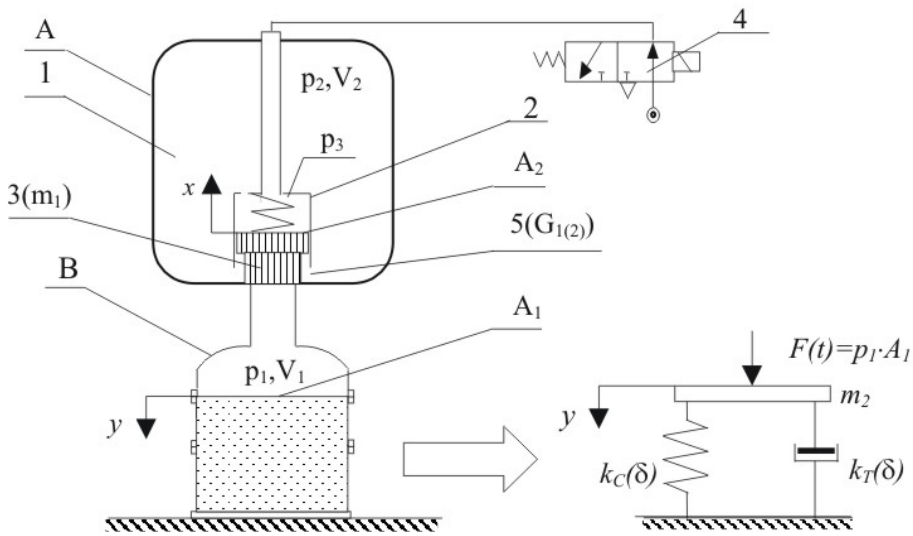

Fig. 1. Layout of the process of impulse compacting of moulding sands: impulse head (A): accumulator (1), self-acting impulse valve (2), valve piston (3), distribution valve (4), outlet (5); moulding box (B)

Because the input function $F(t)$ causing deformation and compaction of moulding sand ought to be known, modelling of the impulse compacting process requires that the mathematical models of the impulse head and the process of sand deformation and compaction are considered jointly.

Taking account of the model of the impulse head and the rheological model of the moulding sand, the impulse compacting process can be described by the following system of differential equations:

$$p_1 \cdot A_1 = m_2 \cdot \frac{d^2 y(t)}{dt^2} + k_T(\delta) \cdot \frac{dy(t)}{dt} + k_C(\delta) \cdot y(t), \tag{1}$$

$$A_2(p_2 - p_3) - c \cdot x - m_1 \cdot g = m_1 \cdot \frac{d^2 x}{dt^2}, \tag{2}$$

$$\frac{\kappa \cdot R \cdot T \cdot G_1}{V_1} = \frac{dp_1}{dt}, \tag{3a}$$

or

$$\frac{\kappa}{y} \cdot \left(\frac{G_1 \cdot R \cdot T}{A_1} - p_1 \cdot \frac{dy}{dt} \right) = \frac{dp_1}{dt}, \tag{3b}$$

$$\frac{-\kappa \cdot R \cdot T \cdot G_2}{V_2} = \frac{dp_2}{dt}, \tag{4}$$

where:

$k_T = f(\delta)$ – attenuation coefficient of moulding sand in function of its compacting degree;

$k_C = f(\delta)$ – elasticity coefficient of moulding sand in function of its compacting degree;

p_1 – absolute pressure in the workspace;

p_2 – absolute pressure in the accumulator;

p_3 – absolute air pressure in the impulse valve chamber;

A_2 – piston face area;

c – constant of the impulse valve spring;

g – acceleration of gravity;

V_1 – workspace volume;

V_2 – accumulator volume;

m_1 – mass of the piston of the self-acting impulse valve;

m_2 – mass of the thickened moulding sand;

s – piston stroke;

x – co-ordinate of the piston position;

y – co-ordinate of the upper layer of moulding sand;

κ – adiabate exponent;
$G_{1(2)}$ – air flow rate from the accumulator to the workspace;
R – gas constant of the air;
T – air temperature in the workspace and in the accumulator;
α – coefficient of air flow rate from the accumulator to the workspace;
$f_1(x)$ – area of air flow from the accumulator to the work space.

The model presented describes the process of impulse compacting of moulding sand that occurs when $k_C>0$ and $k_T>0$.

The system of differential equations given above represents: (1) – deformation process of moulding sand; (2) – piston movement; (3a) – gaseous process in the empty workspace; (3b) – gaseous process in the workspace with moulding sand; (4) – gaseous process in the accumulator.

The system of equations (2), (3a) and (4) describes the head dynamics and airflow in the empty workspace. The system of equations (1), (2), (3b) and (4) describes the head dynamics and airflow in the workspace that includes moulding sand.

The airflow rate $G_{1(2)}$ from the accumulator to the workspace can be determined from the relationship:

$$G_{1(2)} = K \cdot \alpha \cdot f_1(x) \cdot p_{1(2)} \cdot \sqrt{\frac{1}{R \cdot T}} \cdot \varphi(\varepsilon), \tag{5}$$

where:

$$\varepsilon = \frac{p_1}{p_2}, \qquad K = \sqrt{\frac{2 \cdot \kappa}{\kappa - 1}},$$

$$\varphi(\varepsilon) = \begin{cases} 0.2588 & \text{for} \quad 0 < \varepsilon \le 0.53, \\ \sqrt{\varepsilon^{2/\kappa} - \varepsilon^{\kappa+1/\kappa}} & \text{for} \quad 0.53 < \varepsilon \le 1. \end{cases}$$

In order to solve the system of differential equations (1)–(4), it is necessary to know the parameters that characterise rheological properties of moulding sand, i.e., $k_C=f(\delta)$ and $k_T=f(\delta)$.

The relationships describing the changes of viscous and elastic properties in function of the sand compacting degree were determined on the grounds of experimental results [7]. Their forms were found as follows:

$$k_C(\delta) = b_1 \cdot \exp[b_2 \cdot V_L(\delta)], \qquad k_T(\delta) = a_1 \cdot \exp[a_2 \cdot V_L(\delta)], \tag{6}$$

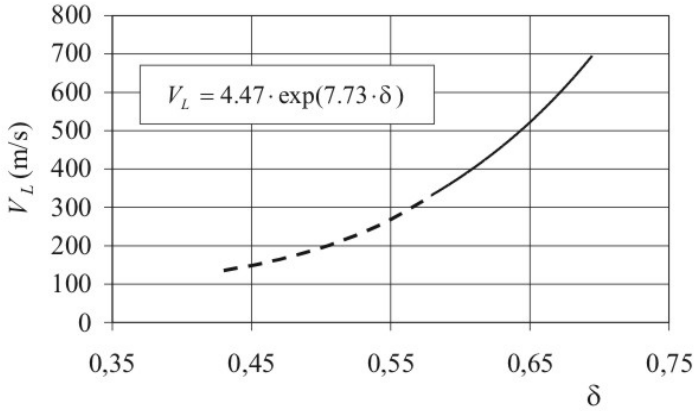

Fig. 2. $V_L = f(\delta)$ relationship for moulding sand and Bentomak bentonite

a)

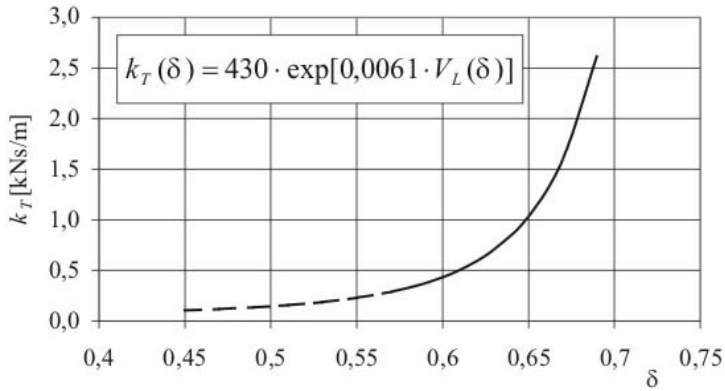

b)

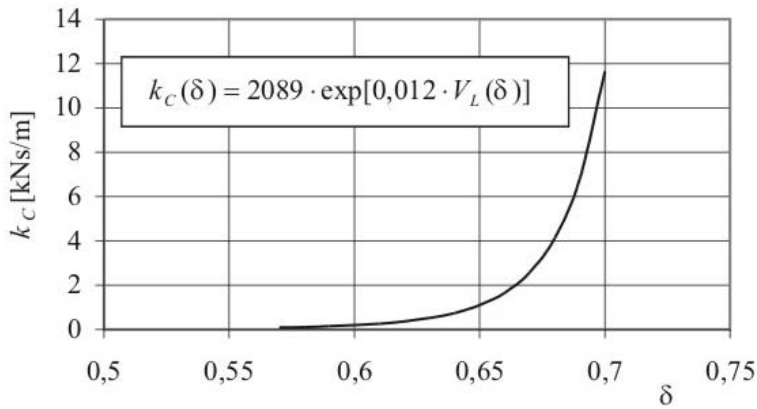

Fig. 3. Relationship describing viscous and elastic properties $k_T = f(\delta)$ (a) and $k_C = f(\delta)$ (b) of moulding sand and Bentomak bentonite

where:

a_i, b_i – coefficients,

V_L (δ) – propagation velocity of longitudinal ultrasonic wave in moulding sand in function of sand compacting degree.

As results from relationship (6), the coefficients $k_C = f(\delta)$ and $k_T = f(\delta)$ can be determined, provided that the propagation velocity V_L of longitudinal ultrasonic wave in moulding sand in function of sand compacting degree is known. The relationship $V_L = f(\delta)$ can be determined on the grounds of ultrasonic test carried out with the use of a material tester of type 543.

Figure 2 shows an example of relationship, i.e. $V_L = f(\delta)$, determined based on ultrasonic measurements of moulding sand with 6% of Bentomak bentonite, humidity W=3.17%.

Figure 3 shows the $k_C = f(\delta)$ and $k_T = f(\delta)$ relationships described by relationships (6) and $V_L = f(\delta)$.

3. Results of simulation

Simulation of the mathematical model of the process of impulse compacting of moulding sands was ran in the Matlab-Simulink environment. The simulation tests were carried out for the empty workspace and the workspace filled with moulding sand.

Figure 4 shows the relationships representing the changes of air pressure in the accumulator and in the empty workspace. Figure 5 shows the changes of air pressure in the accumulator of the impulse head and in the workspace above moulding sand. The test results were obtained with an initial pressure $p_0 = 0.5$ MPa in the accumulator of the impulse head.

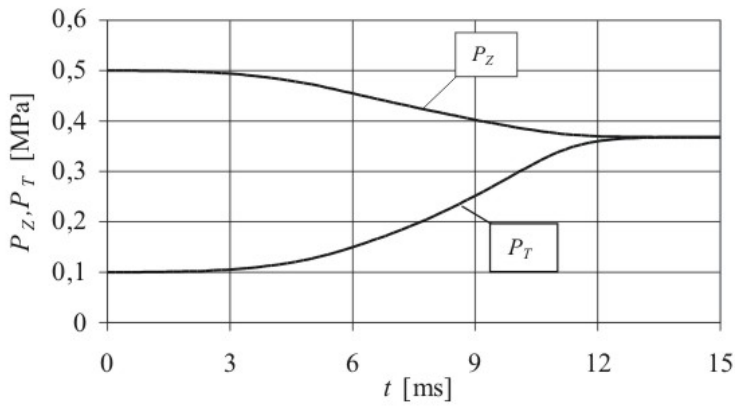

Fig. 4. Time relationships of air pressure in the impulse head (P_Z) and in the empty workspace (P_T)

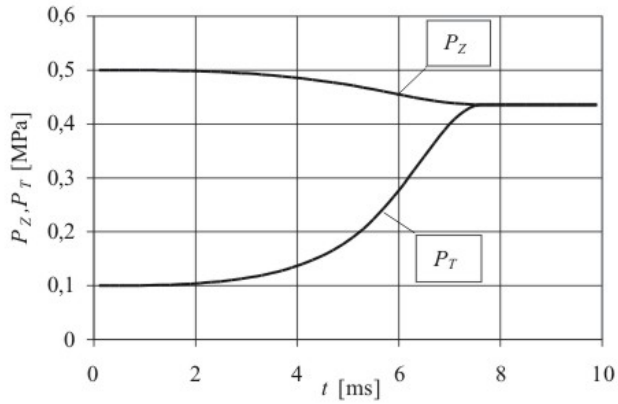

Fig. 5.Time relationships of air pressure in the impulse head (P_Z) and in the workspace (P_T) filled with moulding sand with Bentomak bentonite

Based on the time relationships of air pressure in the empty workspace and in the space above moulding sand it can be concluded that higher rate of pressure rise and higher pressure in steady state are obtained in the process with moulding sand. This results from smaller volume of the workspace whose substantial part is filled with moulding sand.

The simulation results obtained allow us to state that the impulse head is characterised by very high internal dynamics evidenced by very short compacting time of ca. 10 ms.

4. Summary

A mathematical model of the process of impulse compacting of moulding sands developed at the Laboratory of Automation Principles of the Institute of Machine Engineering and Automation of Wrocław University of Technology and some selected results of simulation tests of this model are presented.

The model developed describes in detail the impulse process, and the results of its examination permit an assessment of the dynamics of the head and the compacting process. The model presented can be used for designing and optimising the heads on impulse machines and for assessing the dynamics of impulse compacting of moulding sands.

References

[1] Orlov G.M.: *Miechanizm dinamičeskogo uplotnieniija form*, Lit. Proizv., 1983, No. 7.
[2] Bast J.: *Mathematisch-naturwissenschaftliche Grundlagen der pneumatischen Verdichtungsverfahren*, Giessereiforschung, 1993, Nr. 1, 45.

[3] Smyksy K.: *Research and analysis of parameters of impulse moulding machine* (in Polish), Doctor's Thesis, ITiMO AGH, Kraków, 1991.
[4] Mikulczyński T., Bogdanowicz J.: *The assessment of effectiveness of moulding sands of a single-valve impulse head*, Acta Metallurgica Slovaca, 1998, 2.
[5] Bogdanowicz J., Mikulczyński T., Samsonowicz Z.: *Attempt to quantitative evaluation of effectiveness of impulse forming* (in Polish), Archives of Institute of Machine Engineering and Automation, 1998, Vol. 18.
[6] Bogdanowicz J., Mikulczyński T.: *Influence of selected factors on effectiveness of air impulse moulding*, Archiwum Budowy Maszyn, 1999, Vol. 46, No. 3.
[7] Ganczarek M.: *Mathematical model of the process of dynamic squeezing of moulding sands* (in Polish), Doctor's Thesis, ITMiA PWr., Wrocław, 2003.

Badania symulacyjne procesu impulsowego zagęszczania mas formierskich

Przedstawiono matematyczny model impulsowego zagęszczania mas formierskich opracowany w Instytucie Technologii Maszyn i Automatyzacji Politechniki Wrocławskiej. Zaprezentowany model jest układem równań różniczkowych, które opisują dynamikę głowicy impulsowej oraz proces deformacji masy formierskiej. Do opisu deformacji masy formierskiej zastosowano lepkosprężysty model reologiczny, który przyjęto na podstawie identyfikacji własności reologicznych masy metodą czasową. Zaprezentowano wyniki badań symulacyjnych procesu impulsowego zagęszczania mas formierskich. Na podstawie analizy uzyskanych wyników badań stwierdzono, że opracowany model w pełni opisuje proces impulsowego zagęszczania mas formierskich. Zatem może on być stosowany do projektowania i optymalizacji głowic maszyn impulsowych oraz projektowania procesu zagęszczania mas formierskich.

ARCHIVES OF CIVIL AND MECHANICAL ENGINEERING

Vol. IV 2004 No. 2

Distortions and deviations caused by spring-back in the case of rectangular draw parts made from homogeneous and heterogeneous metal sheets

G. BRABIE, C. AXINTE
University of Bacau, 157 Marasesti Street, 5500 Bacau, Romania

D. PROFIR
WMW Bacau, 205 Republicii Street, 5500 Bacau, Romania

Spring-back is a phenomenon that seriously affects the quality of parts made by forming processes of metal sheets. The size of distortions of the formed part caused by spring-back depends on different factors, such as: material parameters and chemical composition, working conditions and tool accuracy. The present paper deals with an experimental research into the influence of such sheet material as homogeneous and heterogeneous metal sheets on distortions and deviations caused by spring-back in the case of rectangular draw parts.

Keywords: *spring-back, rectangular parts, homogeneous and heterogeneous metal sheets*

1. Introduction

Spring-back is a phenomenon of elastic nature determined by the distribution of residual stresses in the section of the formed part. Spring-back is not only manifested by the modification of the state of stress/strains in the formed material, but also by the modification of the geometric shape and dimensions of the formed part.

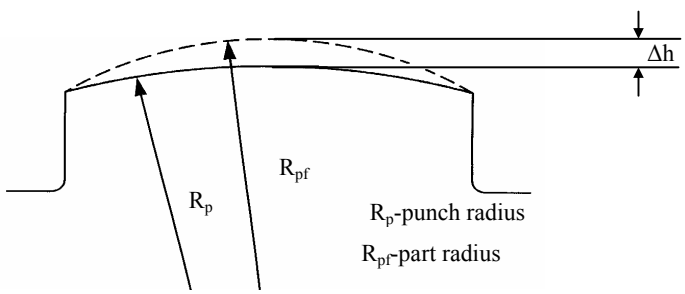

Fig. 1. Spring-back in the case of rectangular part

In the case of deep drawing operations, the spring-back is a complicated problem because of the complex loading and complex geometry of the formed part. In com-

parison with bending operation, in drawing operation the spring-back parameters are the function of the part geometry. In the case of a rectangular draw part shown in Figure 1, main deviations and distortions caused by spring-back can be itemized as follows: modification of the angle of inclination of the part walls, modification of the curvature radius (R) and the difference in height (Δh) [3]. Generally, the spring-back is positive, but its negative values can be registered when the blankholder forces increase and the radii of part are smaller than the radii of punch. The main factors that influence the spring-back phenomenon after drawing are as follows: dimensions and accuracy of the tool (punch and die radii, initial clearances), the working conditions (lubricating conditions, force and shape of blankholder, forming force, forming speed), chemical composition and mechanical properties of material and sheet thickness. Taking account of the influence of the material parameters, it can be concluded that generally materials of higher mechanical strength characteristics lead to an increase in the spring-back intensity [1], [2], [4].

The present paper deals with an experimental research into the influence of the blank material, i.e. homogeneous or heterogeneous metal sheets, on the deviations and distortions caused by spring-back in the case of rectangular draw parts.

2. Experimental conditions

The experimental analysis of spring-back was performed under the following conditions: drawing depth, 22 mm; drawing force, 25 tf; drawing speed, 18 mm/min; blank holding force, 10 kN. In order to compare the behaviour of different materials

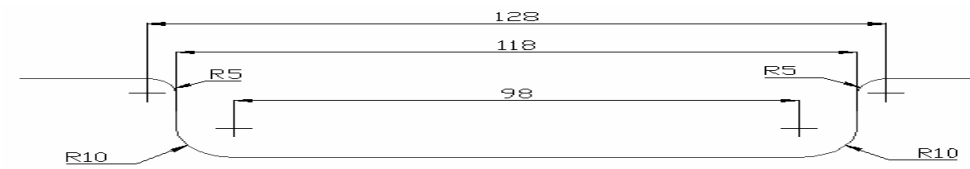

Section in *XOZ* plan

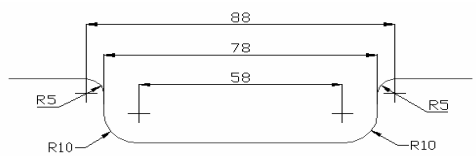

Section in *YOZ* plan

Fig. 2. Dimensions of the finished part

subjected to spring-back, the analysis was carried out using the following three steel sheets: blanks made from homogeneous FEPO 5MBH, SPE 220BH sheets and blanks made from TWB obtained by joining the FEPO 5MBH and SPE 220BH steel sheets by laser welding. The materials used in this study were selected based on the following mechanical characteristics: yielding stress and workhardening coefficient. The FEPO 5MBH steel has lower yielding stress and higher workhardening coefficient in comparison with SPE 220BH steel. The basic dimensions of the finished part and the device used for part drawing are presented in Figures 2a, 2b and 3, respectively. The parameters determined in experimental analysis are shown in Figure 4.

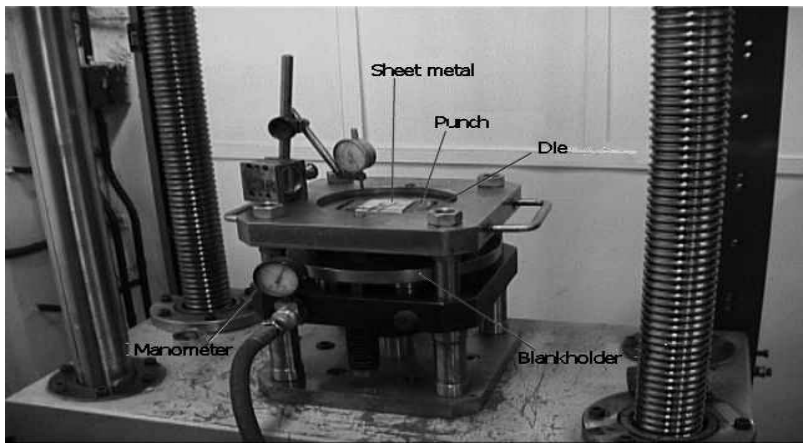

Fig. 3. Device construction

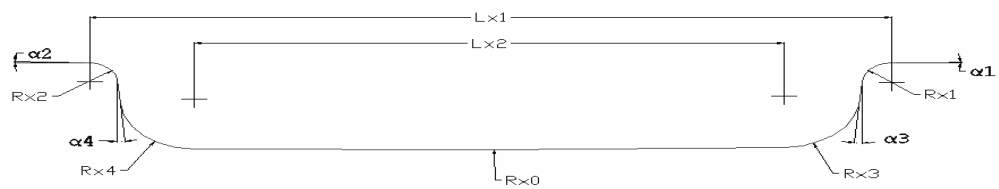

Section in the *XOZ* plane

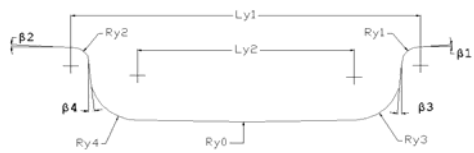

Section in the *YOZ* plane

Fig. 4. Parameters determined from experimental analysis

3. Test results

The experimental results are represented by the longitudinal and transverse sections of the part scanned using a 3D scanning machine and are shown as follows: the part made from FEPO 5MBH steel sheet in Figure 5a and b; the part made from SPE 220BH steel sheet in Figure 6a and b and the parts made from TWBs in Figure 7a and b. The deflections caused by spring-back phenomenon are presented in the Table.

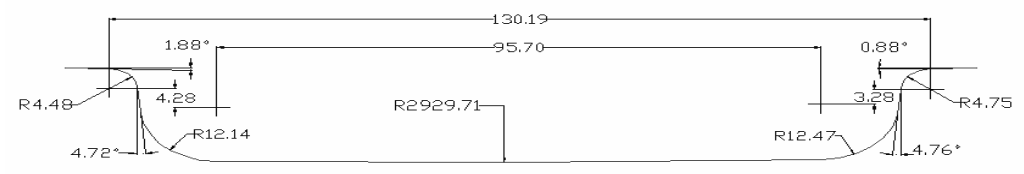

a. *OX* axis

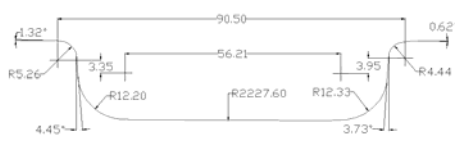

b. *OY* axis

Fig. 5. Spring-back parameters in the case of rectangular part made from FEPO 5MBH steel sheets:

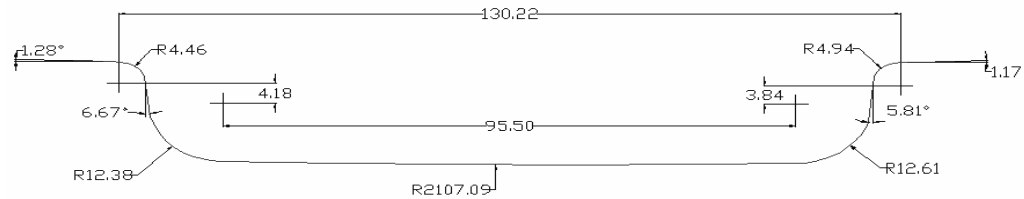

a. *OX* axis

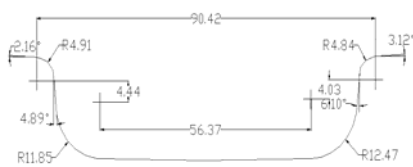

b. *OY* axis

Fig. 6. Spring-back parameters in the case of rectangular part made from SPE 220BH steel

a)

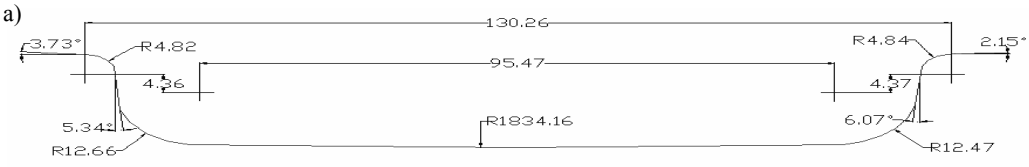

b)

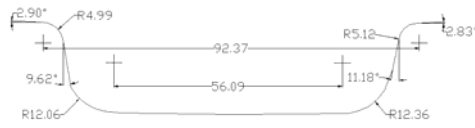

Fig. 7. Spring-back parameters in the case of rectangular part made from TWB steel sheets: a – *OX* axis, b – *OY* axis

Table. Deviations from the nominal dimensions caused by spring-back

XOZ plane	Drawing speed, 18 mm/min; drawing depth, 22 mm; blank holder force, 10 kN										
Material	*Lx*1-128 [mm]	*Lx*2-98 [mm	*Rx*0 [mm]	*Rx*1-5 [mm]	*Rx*2-5 [mm]	*Rx*3-10 [mm]	*Rx*4-10 [mm]	α1 [°]	α2 [°]	α3 [°]	α4 [°]
SPE220BH	2.22	2.5	2107.09	–0.06	–0.54	2.61	2.38	–1.17	–1.28	5.81	6.67
FEPO5MBH	2.19	–2.3	2929.71	–0.25	–0.52	2.47	2.14	–0.88	–1.88	4.76	4.72
TWBs	2.26	–2.53	1834.16	–0.16	–0.18	2.47	2.66	–2.15	–3.73	6.07	5.34
YOZ plane	Drawing speed, 18 mm/min; drawing depth, 22 mm; blank holder force, 10 kN										
Material	*Ly*1-88 [mm]	*Ly*2-58 [mm]	*Ry*0 [mm]	*Ry*1-5 [mm]	*Ry*2-5 [mm]	*Ry*3-10 [mm]	*Ry*4-10 [mm]	β1 [°]	β2 [°]	β3 [°]	β4 [°]
SPE220BH	2.42	–1.63	1600.28	–0.16	–0.09	2.47	1.85	–3.12	–2.16	6.1	4.89
FEPO5MBH	2.5	–1.79	2227.6	–0.56	–0.26	2.33	2.2	–0.62	–1.32	3.73	4.45
TWBs	4.37	–1.91	1074.83	–1.91	–0.01	2.36	2.06	–2.83	–2.9	11.18	9.62

4. Conclusions

1. The distortions caused by spring-back are as follows: inclination of the part walls, inclination of the flange and bottom curvature. These distortions are registered in both sections – longitudinal and transverse – of the formed part for all materials being analysed.

2. The deviations from the nominal dimensions occur as follows: in the plane *XOZ* for the following dimensions: *Lx*1, *Lx*2, *Rx*0, *Rx*1, *Rx*2, *Rx*3, *Rx*4, α1, α2, α3, α4; in the plane *YOZ* at the following dimensions: *Ly*1, *Ly*2, *Ry*0, *Ry*1, *Ry*2, *Ry*3, *Ry*4, β1, β2, β3, β4. In the same plane, between the deviations on both sides of the part there are observed small differences. They occur not only in the case of TWBs, but also in the

case of homogeneous steel sheets. In the case of parts made from TWBs, these differences are caused by the differences in the mechanical properties of the steel sheets that make the blank. In the case of the parts made from homogeneous steel sheets, the differences can be due to the imperfections of the metal sheet structure.

3. In the case of homogeneous metal sheets, the deviations caused by spring-back were registered for all nominal dimensions of the formed parts. Contradictory aspects were observed for the influence of the metal sheet properties on the size and location of the deviations. Thus, the deviations were considerably sharper in the case of the parts made from SPE 220BH steel sheets at the following nominal dimensions: $Lx1$, $Lx2$, $Rx2$, $Rx3$, $Rx4$, $\alpha 1$, $\alpha 3$, $\alpha 4$ in the *XOZ* plane, and $Ry3$, $\beta 1$, $\beta 2$, $\beta 3$, $\beta 4$ in the *YOZ* plane. In the case of parts made from FEPO 5MBH steel sheet, the sharpest deviations were observed at the following nominal dimensions: $Rx0$, $Rx1$ and $\alpha 2$ in the plane *XOZ* and $Ly1$, $Ly2$, $Ry0$, $Ry1$, $Ry2$ and $Ry4$ in the plane *YOZ*. The general conclusions resulting from this analysis can be drawn as follows:

- an increase in the yielding stress and a decrease in the workhardening coefficient can be favourable for an increase in the spring-back intensity in certain regions of the formed part, i.e. in the left and right walls, the flange and the region of connection between bottom and walls;
- a decrease in the yielding stress and an increase in the workhardening coefficient can determine an increase in the spring-back intensity in other regions of the formed part, i.e. in the bottom and the region in connection between flange and walls;
- an increase in the yielding stress and a decrease in the workhardening coefficient can be favourable for an increase in the spring-back intensity in the longitudinal section of the formed part; a decrease in the yielding stress and an increase in the workhardening coefficient can determine an increase in the spring-back intensity in the transverse section of the formed part.

4. In the case of parts made from TWBs, the deviations are sharper than in the case of parts made from homogeneous metal sheets at the following nominal dimensions: $Lx1$, $Lx2$, $Rx4$, $\alpha 1$, $\alpha 2$, $\alpha 3$ in the plane *XOZ* and $Ly1$, $Ly2$, $\beta 2$, $\beta 3$, $\beta 4$ in the plane *YOZ*. Generally, the sharpest deviations occur in the half-part made from steel sheets having smaller yielding stress and higher workhardening coefficient. The influence of the weld line was observed in the bottom part. In this case, the bottom curvature for the part made from TWB is smaller in comparison with that for the parts made from homogeneous metal sheets.

Acknowledgement

This research was performed with the financial support of the European Commission.

References

[1] Tang C.S.: *Analysis of springback in sheet forming operation*, Advanced Technology of Plasticity, 2001, Vol. I, pp. 193–197.
[2] Han S.S., Park K.C.: *An investigation of the factors influencing springback by empirical and simulative techniques*, Proc. of Numisheet'99, Besancon, France, 1999, pp. 53–57.
[3] *** *Sheet Steel Forming Handbook*, SSAB Tunnplat, 3rd edition, 2002.
[4] Pearce R.: *Sheet metal forming*, The Adam Hilger Series on New Manufacturing Processes and Materials, Bristol, 1991.

Powrotne sprężyste odkształcenia i przemieszczenia w prostokątnych wytłoczkach wykonanych z jednorodnych i niejednorodnych blach

Odkształcenia sprężyste istotnie wpływają na jakość wyrobów tłoczonych. Zależą one od różnych czynników takich jak: właściwości materiału, skład chemiczny, warunki odkształcania i dokładność wykonania narzędzi. Przedstawiono badania doświadczalne pokazujące wpływ warunków odkształcania blach wykonanych z materiałów jednorodnych i niejednorodnych na odkształcenia i przemieszczenia sprężyste prostokątnych wytłoczek. Zaobserwowano, że w wytłoczkach wykonanych z blach jednorodnych zwiększenie granicy plastyczności i zmniejszenie współczynnika umocnienia materiału wpływa na zwiększenie odkształceń powrotnych w następujących obszarach wytłaczanych wyrobów: ściana, kołnierz i obszar zawarty między dnem a ścianami. Zmniejszenie natomiast granicy plastyczności i wzrost współczynnika umocnienia wywołują zwiększenie odkształceń sprężystych w innych obszarach wytłoczki, tj. w samym dnie i obszarze zawartym pomiędzy kołnierzem a ścianami. W wytłoczkach z blach niejednorodnych spawanych laserem odkształcenia sprężyste są większe niż w wytłoczkach z blach jednorodnych.

ARCHIVES OF CIVIL AND MECHANICAL ENGINEERING

Vol. IV 2004 No. 2

Determination of the weld metal properties and behaviour in the case of tailor-welded blanks using the parallel tensile test and image-analysis method

G. BRABIE, B. CHIRITA, C. CHIRILA
University of Bacau, 157 Marasesti Street, 5500 Bacau, Romania

The quality of a weld in the tailor-welded blank is very important for the success of the forming operation. The mechanical properties of the weld metal can be determined by applying different methods, such as: parallel test, normal test, microhardness test, etc. In the present paper, the mechanical properties of the weld metal in a tailor-welded sheet made by joining similar metals were investigated. The investigation was performed by applying the microhardness and parallel tests in conjunction with the rule of mixture. The analysis of the behaviour of the tailor-welded blanks by examining the strain variation during tensile parallel test of tailor-welded sheets applying the image-analysis method is also presented.

Keywords: *weld metal properties, parallel test, rule of mixture, image analysis, strain distribution*

1. Introduction

A tailor-welded blank (TWB) consists of two or more sheets that are welded together to make a single blank prior to forming (Figure 1). These sheets can be identical, or they can be of different thickness, mechanical properties, or surface coatings. The blanks are joined either by mash seam welding or by laser beam welding, electron-beam welding, and induction welding.

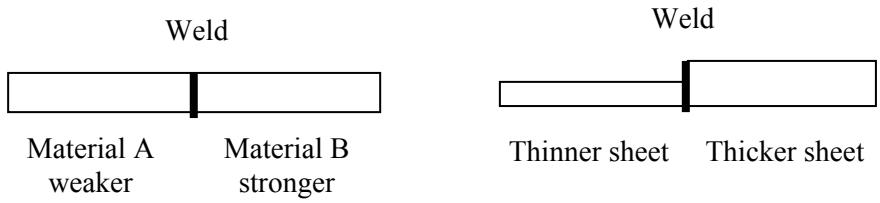

Fig. 1. Tailored blanks

The quality of the weld in the tailor-welded blank is very important for the successful forming operation. Physical testing of the weld metal is very important to determine the behaviour of the TWB during forming. Generally, for a steel TWB the basic metal has significantly lower yield strength and tensile strength and hence higher ductility than the weld metal [1], [2]. The mechanical properties of the weld metal can be

determined by applying different methods, such as: parallel test, normal test, microhardness test, etc. In the present paper, the mechanical properties of the weld metal in a tailor-welded sheet were investigated by applying the microhardness and parallel tensile tests in conjunction with the rule of mixture, and by analysing the strain variation during parallel tensile test using the image analysis method.

2. Determination of weld metal properties from parallel test

In order to determine the weld metal properties, a parallel test can be done in conjunction with the *rule of mixture*. According to this rule, the stress–strain tensile test must be performed using specimens cut from basic materials and from TWB. The following relation gives the total load applied to a specimen:

$$F = \sigma_1 A_1 + \sigma_2 A_2 + \sigma_w A_w , \tag{1}$$

where: σ_1, σ_2 are the stresses corresponding to the areas of the basic materials; σ_w is the average stress corresponding to the weld area; A_1, A_2 and A_w are the cross section areas of the basic and weld metals, respectively. The longitudinal strains are assumed to be constant across the TWB specimen, so that:

$$\varepsilon_1 = \varepsilon_2 = \varepsilon_w . \tag{2}$$

Based on the Ludwik–Hollomon equation, relation (1) takes the following form:

$$F = \left(K_1 \varepsilon_1^{n_1}\right) A_1 + \left(K_2 \varepsilon_2^{n_2}\right) A_2 + \sigma_w A_w . \tag{3}$$

An average stress will result from relation (3) as follows:

$$\sigma_w = \frac{F - \left(K_1 \varepsilon_1^{n_1}\right) A_1 - \left(K_2 \varepsilon_2^{n_2}\right) A_2}{A_w} . \tag{4}$$

By taking into account assumption (2), equation (4) can be rewritten as:

$$\sigma_w = \frac{F - \left(K_1 \varepsilon_w^{n_1}\right) A_1 - \left(K_2 \varepsilon_w^{n_2}\right) A_2}{A_w} . \tag{5}$$

Equation (5) defines the stress–strain relation for the weld metal. If the basic materials are the same and the thickness of sheets is the same, the following parameters of the materials and sheets will have equal values:

$$K_1 = K_2 = K, \quad n_1 = n_2 = n, \quad A_1 = A_2 = A .$$

Hence, Equation (5) can be rearranged as follows:

$$\sigma_w = \frac{F - 2\left(K\ \varepsilon_w^n\right)A}{A_w} = \frac{F - \left(K\ \varepsilon_w^n\right)\left(A_t - A_w\right)}{A_w}, \tag{6}$$

where the cross section area of the basic materials was replaced by $A=(A_t–A_w)/2$. The area A_w of the weld metal cross-section can be obtained using the following methods: the direct measurement of the weld width; the measurement of a metallographic section; the determination of microhardness profiles [3], [4].

The parallel test was performed in the LMecA – ESIA laboratories, Annecy, France, with an INSTRON-5569 Tensile Testing Machine. Standard specimens were used in the test. The specimens were made from TWBs and obtained by joining the same metals: SPE 220BH and FEPO 5MB. The width of the weld was determined using a microhardness profilometer. The weld metal properties obtained from the parallel test were compared with the properties obtained from the image analysis.

The results obtained have been presented as follows: hardness variation along the width of the specimens (Figure 2), estimated values of A_w area (Table), true stress–strain curves for the weld metals (Figures 3 and 4).

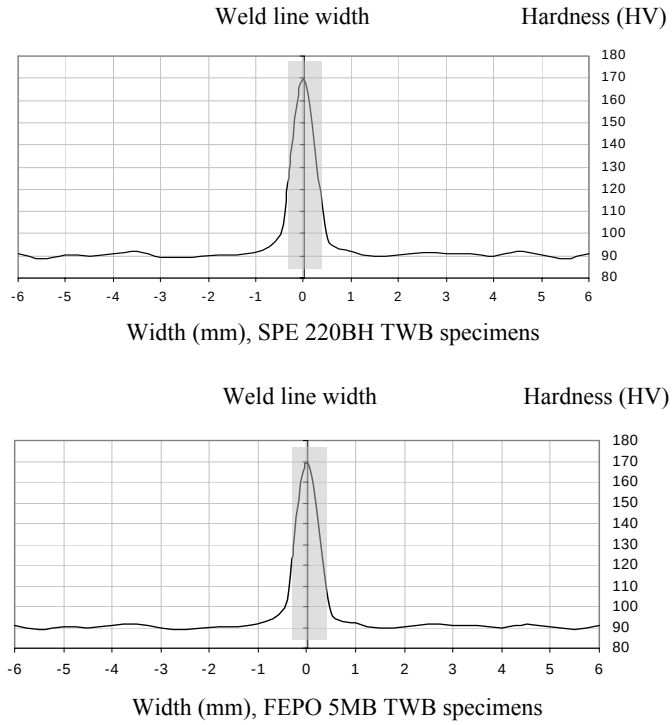

Fig. 2. Hardness variation along the width of the specimens

Table. Estimated values of A_w area

TWBs	Sheet thickness (mm)	Width estimating method	Width value (mm)	A_w area (mm)
TWBs made in SPE 220BH steel sheets	0.7	direct measurement	0.64	0.448
		hardness measurement		
TWBs made in FEPO 5BM steel sheets	0.75	direct measurement	0.65	0.4875
		hardness measurement		

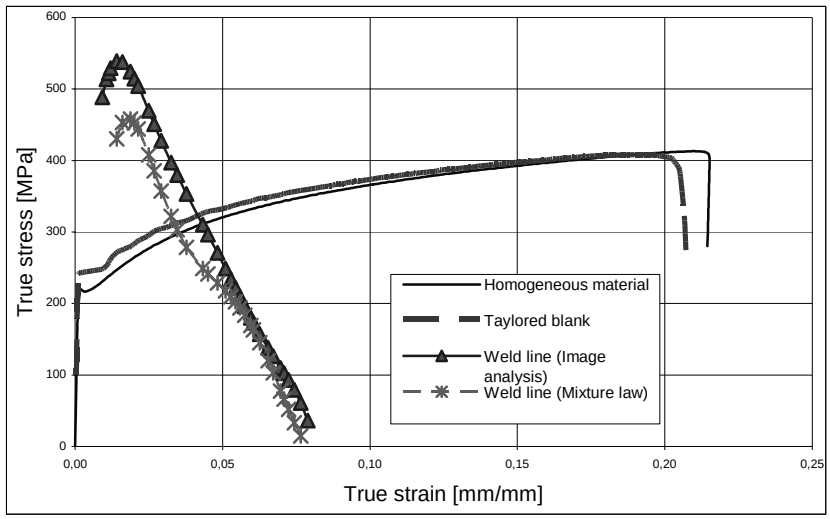

Fig. 3. True stress–strain curves for the weld metal for TWB–SPE 220BH TWB specimens

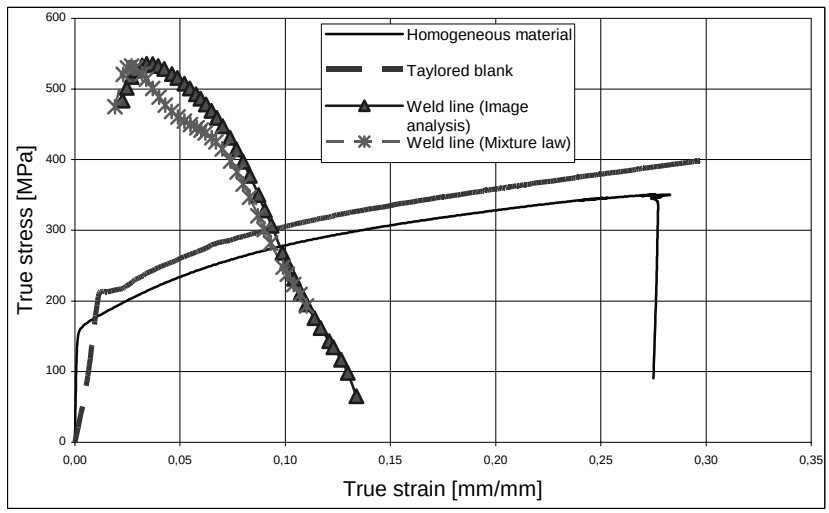

Fig. 4. True stress–strain curves for the weld metal for TWB–FEPO 5MB TWB specimens

3. Determination of strain variation during the tensile test of TWB sheets by using the image-analysis method

The tests were performed with an INSTRON-5569 Tensile Testing Machine. The parallel tensile test was applied and standard specimens were used. The strain was measured based on the method of image analysis using a Hamamatsu C4742-95 digital video camera. The specimens were prepared in such a way that they were made of the SPE 220BH steel sheet as basic material of TWB. Each test was repeated three times under the same experimental conditions and using the same type of specimen. The processing of the experimental results was performed using a SEPT-D LMECA – 0.5.0.15 software version.

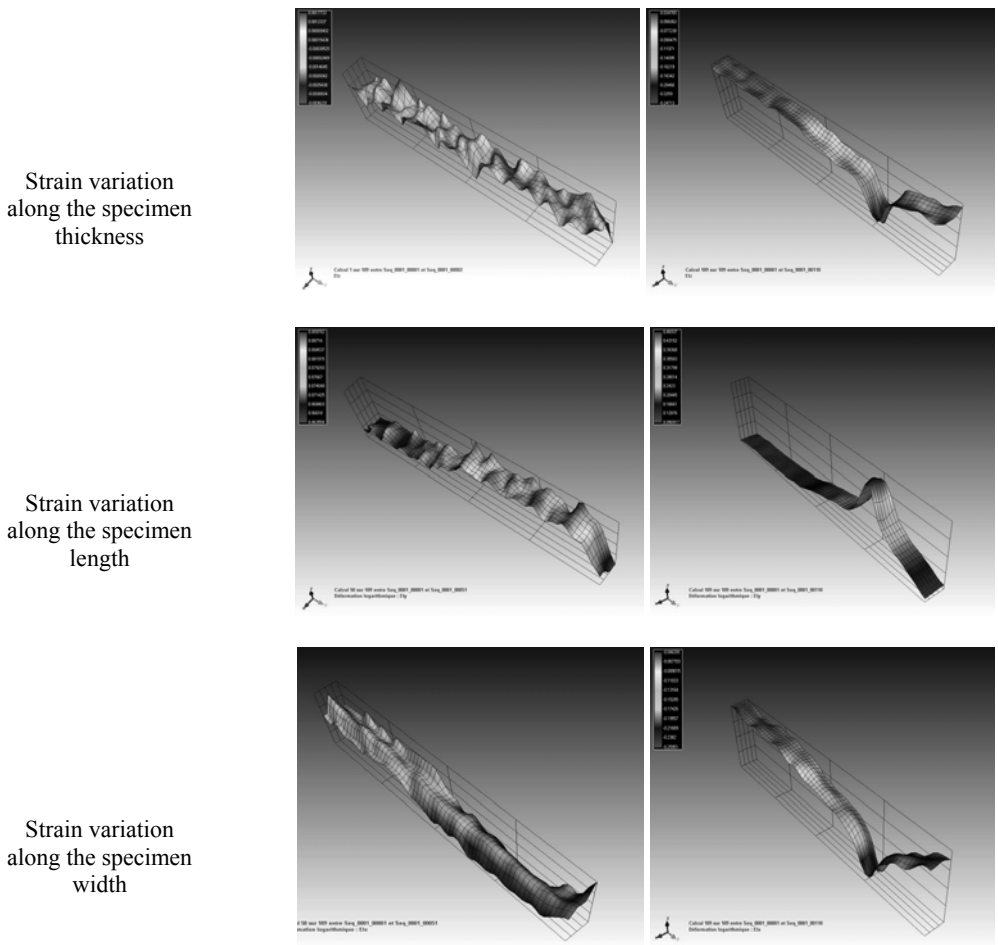

Fig. 5. Strain variations in parallel test – from the initial stage of the test till fracture, TWB made from SPE 220 BH steel

The results obtained have been presented as follows: strain variations in parallel test – from the half stage of the test till fracture, TWB made from SPE 220 BH steel (Figure 5), the specimens tested in parallel: zone of necking and fracture (Figure 6).

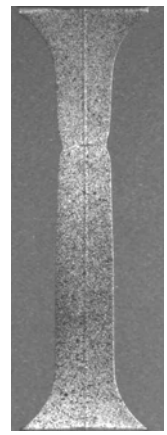

Fig. 6. The specimens tested in parallel: zone of necking and fracture

4. Conclusions

1. *Conclusions drawn for mechanical properties of weld metal*

In the case of parallel test for both TWBs, the strains of the weld metal in elastic region could not be determined. In the plastic region, both methods, i.e. – rule of mixture and image analysis, lead to approximately the same result.

The tensile strength of the weld metal is 1.6 times greater than that of the basic material in the case of TWBs made from SPE 220BH and 1.3 times greater in the case of TWBs made from FEPO 5MB.

2. *Conclusion drawn for strains' distribution*

Analysis of the graphs in Figure 5, which represent the strain variation, allows us to draw the following conclusions:

- the strain variation along the specimen thickness presents a smaller intensity along the weld line in comparison with the matrix,
- the strains along the specimen length are uniformly distributed in the matrix and weld metal till the necking stage occurs; the fracture will occur first in the weld metal as can be seen in Figure 6,
- the strains along the specimen width are mainly located in the matrix, the weld metal presents only small strains.

3. *General conclusions:*

Based on the hardness variation in the transverse section of a specimen and on the strain variation along the specimen width, it can be concluded that the analysis of the

mechanical properties of TWB should take into account only the behaviour of basic materials and weld materials, whereas the heat affected zone (HAZ) does not seem to have any influence.

Based on the uniform strain distribution along the width, thickness and length of a specimen, the assumption that the longitudinal strains are constant across the TWB specimen applied in the rule of mixture can be considered as correct. Hence, we can conclude that in the determination of weld metal properties, the application of the parallel test in conjunction with rule of mixture is benefical for the accuracy of results.

Acknowledgements

This research was performed with the financial support of the European Commission. The authors are grateful to Prof. R. Arrieux, Prof. L. Tabourot and Eng. O. Incandela (Univ. of Savoie, ESIA Annecy, France) for their help.

References

[1] *Tailor welded blank design and manufacturing manual*, http://www.a-sp.org
[2] *Annual book of ASTM Standards*, 1990.
[3] Lee J.K., Chun B.K.: *Numerical investigation of TWB forming and springback*, Simulation of Mat. Proc. Theory, 2001, pp. 729–734.
[4] Abdullah K. et al.: *Tensile testing for weld deformation properties in similar gage TWBs using the rule of mixture*, J. of Mat. Proc. Tech., 2001, 112, pp. 91–97.

Określenie właściwości i zachowania się blach spawanych laserem w próbie równoległego rozciągania i metodą analizy obrazu

Badano właściwości mechaniczne spawanych laserem blach wykonanych z podobnych materiałów. Właściwości blach określano przez pomiary ich mikrotwardości oraz w próbie równoległego rozciągania; do rozdziału właściwości materiałów w poszczególnych strefach stosowano zasadę proporcjonalności. Aby ocenić rozkład odkształceń w czasie równoległej próby rozciągania, zastosowano analizę obrazu. Zarówno badania właściwości materiału w próbie równoległego rozciągania połączonej z pomiarami mikrotwardości, jak i analiza obrazu w obszarze odkształceń plastycznych prowadzą do podobnych wyników. Opierając się na zmianach mikrotwardości w przekroju poprzecznym próbek oraz na odkształceniach szerokości próbek stwierdzono, że mechaniczne właściwości blach połączonych laserem mogą być określone jedynie na podstawie właściwości materiałów użytych do wykonania blach kompozytowych z całkowitym pominięciem oddziaływania strefy wpływu ciepła. Ostatecznie wykazano, że próba równoległego rozciągania blach spawanych lasem w powiązaniu z pomiarami mikrotwardości daje bardzo dobre informacje o właściwościach spawanych blach.

ARCHIVES OF CIVIL AND MECHANICAL ENGINEERING

Vol. IV 2004 No. 2

An approximate method for determining static and dynamic stiffnesses of machine tools with rolling guideways

D. ŚNIEGULSKA-GRĄDZKA, M. KLASZTORNY, M. SZAFARCZYK
Warsaw University of Technology, Narbutta 85, 02-524 Warsaw

The paper develops computer-aided design of reconfigurable/modular machine tools with rolling guideways, at the stage of conceptual design. The main static and dynamic stiffnesses in the tool−workpiece area are proposed for assessment of possible configurations of a machine tool. These stiffnesses are understood as reversals of the main relative compliances of the tool with the workpiece under static and dynamic conditions. A machine tool is modelled approximately as a multi-body system with spatial linear viscoelastic interfaces. Dynamic stiffnesses are derived for three harmonic forces coinciding with the circumferential, feed and passive-pressure components of the tool−workpiece interaction. A computational algorithm for determining these stiffnesses has been formulated and programmed. The approximate modelling of a machine tool has been performed for the VENUS 250 NC lathe, designed and produced by the Centre of Machine Tool Design and Research, CBKO-Pruszków, Poland. Results of the computations are presented in the form of dynamic stiffness−frequency diagrams.

Keywords: *machine tool, conceptual design, static stiffness, dynamic stiffness*

1. Introduction

Computer-aided design of machine tools with rolling guideways (MTRGs) is commonly applied in modern manufacturing industry. Professional CAx systems, such as CATIA or UNIGRAPHICS, have some possibilities for evaluating static and dynamic properties of a machine tool. However, these systems are too expensive to be implemented in small design offices and require a lot of expertise from the user–designer. Moreover, a CAD project of the machine tool has to be advanced to apply these systems.

At the stage of conceptual design, the optimal configuration should be selected taking into account both manufacturing requirements and static–dynamic properties of the machine. This decision is vital for achieving a low-cost and rapid design process. Research centres involved in design of reconfigurable and modular machine tools are searching for effective methods for assessing various configurations of the machine tool at the stage of conceptual design [1–3]. Today, after accepting a structural configuration of the machine tool, advanced verifying or optimising computation is performed using FEM [4, 5].

Theoretical and experimental research on machine tools is also undertaken in Poland, e.g. [6–10]. Grudziński and Zapłata [6] developed dynamics of machine tools with slideways via modifying a classic theory of frictional self-excited vibrations.

Jastrzębski and Szwengier [7] applied the hybrid (rigid–flexible) finite element method to the analysis of static properties of machine tools with slideways. The authors took into account physical non-linearity of the contacting elements, i.e. one-side elastic characteristics, slide friction, structural clearances and initial clamps. The equations of static equilibrium are solved in an iterative loop assuming a linear initial model of the machine.

Bodnar and Schütte [8] presented a method for experimental determining the static stiffness and the static friction forces (of a very low value) in rolling guides. They foud that those characteristics are nonlinear and strongly affected by geometrical errors of the contacting elements. However, they considered only a rolling-contact joint with a single ball-shaping rolling element.

Konowalski [9] presented experimental values of contact deflections of needle roller flat cages used in slideway connections of machine tools. The author determined the static and dynamic stiffness characteristics related to normal contact deflections and compared them with the catalogue data.

Skoczyński and Krzyżanowski [10] presented a method for evaluating selected dynamic properties of lathes, which is based on machining accuracy of test pieces and desired production tasks. The authors established evaluation indexes that are able to account for relationships between properties of the machine tool structure and test piece machining accuracy. However, this approach requires using the machine tool prototype whose dynamic properties cannot be predicted theoretically.

A research team from University of Michigan, Ann Arbor, USA, has developed a method for conceptual design of modular machine tools [11, 12]. In this method, a library of modular sub-assemblies, including stiffness, is used. After designing a structural configuration satisfying technological tasks, the designer estimates dynamic stiffness of the machine tool.

2. A concept of the main static and dynamic stiffnesses of an MTRG

Static and dynamic properties of an MTRG can be assessed with the so-called static and dynamic stiffnesses, understood as reversals of the relative compliances in the tool–workpiece area [13]. In this study, six main stiffnesses are proposed for assessing. They are the reversals of the main relative compliances corresponding to three harmonic forces coinciding with circumferential, feed and passive-pressure components of the tool–workpiece interaction. Dynamic compliances result from steady-state responses of the MTRG to respective harmonic excitations. The main stiffnesses and compliances of a machine tool are understood according to definitions formulated by Wrotny [14].

Static and dynamic stiffnesses of an MTRG can be estimated using an approximate model in the form of a multi-body system with spatial linear viscoelastic interfaces. Such approach can be performed on a 3D CAD conceptual project of an MTRG.

3. Approximate dynamic modelling of an MTRG

In this study, the VENUS 250 NC lathe (V250) is analysed as an example of an MTRG. This machine has been designed and produced by the Centre of Machine Tool Design and Research, CBKO-Pruszków, Poland [15]. A structural scheme of the machine, based on [15], is shown in Figure 1. An approximate dynamic model is assumed in the form of four rigid bodies connected with deformable interfaces, i.e.:

B1 – a bed + a headstock frame + a spindle motor + additional masses,

B2 – a longitudinal slide + additional masses,

B3 – a cross slide + a tool head + a tool disk + a cutting tool (CT),

B4 – a spindle + a workpiece chuck + a cylinder sleeve + a workpiece (WP).

The interfaces are modelled as spatial orthogonal sets of linear viscoelastic Voigt constraints. The V250 lathe has four interfaces, i.e.:

(p) – vibroisolation pads between the bed and the foundation,

(l) – rolling carriages and a ball screw of the longitudinal slide,

(c) – rolling carriages and a ball screw of the cross slide,

(s) – rolling bearings and a driving belt of the spindle.

The remaining assumptions are as follows. A spindle motor and servo-mechanisms are ideal. The foundation is rigid in comparison to vibroisolation pads.

Each rigid body has 6DOF. Since the displacements are very small, vibrations of each rigid body are described with 3 translations and 3 rotations, defined in local Cartesian coordinate systems, as presented in Figure 1. The local coordinate systems take into account the slides' structural slope equal to 35°.

The kinetic energy of V250 is described by a well-known general formula [16]

$$E_{\mathrm{k}} = \frac{1}{2}\dot{\mathbf{q}}^{\mathrm{T}}\mathbf{B}\dot{\mathbf{q}}, \tag{1}$$

in which

$$\begin{gathered}
\mathbf{q} = \operatorname{col}\left(\mathbf{q}_1, \mathbf{q}_2, \mathbf{q}_3, \mathbf{q}_4\right), \\
\mathbf{q}_i = \operatorname{col}\left(q_{1i}, q_{2i}, q_{3i}, q_{4i}, q_{5i}, q_{6i}\right), \quad i = 1,2,3,4, \quad (\,)^{\bullet} = d/dt, \\
\mathbf{B} = \operatorname{diag}\left(\mathbf{B}_1, \mathbf{B}_2, \mathbf{B}_3, \mathbf{B}_4\right), \\
\mathbf{B}_i = \begin{bmatrix}
M & 0 & 0 & 0 & S_{xy} & -S_{xz} \\
 & M & 0 & -S_{xy} & 0 & S_{yz} \\
 & & M & S_{xz} & -S_{yz} & 0 \\
 & & & I_x & -D_{xy} & -D_{xz} \\
 & & & & I_y & -D_{yz} \\
\text{symm.} & & & & & I_z
\end{bmatrix}_i,
\end{gathered} \tag{2}$$

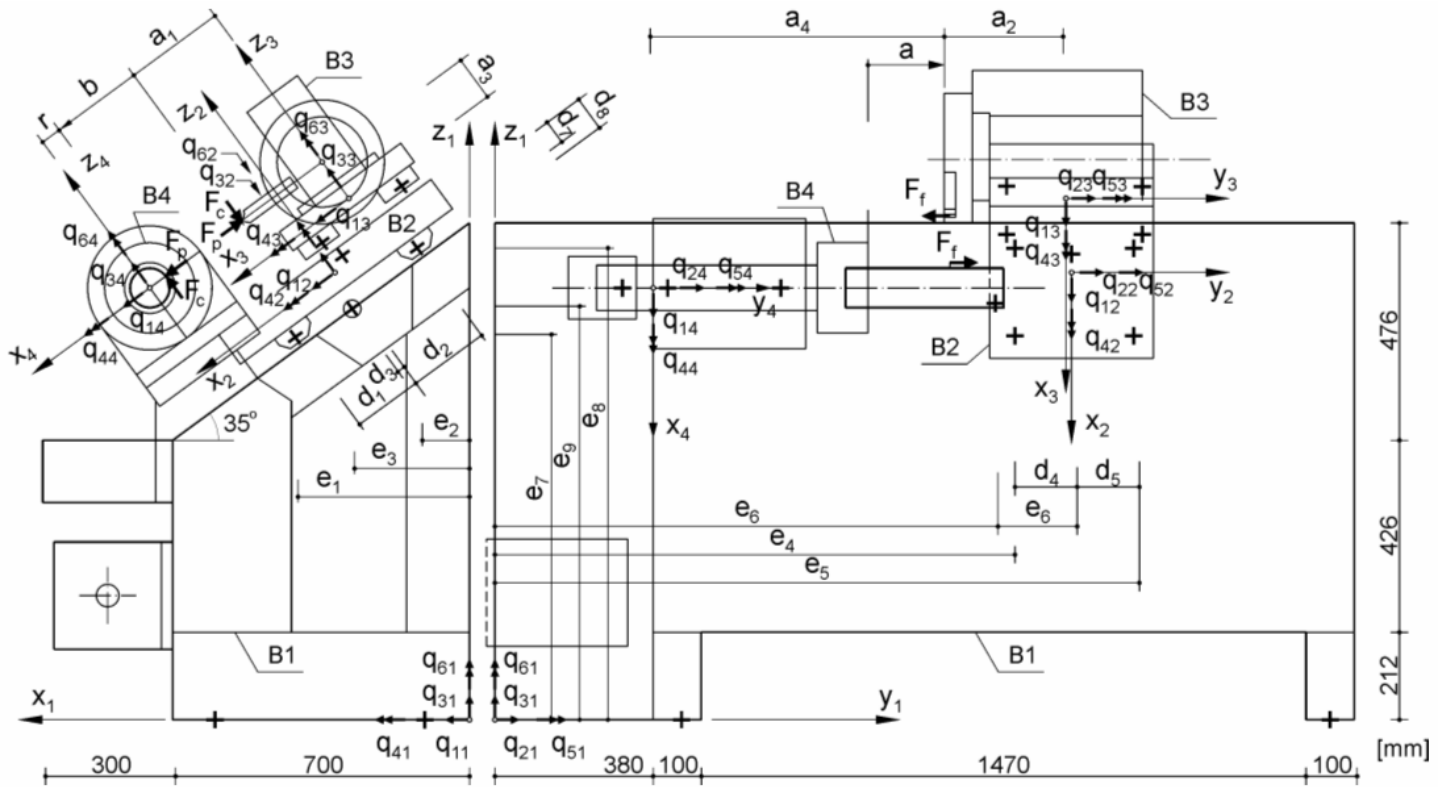

Fig. 1. A VENUS 250 NC lathe [15]. The structural configuration with the main dimensions. A set of the generalized coordinates **q**. The sub-assemblies: rigid bodies and viscoelastic interfaces. Dimensions related to rolling bearings and a horizontal ball screw of the longitudinal slide. The CT–WP interaction components at the stand-off distance b of CT from WP

where: **q** – vector of generalized coordinates, M – mass, S_{xy}, S_{yz}, S_{xz} – static moments; I_x, I_y, I_z – moments of inertia, D_{xy}, D_{yz}, D_{xz} – moments of deviation of the i^{th} rigid body in the $x_i y_i z_i$ coordinate system. An algorithm for computations of the geometric mass characteristics, developed in this study, is based on division of each rigid body into regular elements (rectangular and triangular plates, cubicoids, cylinders, etc.) and on Steiner's theorem. For V250, the B1 body was divided into 43 elements, B3 – into 6 elements, B4 – into 4 elements (see Figure 1). The B2 body was treated as a single cubicoid.

Four vibroisolation pads supported a V250 lathe; each of the pads is modelled as a set of three orthogonal Voigt constraints of stiffness values k_v^p, k_h^p and damping coefficients c_v^p, c_h^p, respectively in the vertical and horizontal directions. The longitudinal slide is guided by four rolling carriages; each of them is modelled as a set of two orthogonal Voigt constraints of stiffness values k_v^l, k_h^l and damping coefficients c_v^l, c_h^l. A longitudinal ball screw is modelled as a single horizontal constraint of parameters k_y^l, c_y^l. The cross slide is also guided by four rolling carriages; each of them is modelled as a set of two orthogonal constraints of parameters $k_v^c, k_h^c, c_v^c, c_h^c$. The cross ball screw, inclined at an angle of 35°, is modelled as a single constraint of parameters k_x^c, c_x^c. Rolling bearings of the spindle are reflected by two sets (3 + 2) of orthogonal constraints, located at the spindle axis, of parameters $k_v^s, k_h^s, k_y^s, c_v^s, c_h^s, c_y^s$. The driving belt is modelled as a single rotational constraint with respect to the spindle axis, of parameters k_φ^s, c_φ^s. Central points of constraints modelling flexible interfaces are marked in Figure 1 with symbol +.

The elastic strain energy and the damping power of V250 are expressed by square forms of the well-known general shapes, i.e. (e.g. [16])

$$E_p = \frac{1}{2}\mathbf{q}^{\mathrm{T}}\mathbf{K}\mathbf{q}, \quad \Phi = \frac{1}{2}\dot{\mathbf{q}}^{T}\mathbf{C}\dot{\mathbf{q}}\ , \tag{3}$$

where: **K** – stiffness matrix, **C** – damping matrix of a linear dynamic model of a machine tool. For V250 lathe one obtains the following final results:

$$\mathbf{K} = \begin{bmatrix} \mathbf{K}_{11}^p + \mathbf{K}_{11}^l + \mathbf{K}_{11}^s & \mathbf{K}_{12}^l & 0 & \mathbf{K}_{14}^s \\ & \mathbf{K}_{22}^l + \mathbf{K}_{22}^c & \mathbf{K}_{23}^c & 0 \\ & & \mathbf{K}_{33}^c & 0 \\ \text{symm.} & & & \mathbf{K}_{44}^s \end{bmatrix}, \tag{4}$$

with

$$
\begin{aligned}
&\mathbf{K}_{11}^{p} = \mathbf{A}_{p}^{T}\{\mathbf{k}\}_{p}\mathbf{A}_{p}, \quad \{\mathbf{k}\}_{p} = \operatorname{diag}\left(k_{h}^{p}, k_{h}^{p}, k_{v}^{p}, k_{h}^{p}, k_{h}^{p}, k_{v}^{p}, k_{h}^{p}, k_{h}^{p}, k_{v}^{p}, k_{h}^{p}, k_{h}^{p}, k_{v}^{p}\right),\\
&\begin{bmatrix} \mathbf{K}_{11}^{l} & \mathbf{K}_{12}^{l} \\ \mathbf{K}_{21}^{l} & \mathbf{K}_{22}^{l} \end{bmatrix} = \mathbf{A}_{l}^{T}\{\mathbf{k}\}_{l}\mathbf{A}_{l}, \quad \{\mathbf{k}\}_{l} = \operatorname{diag}\left(k_{v}^{l}, k_{h}^{l}, k_{v}^{l}, k_{h}^{l}, k_{v}^{l}, k_{h}^{l}, k_{v}^{l}, k_{h}^{l}, k_{y}^{l}\right),\\
&\begin{bmatrix} \mathbf{K}_{22}^{c} & \mathbf{K}_{23}^{c} \\ \mathbf{K}_{32}^{c} & \mathbf{K}_{33}^{c} \end{bmatrix} = \mathbf{A}_{c}^{T}\{\mathbf{k}\}_{c}\mathbf{A}_{c}, \quad \{\mathbf{k}\}_{c} = \operatorname{diag}\left(k_{v}^{c}, k_{h}^{c}, k_{v}^{c}, k_{h}^{c}, k_{v}^{c}, k_{h}^{c}, k_{v}^{c}, k_{h}^{c}, k_{x}^{c}\right),\\
&\begin{bmatrix} \mathbf{K}_{11}^{s} & \mathbf{K}_{14}^{s} \\ \mathbf{K}_{41}^{s} & \mathbf{K}_{44}^{s} \end{bmatrix} = \mathbf{A}_{s}^{T}\{\mathbf{k}\}_{s}\mathbf{A}_{s}, \quad \{\mathbf{k}\}_{s} = \operatorname{diag}\left(k^{s}, k^{s}, k_{y}^{s}, k^{s}, k^{s}, k_{\varphi}^{s}\right).
\end{aligned}
\tag{5}
$$

The superscripts p, l, c and s describe respective interfaces. The damping matrix $\mathbf{C}$ has a detailed form analogous to the stiffness matrix $\mathbf{K}$; letters $\mathbf{K}$, $\mathbf{k}$, k are then replaced with $\mathbf{C}$, $\mathbf{c}$, c in Equations (4), (5). Matrices $\mathbf{A}_p$, $\mathbf{A}_l$, $\mathbf{A}_c$, $\mathbf{A}_s$, determining transformations of the generalized coordinates into the local coordinates of constraints (shortenings/elongations) in respective interfaces, depend on detailed geometry of an MTRG. For example, matrix $\mathbf{A}_l$ for V250 has the form (see Figure 1):

$$
\mathbf{A}_{l} = \begin{bmatrix}
s & 0 & c & e_4 c & e_7 s - e_1 c & -e_4 s & 0 & 0 & -1 & d_4 & d_1 & 0 \\
c & 0 & -s & -e_4 s & e_7 c + e_1 s & -e_4 c & -1 & 0 & 0 & 0 & 0 & -d_4 \\
s & 0 & c & e_5 c & e_7 s - e_1 c & -e_5 s & 0 & 0 & -1 & -d_5 & d_1 & 0 \\
c & 0 & -s & -e_5 s & e_7 c + e_1 s & -e_5 c & -1 & 0 & 0 & 0 & 0 & d_5 \\
s & 0 & c & e_4 c & e_8 s - e_2 c & -e_4 s & 0 & 0 & -1 & d_4 & -d_2 & 0 \\
c & 0 & -s & -e_4 s & e_8 c + e_2 s & -e_4 c & -1 & 0 & 0 & 0 & 0 & -d_4 \\
s & 0 & c & e_5 c & e_8 s - e_2 c & -e_5 s & 0 & 0 & -1 & -d_5 & -d_2 & 0 \\
c & 0 & -s & -e_5 s & e_8 c + e_2 s & -e_5 c & -1 & 0 & 0 & 0 & 0 & d_5 \\
0 & 1 & 0 & e_9 & 0 & e_3 & 0 & -1 & 0 & 0 & 0 & -d_3
\end{bmatrix},
\tag{6}
$$

with

$$
\begin{aligned}
&s = \sin 35^{\circ}, \quad c = \cos 35^{\circ},\\
&d_1 = 163\,\text{mm}, \; d_2 = 187\,\text{mm}, \; d_3 = 13\,\text{mm},\\
&d_4 = 125\,\text{mm}, \; d_5 = 125\,\text{mm}, \; d_6 = 161\,\text{mm},\\
&e_1 = 400\,\text{mm}, \; e_2 = 108\,\text{mm}, \; e_3 = 268\,\text{mm},\\
&e_4 = 1047\,\text{mm} + a, \; e_5 = 1297\,\text{mm} + a, \; e_6 = 1011\,\text{mm} + a,\\
&e_7 = 862\,\text{mm}, \; e_8 = 1060\,\text{mm}, \; e_9 = 932\,\text{mm}.
\end{aligned}
$$

Position of the central point of a cutting edge of the CT is determined by two technological parameters: a – travel of a longitudinal slide, r – radius of machining. A parameter $b = 260$ mm $- r$ determines a cross travel required before starting machining (Figure 1).

4. Calculation of the main static and dynamic stiffnesses of an MTRG

A shape and dimensions of WP are designed, provided that travels of the longitudinal and cross slides are not affected by vibrations of the MTRG. In practice, machining is affected by displacement fluctuations resulting from the WP–CT relative vibrations. These fluctuations can be assessed with the main static and dynamic stiffnesses generally defined in Section 2.

During machining, there appears the WP–CT interaction which has three components (Figures 1 and 2). A circumferential force F_c is perpendicular to both WP and CT axes. A feed force F_f is parallel to WP axis and perpendicular to CT axis. A passive-pressure force F_p is perpendicular to WP axis and parallel to CT axis.

Let us introduce the forces P_v, P_h, P_r varying harmonically in the time t at a unit amplitude, coinciding with the respective components F_c, F_f, F_p of the WP–CT interaction. Then one can define the main translational/rotational relative compliances of WP with CT in the respective plane of action of the force, as shown in Figure 2. Dynamic stiffnesses are defined as reversals of those compliances, i.e.

$$T_v = \frac{P_v}{u_v}, \quad R_v = \frac{P_v}{\varphi_v}, \quad T_h = \frac{P_h}{u_h}, \quad R_h = \frac{P_h}{\varphi_h}, \quad T_r = \frac{P_r}{u_r}, \quad R_r = \frac{P_r}{\varphi_r}, \tag{7}$$

where T_v, T_h, T_r [N/μm] – main translational stiffnesses; R_v, R_h, R_r [N/μrad] – main translational–rotational stiffnesses in the WP–CT area; P_v=1, P_h=1, P_r=1 – amplitudes of harmonic forces with physic excitation frequency $f=\omega/2\pi$; u_v, u_h, u_r [μm], φ_v, φ_h, φ_r [μrad] – amplitudes of steady-state responses of the MTRG to the loads

$$P_v(t) = P_v \sin \omega t, \quad P_h(t) = P_h \sin \omega t, \quad P_r(t) = P_r \sin \omega t, \tag{8}$$

respectively.

The steady-state dynamic response of the MTRG to each harmonic component of the WP–CT interaction, i.e.

$$\mathbf{q}(t) = \mathbf{q}_s \sin \omega t + \mathbf{q}_c \cos \omega t, \tag{9}$$

is determined from a well-known system of algebraic equations (e.g. [16])

$$\begin{bmatrix} \mathbf{K} - \omega^2 \mathbf{B} & -\omega \mathbf{C} \\ \omega \mathbf{C} & \mathbf{K} - \omega^2 \mathbf{B} \end{bmatrix} \begin{bmatrix} \mathbf{q}_s \\ \mathbf{q}_c \end{bmatrix} = \begin{bmatrix} \mathbf{F}_s \\ \mathbf{0} \end{bmatrix}, \tag{10}$$

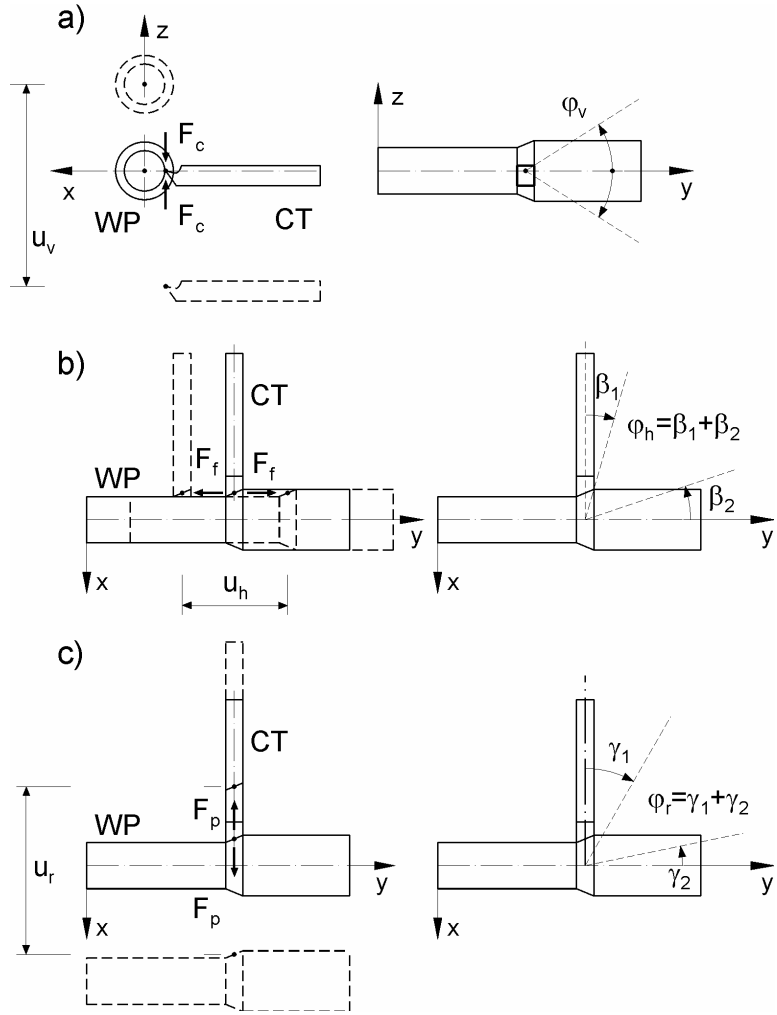

Fig. 2. The main relative displacements for circumferential, feed and passive-pressure components of the CT–WP interaction

where for V250 (see Figures 1 and 2) we have:

$$
\begin{aligned}
&\mathbf{F}_s = \mathrm{col}\left(\mathbf{0},\mathbf{0},\mathbf{F}_3,\mathbf{F}_4\right),\\
&\mathbf{F}_3 = P_v \cdot \mathrm{col}\left(0,0,-1,a_2,a_1,0\right), \quad \mathbf{F}_4 = P_v \cdot \mathrm{col}\left(0,0,1,a_4,r,0\right),\\
&\mathbf{F}_3 = P_h \cdot \mathrm{col}\left(0,-1,0,a_3,0,-a_1\right), \quad \mathbf{F}_4 = P_h \cdot \mathrm{col}\left(0,1,0,0,0,-r\right),\\
&\mathbf{F}_3 = P_r \cdot \mathrm{col}\left(-1,0,0,0,-a_3,-a_2\right), \quad \mathbf{F}_4 = P_r \cdot \mathrm{col}\left(1,0,0,0,0,-a_4\right),\\
&a_1 = 218\,\mathrm{mm}, \quad a_2 = 261\,\mathrm{mm}, \quad a_3 = 107\,\mathrm{mm}, \quad a_4 = 511\,\mathrm{mm} + a.
\end{aligned}
\tag{11}
$$

For V250 lathe, the main relative translations and rotations in the WP–CT area are calculated from the following formulae (see Figures 1 and 2)

$$\begin{aligned}
u_v(t) &= u_{vs}\sin\omega t + u_{vc}\cos\omega t = q_{34} + a_4 q_{44} - q_{33} + a_2 q_{43} + a_1 q_{53},\\
\varphi_v(t) &= \varphi_{vs}\sin\omega t + \varphi_{vc}\cos\omega t = q_{43} - q_{44},\\
u_h(t) &= u_{hs}\sin\omega t + u_{hc}\cos\omega t = q_{24} - rq_{64} - q_{23} + a_3 q_{43} - a_1 q_{63},\\
\varphi_h(t) &= \varphi_{hs}\sin\omega t + \varphi_{hc}\cos\omega t = q_{64} - q_{63},\\
u_r(t) &= u_{rs}\sin\omega t + u_{rc}\cos\omega t = q_{14} - a_4 q_{64} - q_{13} - a_3 q_{53} - a_2 q_{63},\\
\varphi_r(t) &= \varphi_{rs}\sin\omega t + \varphi_{rc}\cos\omega t = q_{64} - q_{63}.
\end{aligned} \tag{12}$$

For $f = 0$ one obtains the main static stiffnesses in the WP–CT area, with the generalized coordinates computed as a solution of a well-known system of algebraic equations, i.e.

$$\mathbf{Kq} = \mathbf{F}_s\,. \tag{13}$$

5. Numerical analysis and conclusions

Taking into account the approximate method for dynamic modelling of an MTRG developed in this study, a computer algorithm has been formulated for calculating the main static and dynamic stiffnesses of a VENUS 250 NC lathe. Subassemblies B1, B2, B3, B4 have been divided into regular rigid elements using a 3D CAD conceptual model of the MTRG [15]. Values of stiffness and damping coefficients of the interfaces, taken from the catalogues [17–19] or estimated from the experiments [20, 21], equal

$$\begin{aligned}
&k_v^p = 121 \text{ MN/m}, \quad k_h^p = 40.3 \text{ MN/m}, \quad c_v^p = 118 \text{ kNs/m}, \quad c_h^p = 68.4 \text{ kNs/m},\\
&k_v^l = k_v^c = 1100 \text{ MN/m}, \quad k_h^l = k_h^c = 637 \text{ MN/m}, \quad k_y^l = 970 \text{ MN/m}, \quad k_x^c = 900 \text{ MN/m},\\
&c_v^l = c_v^c = 32.6 \text{ kNs/m}, \quad c_h^l = c_h^c = 24.8 \text{ kNs/m}, \quad c_y^l = 38.2 \text{ kNs/m}, \quad c_x^c = 16.2 \text{ kNs/m},\\
&k^h = 685 \text{ MN/m}, \quad k_y^h = 1020 \text{ MN/m}, \quad k_\varphi^h = 891 \text{ Nm/rad},\\
&c^h = 2.6 \text{ kNs/m}, \quad c_y^h = 4.5 \text{ kNs/m}, \quad c_\varphi^h = 0.597 \text{ Nms/rad}.
\end{aligned}$$

A rotational service velocity of the spindle equals 30–4500 rot/min yielding physic service frequency of 0.5–75 Hz. The main dynamic stiffnesses, derived in a physic frequency interval f ranging from 1 to 400 Hz, are drawn in Figures 3–8. Higher frequencies are observed only for theoretical recognition. The horizontal lines represent the main static stiffnesses, while the vertical lines are located at the natural frequencies of V250. The dynamic stiffnesses were computed for technological parameters a = 400 mm, r = 125 mm.

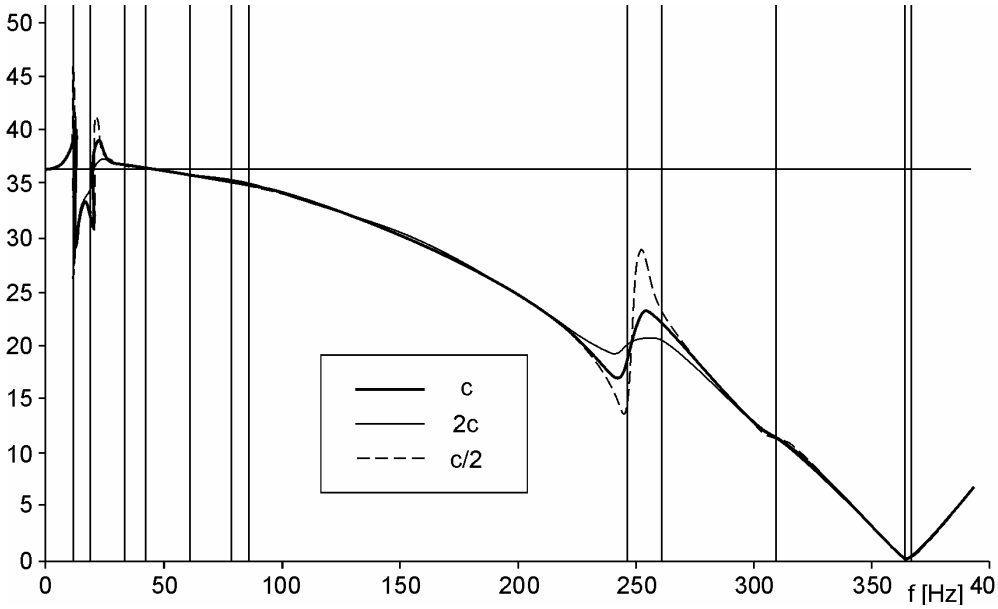

Fig. 3. The VENUS 250 NC lathe. The translational stiffness T_v [N/μm] versus the frequency f

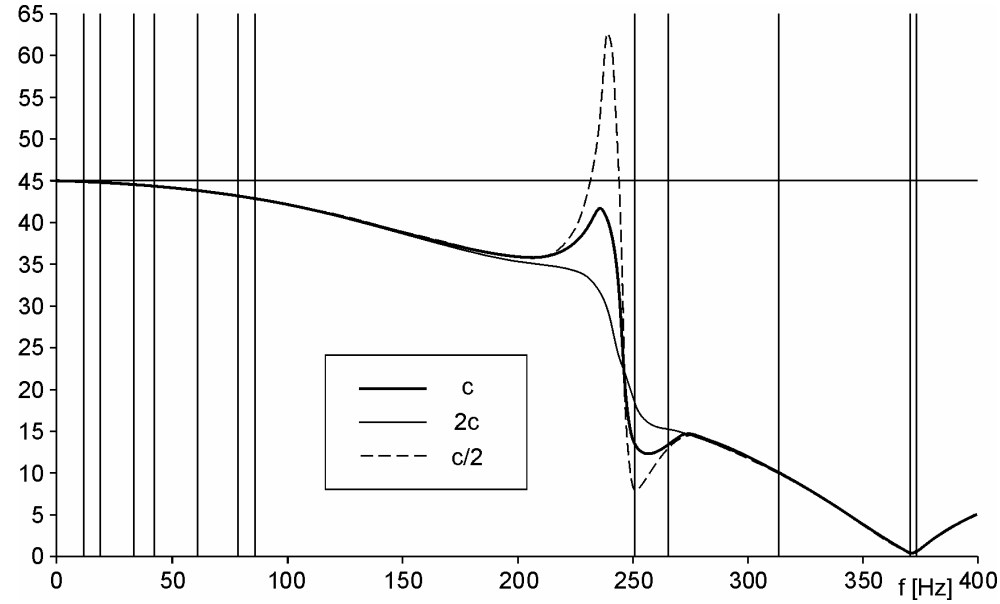

Fig. 4. The VENUS 250 NC lathe. The translational–rotational stiffness R_v [N/μrad] versus the frequency f

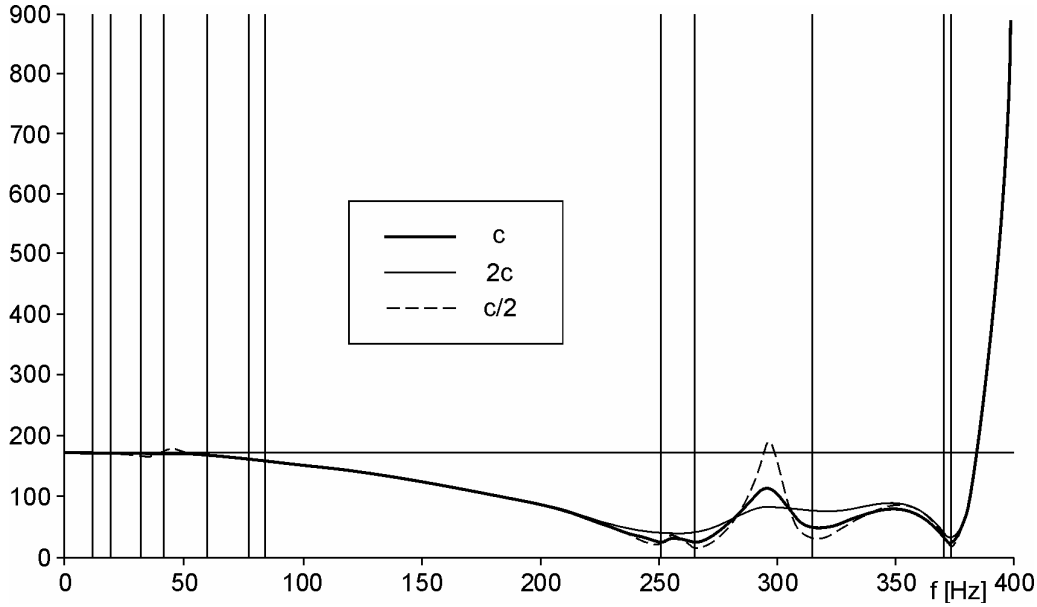

Fig. 5. The VENUS 250 NC lathe. The translational stiffness T_h [N/μm] versus the frequency f

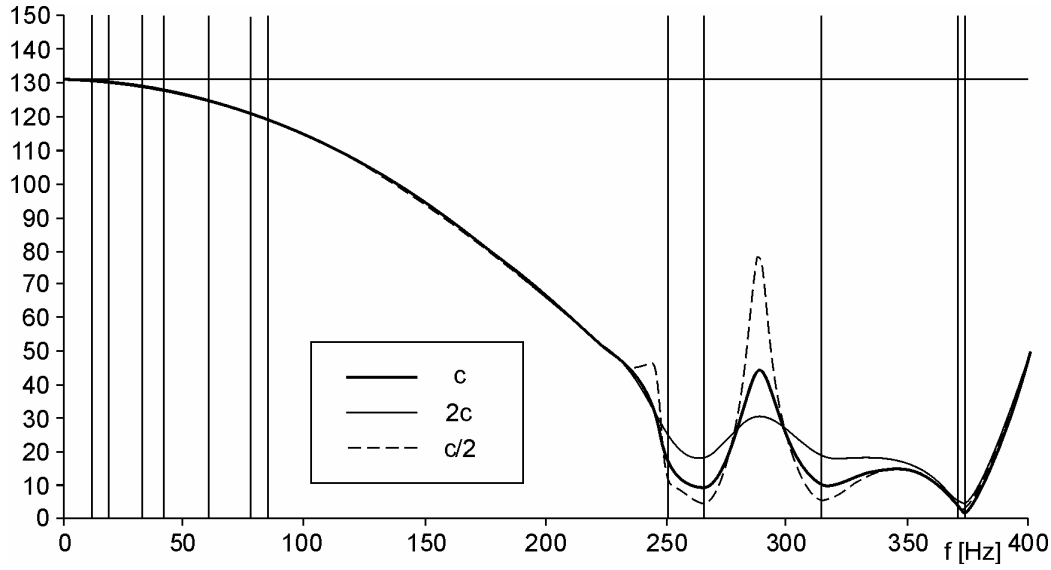

Fig. 6. The VENUS 250 NC lathe. The translational–rotational stiffness R_h [N/μrad] versus the frequency f

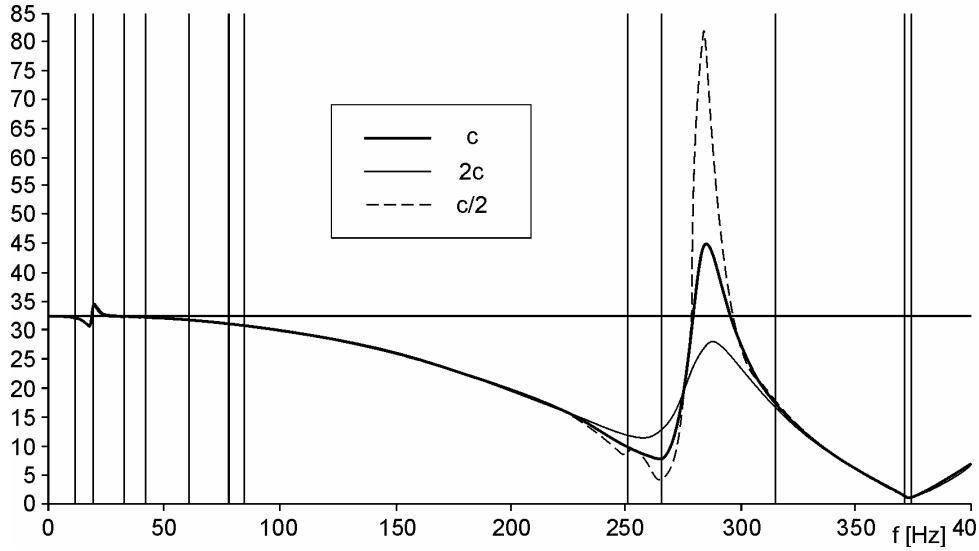

Fig. 7. The VENUS 250 NC lathe. The translational stiffness T_r [N/μm] versus the frequency f

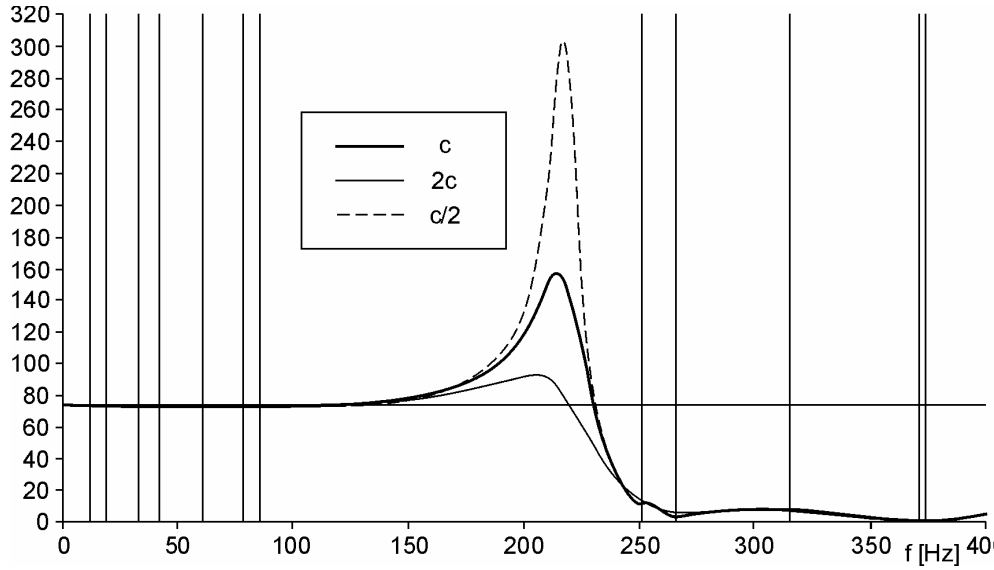

Fig. 8. The VENUS 250 NC lathe. The translational–rotational stiffness R_r [N/μrad] versus frequency f

Since damping coefficients have only approximate values, the dynamic stiffness–frequency diagrams are derived for three levels of damping: 1) the main values of damping set up in this point (solid thick line), 2) the main values increased twice (solid thin line), 3) the main values decreased twice (broken thin line).

Solving the eigenproblem, one obtains the first modal system of the MTRG dominated by torsional vibrations of the spindle. The next six modal systems describe global vibrations of the MTRG resulting from vibroisolation pads' deformations. The next modal systems exhibit relative vibrations of the sub-assemblies of V250.

The main dynamic stiffnesses are practically independent of a damping level outside the resonance zones. As expected, in the forced resonance zones, dynamic stiffnesses are substantially affected by damping.

The results for frequencies >350 Hz are unacceptable from a practical point of view, since dynamic stiffnesses are close to zero. This results from the simplifications of the dynamic model of the machine as well as from too light damping at higher frequencies.

The method developed in this study is useful and effective for predicting static and dynamic behaviour of a machine tool with rolling guideways, for service excitation frequencies. This method, applied at the stage of a conceptual design, results in a low-cost and short-time design of an MTRG. However, the use of this method in practice should be proceeded by appropriate validation experiments.

The method presented in this study can be easily generalized and extended to selected types of reconfigurable/modular machine tools with rolling guideways.

References

[1] *Study and definition of the machining workstation reference architecture (MAREA)*, Project No. BE-5624, Project Coordinator: WTCM/CRIF, Mech. Eng., Synthesis Report, Leuven, Belgium, 1995.

[2] Toenshoff H.K., Mey M., Schunelle A.: *An approach for the concurrent development and manufacturing of modular machine tools*, Production Engineering, 1998, Vol. 5, No. 1, 63–66.

[3] *Modular synthesis of advanced machine tools (MOSYN)*, Project No. BE95-1532, Project Coordinator: IFW, Synthesis Report, Hannover, Germany, 1998.

[4] Zatarain M., Lejarni E., Eyana F.: *Modular synthesis of advanced machine tools*, Annals of the CIRP, 1998, Vol. 17, No.1, 333–336.

[5] Nemeth I., Fisette P., Van-Brussel H.: *Conceptual design of 3-axis machine tools*, Proc. 32nd CIRP Int. Sem. on Manufacturing Systems, Leuven, Belgium, 1999, pp. 239–248.

[6] Grudziński K., Zapłata M.: *Badania ruchu ślizgowego w zespole napędowo-posuwowym obrabiarki metodą symulacji komputerowej*, Postępy Technologii Maszyn i Urządzeń, 1992, Z. 1, 3–26.

[7] Jastrzębski D., Szwengier G.: A*naliza statycznych właściwości układów nośnych obrabiarek hybrydowa metodą elementów skończonych*, Postępy Technologii Maszyn i Urządzeń, 1993, Nr 2, 21–41.

[8] Bodnar A., Schütte O.: P*roblems of experimental determination of static properties of machine tool units supported by rolling guides*, Advances in Technology of Machines and Mechanical Equipment, 2000, Vol. 24, No. 3, 1–11.

[9] Konowalski K.: *Experimental examinations of contact deflections in the rolling elements of slideway connections*, Annals of DAAAM for 2000 & Proc. 11th Int. DAAAM Symposium, pp. 233–234.
[10] Skoczyński W., Krzyżanowski J.: *Some aspects of machine tool properties evaluation*, Conf. on Modern Trends in Manufacturing, Wrocław, 2002, pp. 217–238.
[11] Moon Y., Kota S.: *Generalized kinematic modelling method for reconfigurable machine tools*, MECH/5946, Proc. 25th Biannual Mechanism Design Conference, Atlanta (CA, USA), 1998, pp. 1–12.
[12] Moon Y., Kota S.: *A methodology for automated design of reconfigurable machine tools*, Proc. 32nd CIRP Int. Sem. on Manufacturing Systems, Leuven, Belgium, 1999, pp. 297–303.
[13] Marchelek K.: *Dynamika obrabiarek*, WNT, Warszawa, 1991.
[14] Wrotny L.: *Podstawy konstrukcji obrabiarek*, WNT, Warszawa, 1973.
[15] *VENUS 250 NC lathe, Conceptual Project* (in Polish), Centre of Machine Tool Design and Research, CBKO-Pruszków, Poland, 1997.
[16] Langer J.: *Dynamics of Structures* (in Polish), WPWr Press, Wrocław, 1980.
[17] *INA Linear Guidance Systems*, LIF Publ., Homburg, 2000.
[18] *Technical Manual for Optibelt – RB Ribbed Belt Drives*, Hoexter, Germany.
[19] *Vibroisolation pads*, Bilz Schwingungstechnik GmbH, Loenberg, Germany, 2002.
[20] *Experimental investigations of a prototype of VENUS 250 NC lathe* (in Polish), Center of Machine Tool Design and Research, CBKO-Pruszków, Poland, 1998.
[21] Śniegulska D., Klasztorny M., Szafarczyk M.: *Identification of stiffness and damping of rolling guidance systems in machine tools*, Proc. 2nd Int. Conf. in Advances in Production Engineering, Warsaw (Poland), 2001, Vol. 2, pp. 373–382.

Przybliżona metoda wyznaczania sztywności statycznych i dynamicznych obrabiarek z prowadnicami tocznymi

W pracy rozwinięto komputerowo wspomagane projektowanie obrabiarek przekształcalnych i modularnych z prowadnicami tocznymi na etapie projektu wstępnego. Aby ocenić właściwości statyczne i dynamiczne możliwych konfiguracji maszyny, zaproponowano zbiór głównych sztywności statycznych i dynamicznych w obszarze narzędzie–przedmiot obrabiany. Sztywności te są rozumiane jako odwrotności głównych podatności względnych między narzędziem a przedmiotem obrabianym, odpowiednio w warunkach statycznych i dynamicznych. Obrabiarka jest modelowana jako układ wielu ciał sztywnych połączonych ze sobą i z podłożem liniowymi więziami lepkosprężystymi. Sztywności statyczne i dynamiczne wyznaczono dla sił skupionych przyłożonych zgodnie z obwodową, posuwową i odporową składową interakcji narzędzie–przedmiot obrabiany. Opracowano i zaprogramowano komputerowy algorytm wyznaczania tych sztywności. Przybliżone modelowanie obrabiarek zostało przeprowadzone w odniesieniu do tokarki VENUS 250 sterowanej numerycznie, zaprojektowanej i produkowanej przez Centrum Badawczo-Konstrukcyjne Obrabiarek w Pruszkowie. Wyniki obliczeń przedstawiono w postaci wykresów sztywności dynamicznych w funkcji częstotliwości wzbudzania.

ARCHIVES OF CIVIL AND MECHANICAL ENGINEERING

Vol. IV 2004 No. 2

Dynamic load tests in bridge management

J. BIEŃ, J. KRZYŻANOWSKI, P. RAWA, J. ZWOLSKI
Wrocław University of Technology, Wybrzeże Wyspiańskiego 27, 50-370 Wrocław

The potential application of dynamic test results in the bridge management process is considered. The classification of the bridge dynamic tests, based on the method of vibration excitation, is proposed and four main types of tests are distinguished: excitation by traffic, by special vehicles, by force-generating devices and by means of special techniques. All testing methods are illustrated by examples of the tests performed by the authors. Special attention is paid to the possibilities of damage detection by means of monitoring the bridge dynamic parameters. Advantages and disadvantages of the testing methods presented are discussed taking into account their usefulness in the computer-based Bridge Management Systems.

Keywords: *bridges, dynamic tests, Bridge Management Systems*

1. Introduction

Bridge structures are exposed to various dynamic loads, e.g. moving live loads, time-varying wind loads, etc. The dynamic effects are taken into account while designing bridges and play an important role in the whole life of the structures. The results of the experimental dynamic analysis carried out for many years offer valuable information, e.g. [1–6], for comprehensive bridge management. The main methods of dynamic bridge testing and their potential applications in the computer-based Bridge Management Systems are presented in Figure 1. Two basic types of bridge dynamic tests can be distinguished in the classification proposed: structure dynamic response tests and structure vibration tests.

Dynamic response tests are performed to obtain dynamic characteristics of the bridges under normal traffic or under special vehicles with controlled parameters. These types of tests enable the determination of the following parameters:

- stresses and strains in the bridge components – the basic data for fatigue analysis;
- a dynamic load factor (dynamic load allowance) – a measure of bridge dynamic sensitivity;
- vibration frequencies, mode shapes, vibration amplitude and damping under the live loads.

In the vibration tests, special force-generating devices or other special techniques are used for the excitation of the bridge vibration. The main goals of this kind of test are as follows:

- the determination of the natural frequencies of bridge vibration,

• the identification of the corresponding mode shapes, amplitudes and damping characteristics of the structure.

The results of both types of dynamic tests include very important information, which can be used as tools supporting selected elements of the bridge management process (Figure 1):

• the fatigue analysis based on experimental data;

• the analysis of bridge serviceability taking into account the users comfort (vibration frequency, amplitude, acceleration, possibility of resonance occurrence, etc.);

• the stiffness analysis (displacements under traffic loads, experimental verification of theoretical models, etc.);

• the detection of bridge damages based on the identification of changes in structure dynamic characteristic;

• monitoring of forces in cables (e.g. in cable-stayed bridges) or in other external prestressing tendons.

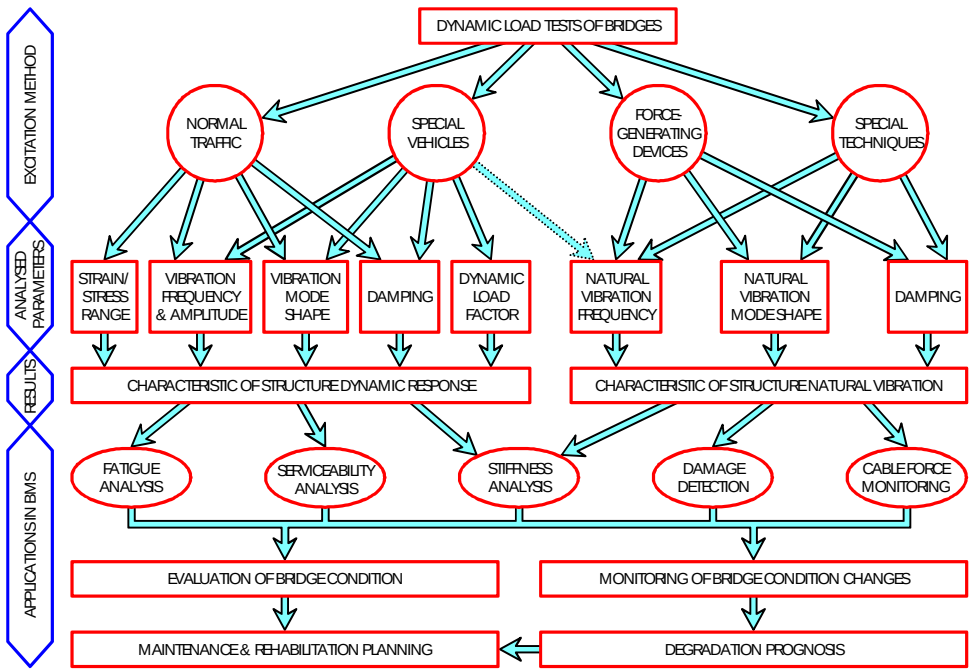

Fig. 1. Dynamic load tests of bridges and their applications in BMS

The characteristics of the bridge dynamic response and bridge natural vibration, based on the results of experimental tests, can be applied to:

• the evaluation of the bridge condition (conformity with designed dynamic parameters, serviceability, dynamic sensitivity, etc.);

• monitoring the bridge condition based on the systematic control of structure dynamic parameters;

• updating the degradation model of the bridge structure;

• the optimization of the planning process in the Bridge Management Systems.

Each of the testing methods considered has specific advantages and disadvantages, which are discussed below based on the examples of the tests performed by the authors.

2. Dynamic tests under traffic

Dynamic tests under normal road or railway traffic are performed to identify the dynamic response of the bridge structure to real live loads, e.g. [2]. This type of dynamic tests has the following main characteristics:

• random nature of loads during the test;

• the vibrating mass of the structure is increased by the mass of the vehicles on the bridge and the dynamic parameters are determined for such a system;

• vehicles are continuously moving along the bridge, which complicates the identification of the vibration forms;

• tests can be performed without any disturbances in the normal operation of the bridge.

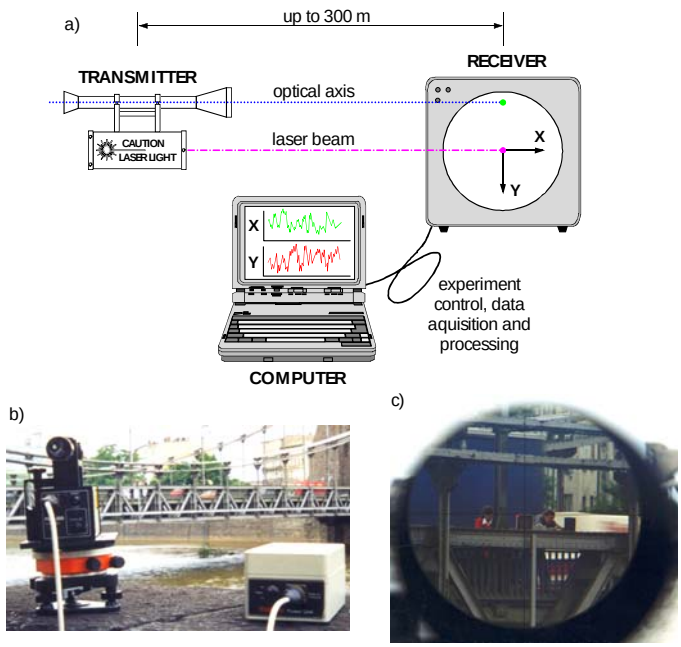

Fig. 2. Laser-based displacement measuring system: a) configuration, b) transmitter on the riverside, c) receiver located on the bridge tested

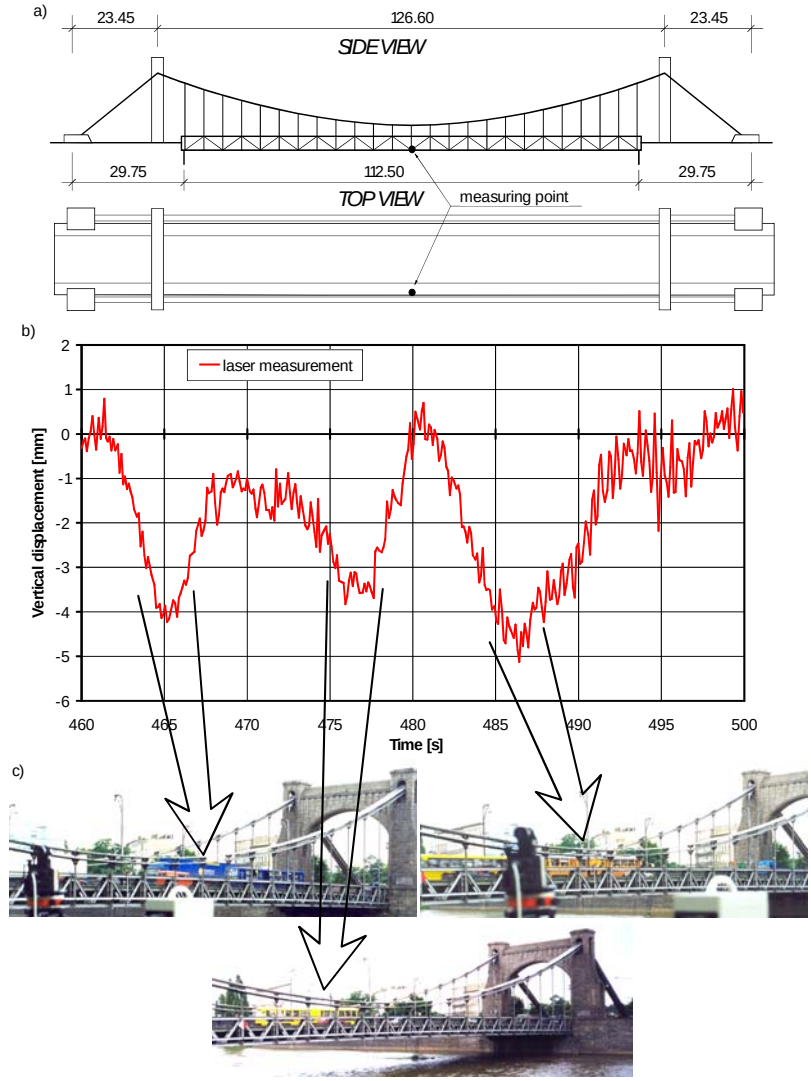

Fig. 3. Vibrations of the Grunwaldzki Bridge over the Odra River in Wrocław: a) bridge scheme and location of measuring point, b) vertical displacements under traffic, c) loads in the selected moments of the test

An example of the monitoring of suspension bridge vibration under road traffic is presented in Figure 2 and Figure 3. Laser-based measuring system applied in this test [7, 8] consists of the laser transmitter and the position-sensitive receiver connected to a laptop computer (Figure 2a). The laser transmitter is placed on a solid base outside the bridge in the distance up to 300 m (Figure 2b) and the receiver is located on the bridge tested (Figure 2c).

The position of the laser beam on the sensitive screen is continuously recorded in two-dimensional space. Vertical displacements of the measuring point in the middle of the span (Figure 3a) are presented in Figure 3b. The measuring system has been coupled with a camera, which enables the identification of the loads configuration during the test (Figure 3c).

3. Dynamic tests by means of special vehicles

In many countries, dynamic tests under special vehicles are standard proof load tests before opening the bridge for use. Heavy trucks or locomotives with controlled parameters (axle loads, geometry, speed, etc.) are usually used as dynamic loads, e.g. [5, 9, 10, 11]. The most important conditions of this type of test are as follows:

- the main parameters of the dynamic loads are known and can be controlled;
- the vibrating mass of the bridge is influenced by the moving mass of the vehicle (vehicles);
- the moving vehicles complicate the identification of the vibration forms;
- tests have to be performed without any other dynamic loads of the bridge.

Fig. 4. Arch viaduct A016 over the highway A4 during load tests

The results of the tests of the arch viaduct A016 [11] over the highway A4 (Figure 4) are presented as an example. Vertical displacements of the measuring points *A* and *B*, located on both sides of the deck in the middle of the span, are shown in Figure 5. The results of the test with normal plain road surface are presented in Figure 5a and displacements during test with artificial "bump" (height of 3 cm) – in Figure 5b.

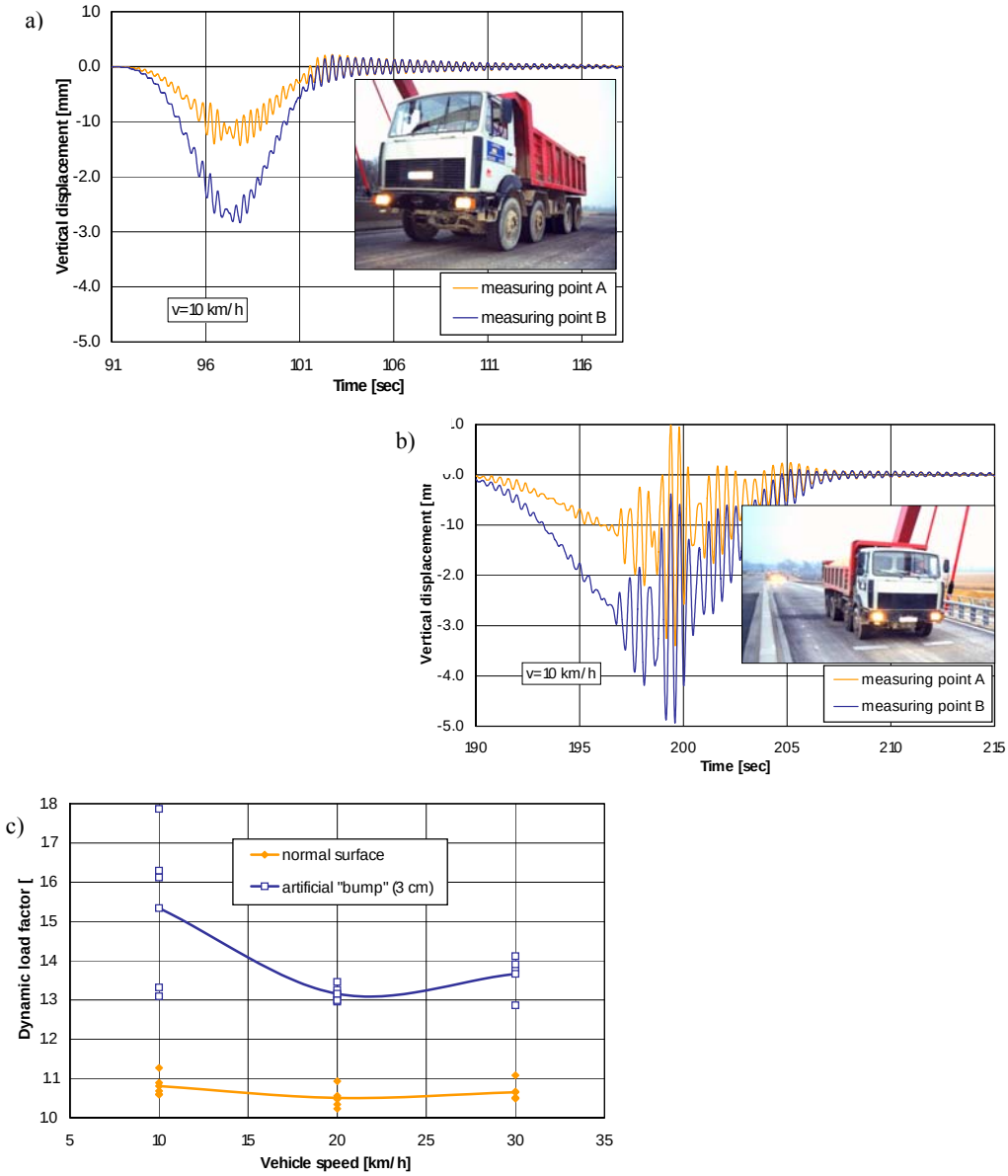

Fig. 5. Dynamic load tests of the viaduct A016 under special vehicle: a) vertical displacement of the deck – test with normal road surface, b) vertical displacement of the deck – test with artificial "bump" (height of 3 cm), c) dynamic load factors for various speeds of vehicle

Dynamic load factors for various speed of the truck – based on the experimental data – are presented in Figure 5c. Five trucks of the same type and the same parameters (axle loads, geometry) were used for each test. Differences within the same test

are probably caused by the various technical conditions of the vehicles. Higher dynamic load factors during "bump" tests show the sensitivity of the structure to the damages of the road surface (e.g. pot holes).

4. Vibration tests using periodic excitation

Vibration tests are conducted mainly by means of force-generating devices, e.g. [1, 4, 12]. The application of a mechanical vibration exciter enables:

- controlling the frequency of the excitation force;
- a free selection of the excitation force location on the structure tested;
- an identification of the resonance frequency while scanning the wide range of the excitation frequencies (mass of the force-generating device can be neglected);
- keeping the structure tested in a steady-state under defined conditions of excitation, including resonant vibration;
- repeatability of the excitation parameters, even after a long time;
- easy transport of the set-up for test execution and short time of disturbances in the traffic during the test.

In last few years, two types of the force-generating devices were constructed and tested at the Institute of Production Engineering and Automation and the Institute of Civil Engineering of the Wrocław University of Technology [6, 13]:

1. Vibration exciter based on the rotation of the unbalanced masses for the frequency between 0 and 15 Hz.
2. Inertial exciter for lower frequencies, between 0 and 5 Hz.

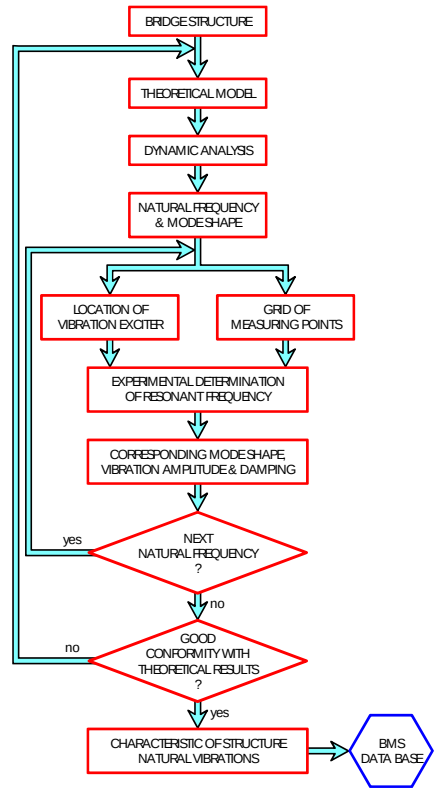

Fig. 6. Procedure of bridge initial testing by means of the vibration exciter

Up to now twelve various types of bridge structures have been tested by means of the exciters. Taking into account accumulated experience, two procedures of the bridge vibration tests have been proposed: preliminary test used for new bridges and monitoring test for bridge structures under operation.

The proposed procedure of initial testing of a new or rehabilitated bridge by means of the vibration exciter is presented in Figure 6. The main steps of the test are ex-

plained by the example of the footbridge B027 [12] shown in Figure 7. They are as follows:

- a theoretical analysis of the structure (FEM) to define natural vibration frequencies and the corresponding mode shapes;
- the determination of the most effective position of the vibration exciter on the tested bridge and selection of the measuring points;
- experimental detection of the resonance frequencies and measurement of the corresponding dynamic parameters; vertical displacements of the bridge deck are presented in Figure 8a and the results of the frequency analysis for excitation frequency of 4.27 Hz – in Figure 8b;
- the comparison of the experimental and theoretical data and storing the dynamic parameters of the structure in a computer-based BMS as a basis for the future tests.

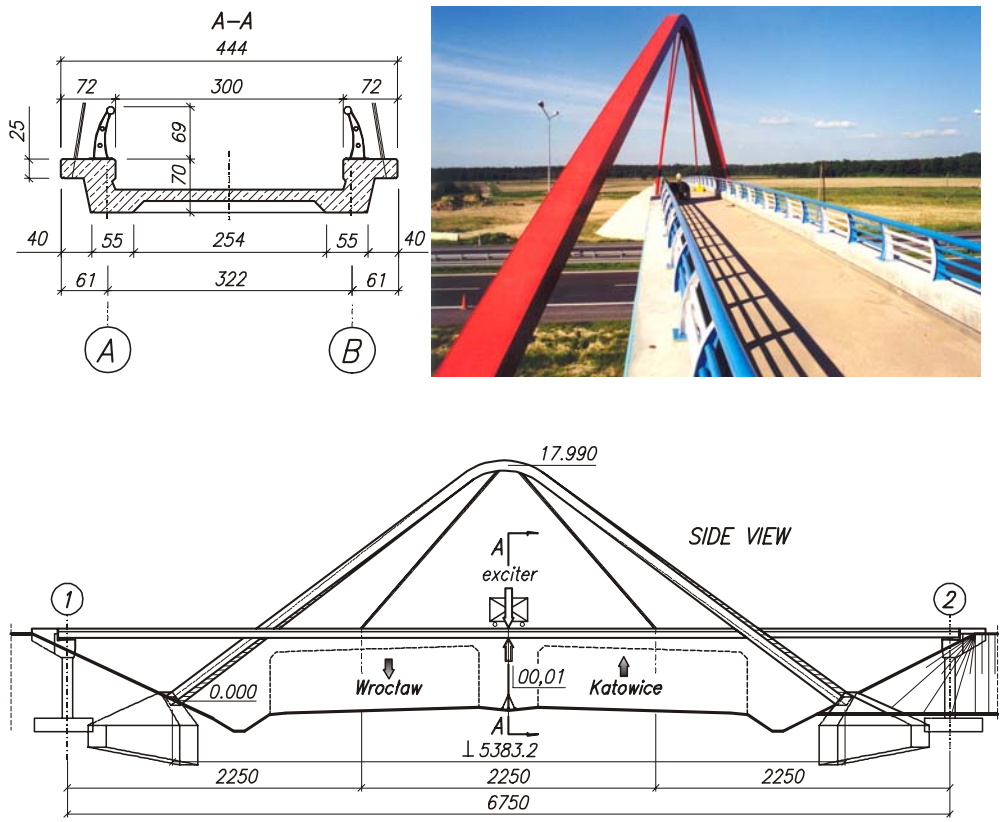

Fig. 7. The footbridge B027 tested over the highway A4

-

The vibration tests are especially useful for monitoring of bridge condition. The systematic control of changes in the dynamic parameters enables detection of bridge condition changes. The testing procedure proposed is presented in Figure 9. The procedure is illustrated by the destructive test of the composite bridge D010 on the highway A4, shown in Figure 10.

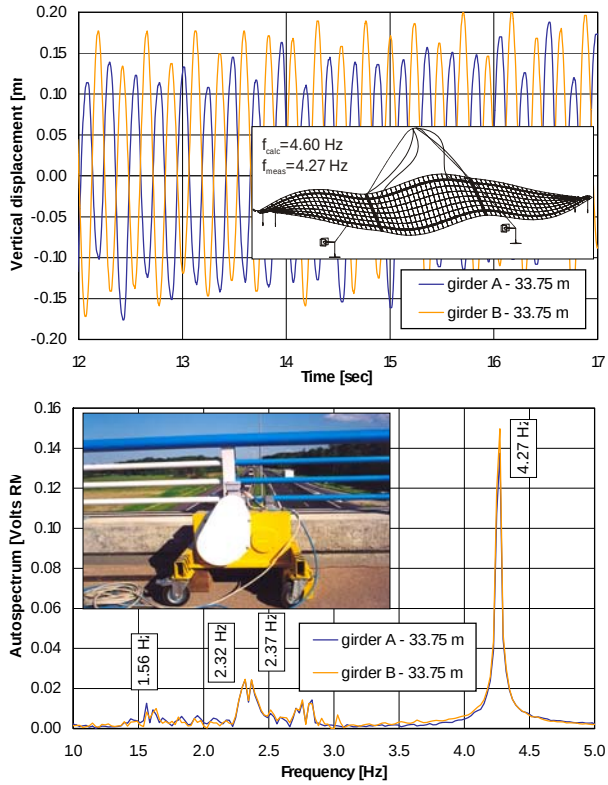

Fig. 8. Vibration test of the footbridge B027: a) vertical displacement of the deck and the calculated and measured vibration frequency and mode shape, b) vibration exciter on the tested structure and the results of the frequency analysis

In the first step, the bridge has been tested according to the procedure presented in Figure 6 to define the dynamic characteristic of the structure without damages. In the next step, one of the steel girders has been cut (Figure 11a) and the vibration tests have been conducted in the following sequence for each level of damage severity:

- the excitation of the bridge with the resonant frequency determined for the structure without damages;
- the determination of changes in vibration amplitude and mode shape due to the damages introduced;
- the determination of changes in the resonant frequency of the damaged structure;

• the measurement of the vibration amplitude and mode shape for new resonant frequency of the bridge.

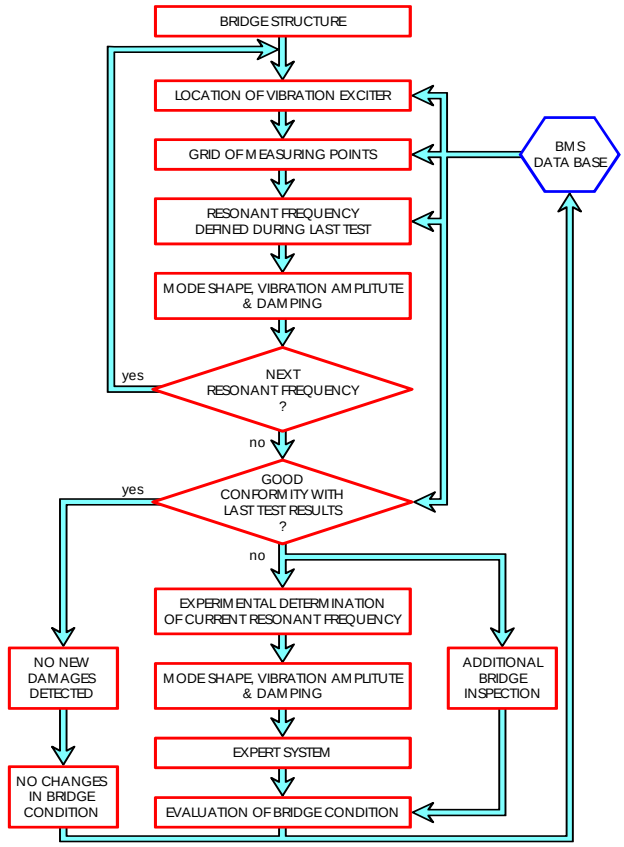

Fig. 9. Procedure of bridge condition monitoring by means of the vibration exciter

The damages affect the amplitude of the bridge vibrations. Figure 11b presents the relationship between the severity of the damage (diminishing of the span stiffness) and the amplitude of vibrations. The results presented have been obtained for constant frequency of excitation and equal resonant frequency of the structure without damages. Amplitude of 0.25 mm for the structure without any damages diminished to 0.16 mm and to 0.04 mm for 12.7% and 19.5% stiffness reduction, respectively.

Changes of the resonant frequencies for two levels of reduction of the span bending stiffness are presented in Figure 11c. For the structure without any damages the frequency is 12.12 Hz and diminishes to 11.77 Hz (in the case of 12.7% stiffness reduction) and to 11.07 Hz for 19.5% stiffness reduction.

The analysis of the test results shows that vibration amplitude of the structure tested is more sensitive to the damages considered than the resonant frequency.

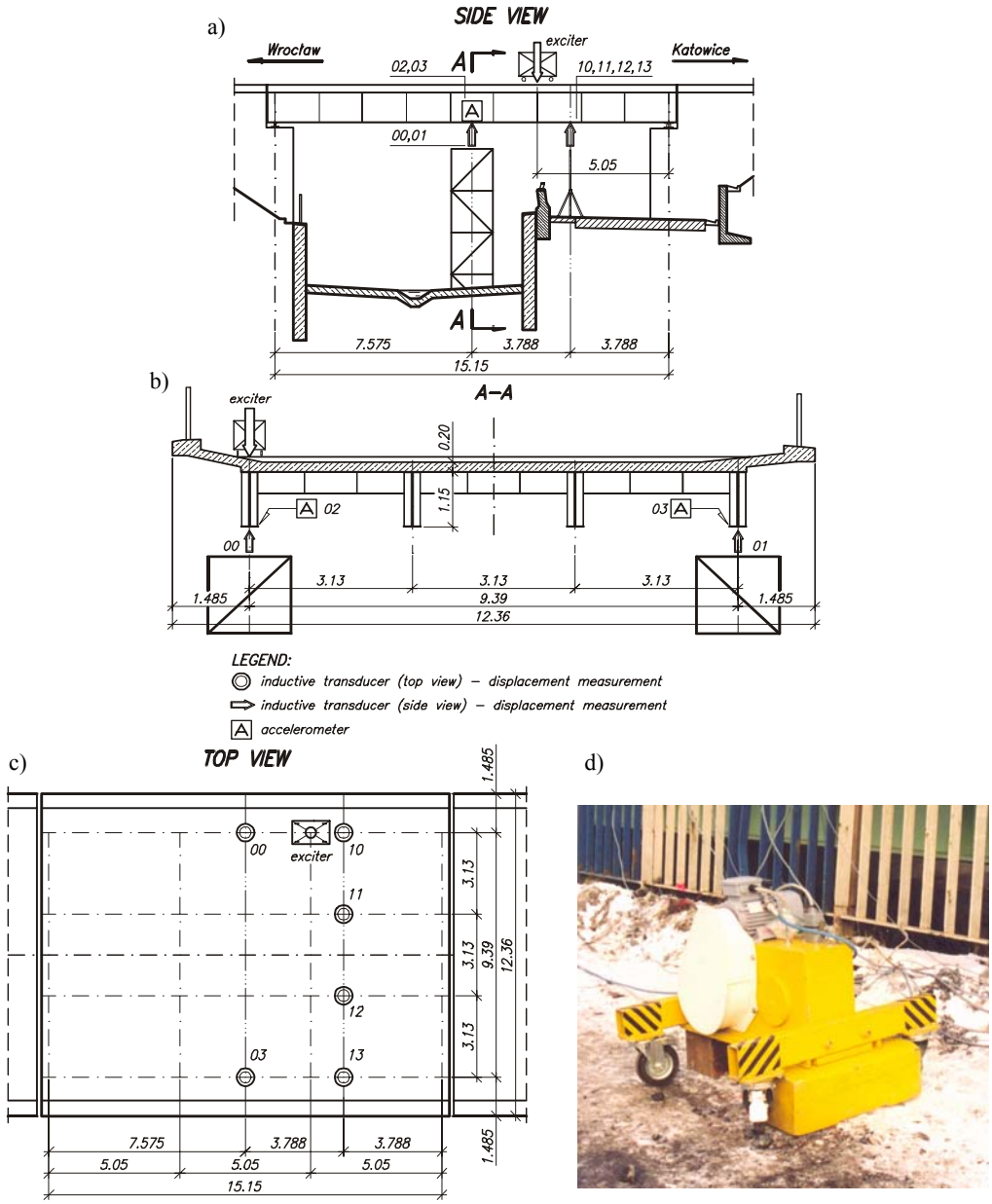

Fig. 10. Bridge D010 on the highway A4: a) side view, b) cross-section A-A, c) top view, d) vibration exciter on the bridge deck

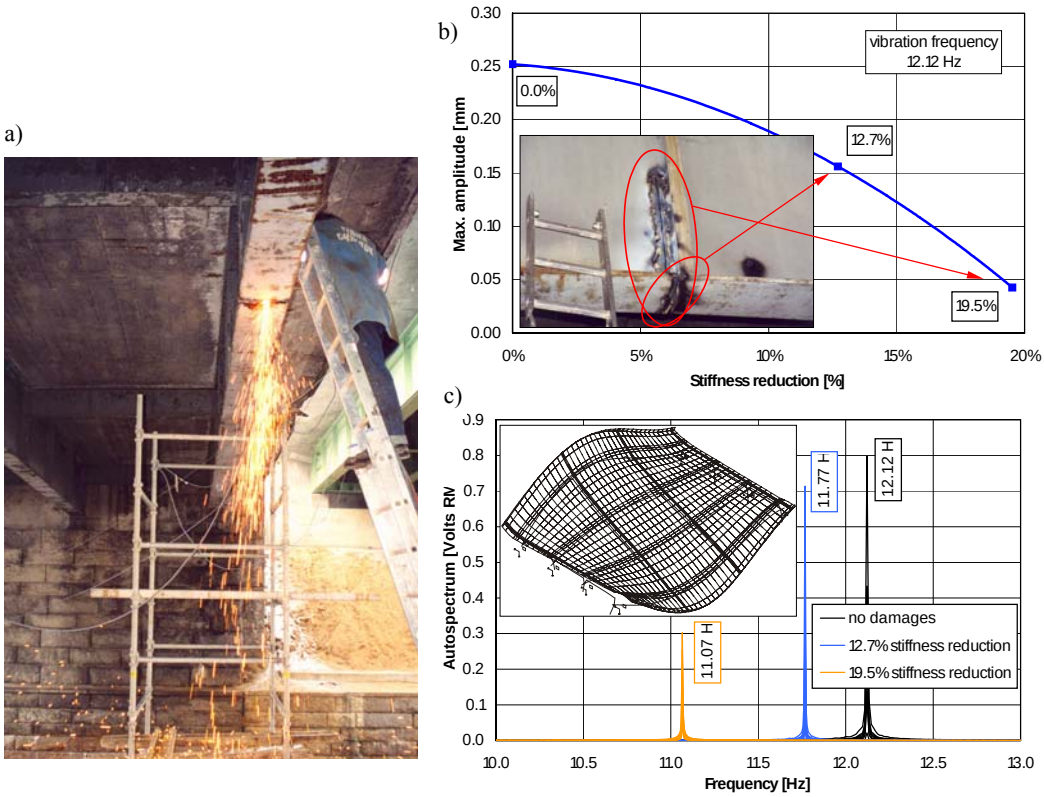

Fig. 11. Destructive test of the bridge D010: a) cutting of the steel girder, b) changes of the vibration amplitude as a function of bending stiffness diminishing, c) changes of the resonance frequency due to reduction of span stiffness for the vibration form shown

5. Special techniques in dynamic testing

Sometimes individual requirements of the bridge test need the application of a special technique of structure excitation. The excitation force, usually of the impulse nature, can be produced by:

- a sudden release of the deflection applied,
- stopping of heavy vehicle,
- dropping a mass on the structure tested, etc.

Special excitation methods can be, for instance, effectively applied in controlling the internal forces in the cables of the cable-stayed bridges. As an example, the selected results of the tests of the Świętokrzyski Bridge over the Vistula River in Warsaw (Figure 12a) are presented. The sudden release of the deflection of the cable (Figure 12b) was used for the vibration excitation. Free vibrations of the tendon tested were measured by means of the set of accelerometers placed on the cable (Figure 12b).

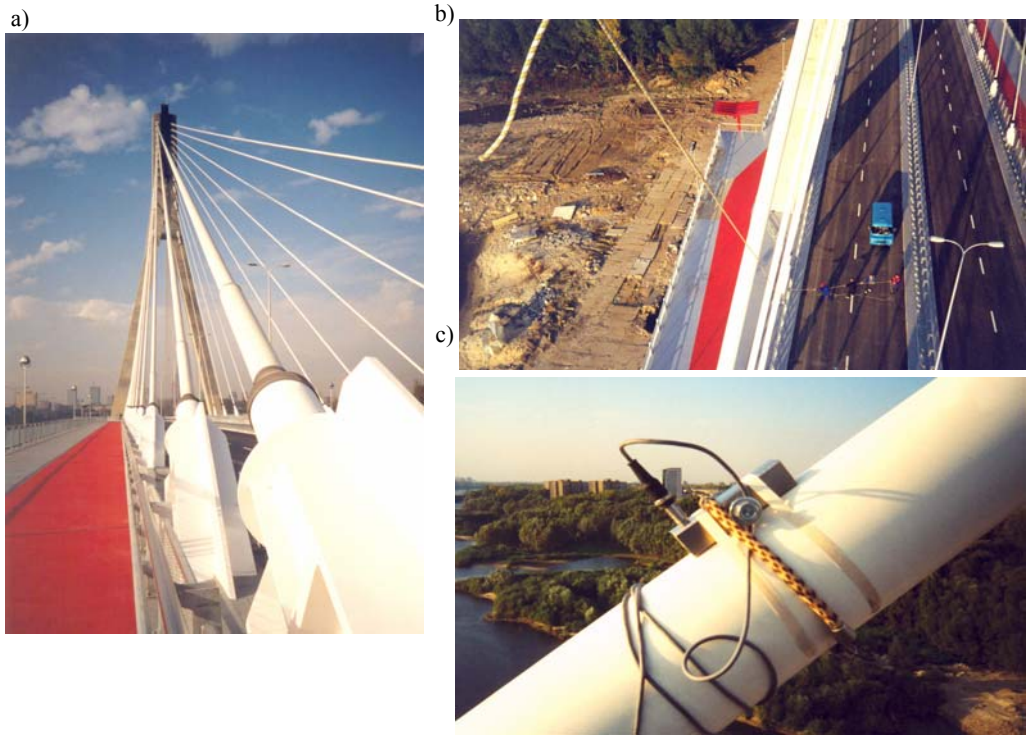

Fig. 12. Cable-stayed bridge over the Vistula River in Warsaw: a) pylon and cable system, b) cable deflection applying c) accelerometers in the middle of cable length

Results of two tests of the cable No. 7S (south) performed before opening the bridge to traffic [10] are presented:

- the vibration tests of the cable before the static tests (no live loads on the bridge);
- the vibration tests during static proof load of the main span 4-5.

First measured frequency f_1 of the cable vibration is presented in the Table. The axial force S_f in the cable was calculated on the basis of the frequency by means of the formula:

$$S_f = (f_1)^2 \cdot 4 \cdot g \cdot (L_f)^2, \tag{1}$$

where:

S_f – the cable force [N],
f_1 – the first frequency of cable vibration [Hz],
g – the mass of the cable [kg/m],
L_f – vibrating length of the cable [m].

Table. Tests of the cable No. 7S of the Świętokrzyski Bridge over the Vistula River in Warsaw

Bridge load	Experimental results		FEM analysis
	First measured frequency of vibration f_1 [Hz]	Calculated cable force S_f [kN]	Cable force S_a [kN]
Dead load	1.282	4 291	3 995
Dead load and proof load on span 4-5	1.416	5 235	5 003

Mass of the cable tested (190 wires, each 7 mm in diameter) was g = 69.58 kg/m. Effective vibrating length of the cable was determined as L_f = 96.86 m taking into account the real prestressing force measured by the hydraulic jacks GP500 during the final stressing of the cable. Details of this procedure applied by the BBR Stahlton AG are presented in [14]. Total length of the cable tested (distance between anchor plates) was L = 98.91 m.

Accelerations perpendicular to the cable axis recorded during the test are shown in Figure 13a. Comparison of the results of the frequency analysis for bridge with no live load and for bridge with the proof load on span 4-5 is presented in Figure 13b.

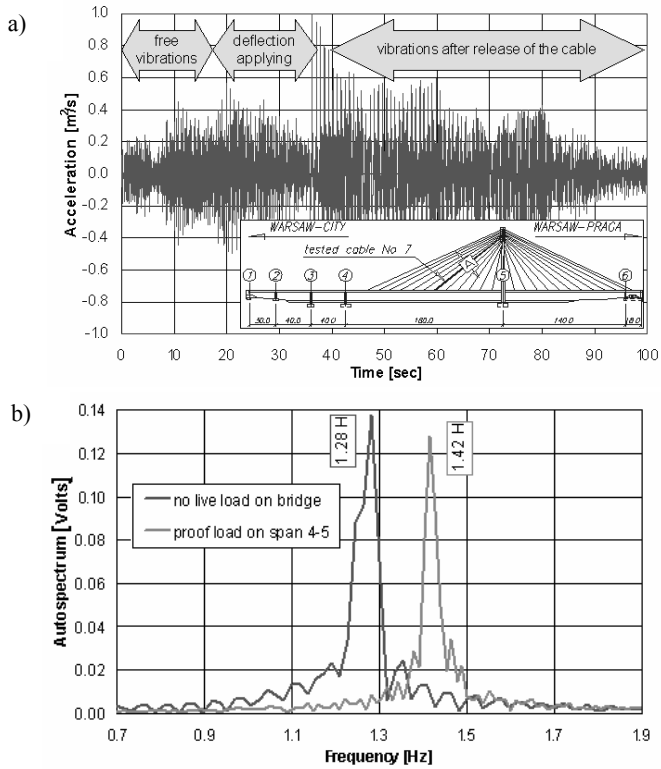

Fig. 13. Tests of the cable No. 7S of the Świętokrzyski Bridge: a) acceleration perpendicular to the cable axis, b) changes of vibration frequencies caused by the proof load

The cable forces S_f based on the experimental tests are compared in the Table with the results (cable force S_a) of the finite element analysis of the structure [15]. The differences range from 4.5 % to 7.5 % and the conformity seems to be satisfactory.

6. Conclusions

Wider experience in dynamic testing of bridges and – on the other hand – needs of more and more efficient methods of bridge management enable the formulation of the following conclusions:

- all considered types of the bridge dynamic tests offer valuable and often unique information which can be used in bridge management;
- various excitation methods and advanced measurement technologies enable precise recording and analyzing the bridge vibration phenomena;
- the dynamic parameters of the bridge structures are sensitive to the structural damages and allow the detection of the damages which are difficult to identify by means of the other methods;
- the systematic monitoring of the changes in bridge dynamic characteristic can be a useful tool for evaluation of structure condition;
- the dynamic tests considered are relatively inexpensive and cause minimal disturbances of the traffic;
- the utilization of the dynamic test results in the Bridge Management Systems needs standardization of the test procedures and measurement techniques to make all the results comparable;
- the unified interpretation of the test results can be ensured by the creation of the specialized knowledge-based expert systems.

Acknowledgement

The financial support given by the Polish State Committee for Scientific Research under Grant No. 8T07E/04020 for the constructing and testing the vibration exciters is greatly acknowledged.

References

[1] Flesch R.G., Kernbichler K.: *A Dynamic Method for the Safety Inspection of Large Prestressed Bridges*, Bridge Evaluation, Repair and Rehabilitation, Kluwer Academic Publishers, 1990, pp. 175–185.

[2] Casas J.R., Aparicio A.C.: *Dynamic Testing of Bridges Using Traffic-Induced Vibration*, Bridge Evaluation, Repair and Rehabilitation, Kluwer Academic Publishers, 1990, pp. 405–420.

[3] Paultre P., Proulx J.: *Dynamic Testing of Large-Scale Structure*, Structural Engineering International, 1997, No. 1, pp. 29–34.

[4] Salawu O.S.: *Assessment of Bridges: Use of Dynamic Testing*, Can J. Civ. Eng., 1997, Vol. 24, pp. 218–228.
[5] Broquet C., Bruhwiler E.: *In situ and Model Tests and Numerical Analysis of a Curved Cable-Stayed Bridge*, Structural Engineering International, 1999, No. 1, pp. 57–62.
[6] Bień J., Gładysz M., Rawa P.: *Vibration Tests of Bridge Structures*, First International Conference on Bridge Maintenance, Safety and Management, IABMAS, Barcelona, Spain, 2002, pp. 105–106 + CD.
[7] Bień J., Rawa P.: *Laser Based Testing and Monitoring of Large Bridges Structures*, Congress of the American Society of Civil Engineers "Structural Engineering in the 21st Century", New Orleans, LA, USA, 1999, pp. 332–335.
[8] Bień J., Rawa P.: *Laser Measurement of Static and Dynamic Displacement of Bridge Structures* (in Polish), Inżynieria i Budownictwo, 2002, No. 3/4, pp. 161–166.
[9] Bień J., Rawa P., Zwolski J.: *Proof Load Tests of Highway Bridges* (in Polish), Inżynieria i Budownictwo, 2001, No. 11, pp. 661–668.
[10] Bień J., Kmita J., Rawa P., Zwolski J.: *Tests of the Świętokrzyski Bridge over the Vistula River in Warsaw* (in Polish), Inżynieria i Budownictwo, 2002, No. 3/4, pp. 166–170.
[11] Bień J., Rawa P., Zwolski J.: *Load Tests of Arch Viaducts over the Highway A4* (in Polish), Inżynieria i Budownictwo, 2002, No. 6, pp. 316–321.
[12] Bień J., Kmita J., Rawa P., Zwolski J.: *Highway A4: Part Wrocław-Nogowczyce. Load Tests of Bridge Structure B027 over Highway A4 – km 218+926.50*, Wrocław University of Technology, Institute of Civil Engineering, Report SPR-60/2001, Wrocław, 2001.
[13] Bień J., Krzyżanowski J., Poprawski W., Skoczyński W., Szymkowski J.: *Experimental Study of Bridge Structure Dynamic Characteristics Using Periodic Excitation*, International Conference on Noise and Vibration Engineering ISMA 2002, Leuven, Belgium, 2002, pp. 555–562.
[14] Bień J., Biliszczuk J., Kmita J., Rawa P., Szymkowski J., Zwolski J.: *Load Tests of the Świętokrzyski Bridge in Warsaw* (in Polish), Wrocław University of Technology, Institute of Civil Engineering, Report SPR-6/2001, Wrocław, 2001.
[15] *Świętokrzyska Route in Warsaw, Design of the Bridge Load Tests*, BMJ Group, Warsaw, 2000.

Zastosowanie wyników dynamicznych badań konstrukcji w zarządzaniu mostami

Omówiono potencjalne możliwości wykorzystania wyników dynamicznych badań konstrukcji w procesie zarządzania mostami. Zaproponowano podział dynamicznych badań mostów w zależności od metody pobudzenia drgań obiektu. W klasyfikacji tej rozróżniono badania z zastosowaniem czterech rodzajów wymuszeń dynamicznych: ruch eksploatacyjny, pojazdy specjalne, urządzenia generujące drgania oraz specjalne techniki wymuszeń. Poszczególne metody badań zostały zilustrowane przykładami testów przeprowadzonych przez autorów. Szczególną uwagę zwrócono na możliwości wykrywania uszkodzeń obiektów mostowych przez monitorowanie ich cech dynamicznych. Omówiono zalety i wady prezentowanych metod badań pod względem ich użyteczności w komputerowych Systemach Zarządzania Mostami.

ARCHIVES OF CIVIL AND MECHANICAL ENGINEERING

Vol. IV 2004 No. 2

Impact of thermal effect on the results of plastometric tests

E. HADASIK, A. PŁACHTA, K. MOKRYŃSKI
Department of Process Modelling and Medical Engineering, Silesian University of Technology
K. KUBIAK,
Department of Material Science, Technical University in Rzeszów

The influence of the temperature rise of a sample on relationship between the flow stress and strain determined in a hot torsion test was evaluated. Measurement of temperature was performed for samples of austenitic steel 0H18N9 and titanium alloy WT22 deformed at temperature of 900 °C at a rate of 10, 100 and 1000 rpm with partial radiation pyrometer and a thermovision system. It was proved that the temperature variations depended on the rate of torsion, which was related to the reaction of the plastometer temperature control system. An increase in the temperature recorded with thermovision camera was by 50% bigger than that recorded with a light pyrometer. This was due to the location of deformation area, which was different than that measured by pyrometer, being located in the middle of sample reference length. Since the local temperature rise differed up to 140 °C from preset temperature, a need for correction of the flow stress was indicated. The corrected values of flow stress, due to temperature variations, showed the differences up to 25% compared to non-corrected values of the flow stress.

Keywords**:** *characteristics of plasticity, torsion test, correction of torque*

1. Introduction

The temperature of sample during hot torsion test is subjected to constant variation and depends on the value of the flow stress σ_p, the value of the strain ε, and on the thermal capacity and conductivity, as well as on the material susceptibility to hardening which determines location of strain. During the hot torsion test the work of deformation is converted into thermal energy, thus rising the temperature of material. Due to a rise of temperature the measured value of flow stress is lower than the value of true stress at the temperature of test [1]. A heterogeneity of strain appearing during the torsion test is responsible for the localization of strain. The local, unstable strain is induced very rapidly, while the torsion rate remains constant. Therefore, it can be assumed that this process must bring about a big, local rise of temperature, which may lead to dynamic structural changes. Hence, a measured flow stress is lower than a true stress at a given temperature, and the effect of temperature increase becomes so significant that the correction should be introduced into the flow stress diagram to account for variation of temperature during deformation [1–4]. In this paper, there is presented a local temperature increase achieved by means of Infometric 960 B thermovision system and a standard equipment of torsion plastometer, a partial radiation pyrometer, TMR 95-d Mauer Optoelektronik type. A method for correction of flow stress value, accounting for variations of temperature during deformation, is proposed.

2. Method of testing

A titanium alloy WT22 and an austenitic steel 0H18N9 of chemical composition as specified in Tables 1 and 2 were tested.

Table 1. Chemical composition of austenitic steel 0H18N9

Content of element (mass %)									
C	Cr	Ni	Mn	Mo	W	P	S	Cu	Al
0.028	18.40	8.90	0.187	0.27	0.16	0.036	0.012	0.10	0.027

Table 2. Chemical composition of titanium alloy WT22

Content of element (mass %)					
Fe	Al	Mn	Cr	V	Mo
0.89	4.72	0.02	0.86	4.60	4.30

The plastometric examinations were carried out with torsion plastometer at the Department of Process Modelling and Medical Engineering of the Silesian University of Technology [5]. Prior to torsion, the samples were heated up to temperature of 1150 °C and kept at this temperature for 180 seconds, then cooled down to the torsion temperature of 900 °C. The torsion was carried out with a rate of 10, 100 and 1000 rpm until a fracture appeared. At the time intervals ΔT, the measured data, i.e. the torque M [Nm], the axial force F [N], the temperature T [°C], the number of twists N [rot] and the time t [s], are recorded in digital form by measurement system of plastometer into the text files. Next, they are introduced into Excel program sheet to be processed by filtration, clipping, thinning and smoothing with the Matlab software. While smoothing the data by means of spline function, a special graphic interface comprised in Spline Toolbox package has been utilized.

The temperature is automatically controlled by temperature regulator connected to pyrometer. This was pyrometer of partial radiation fitted with light beam localizer, enabling precise adjustment of measuring head and estimation of the size of measured area [5]. A uniform distribution of temperature along the sample length is achieved by use of appropriate geometry and spacing of inductor coils [6]. Application of Infometric 960 thermovision system [7] allowed recording in real time the temperature distribution along the measured length of twisted sample.

Based on temperatures recorded by thermovision camera and pyrometer, the calculations of temperature increments ΔT of twisted sample in a given torsion temperature were performed in the function of strain. The strain ε is defined by the following formula [4]:

$$\varepsilon = \frac{2}{\sqrt{3}} \frac{\pi R N}{L}, \tag{1}$$

where:

R – radius of sample [mm],
L – measured length of sample [mm],
N – sample rotations [rot.].

The flow stress σ_p [MPa] was determined from the relationship accounting for the effect of hardening /weakening/ p and material response to the strain rate m:

$$\sigma_p = \sqrt{\left(\frac{\sqrt{3}\cdot M}{2\cdot\pi\cdot R^3}\right)^2 (3+p+m)^2 + \left(\frac{F}{\pi\cdot R^2}\right)^2} \,. \tag{2}$$

3. Results of tests

Figure 1 presents the dependence of temperature and torque on the number of twists obtained during torsion at a given temperature of 1000 °C and diversified torsion rate. Measurement of temperature was carried out with pyrometer over the whole cycle of sample torsion. At a low torsion rate ▒ = 10 rpm the temperature value oscillated about a preset value due to temperature control system. Such oscillations of temperature are reflected in an oscillatory course of torque. At an intermediate torsion rate ▒ = 100 rpm an increase in temperature due to conversion of deformation work

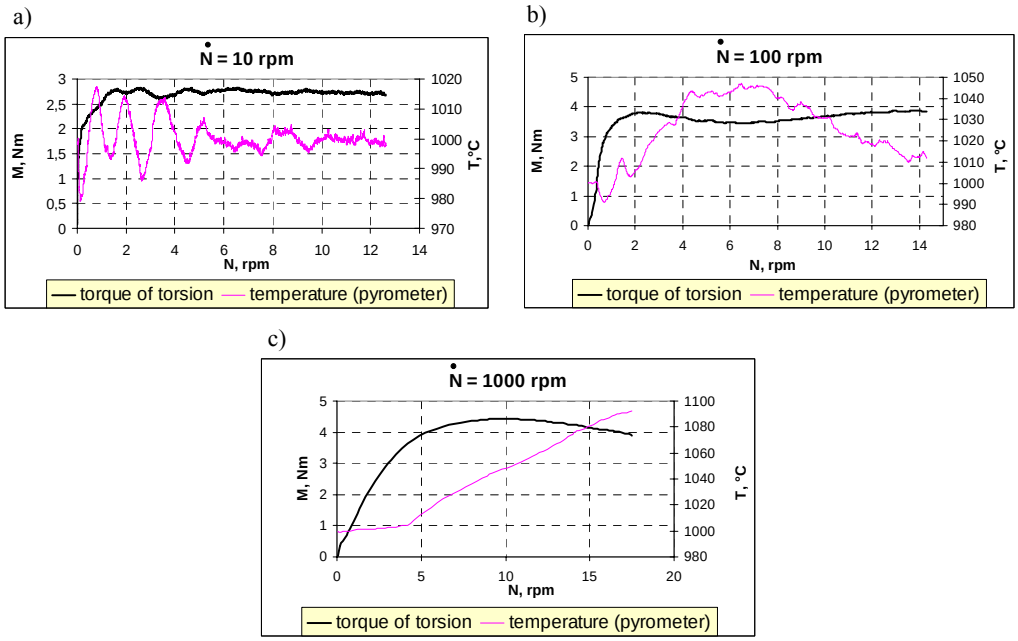

Fig. 1. Dependence of temperature and torque on number of twists for various torsion rates. A temperature is measured with pyrometer. Steel 0H19N9, T = 1000 °C, ▒ = 10 rpm (a), ▒ = 100 rpm (b), ▒ = 1000 rpm (c)

into a heat lasts until its peak value is reached, and then it drops to a preset value. This results from the reaction of control system, which would require for activation a specific increase of temperature and time. The drop of temperature results in an increase of torque value. At a high torsion rate ▒ = 1000 rpm, with the torsion time until the fracture occurrence being about 1 s, the control system could not have time to respond to temperature variations. Within this range of speed there is observed a constant rise of temperature during torsion.

An example of temperature distribution along the length of twisted plastometric sample obtained with thermovision camera is presented in Figure 2. In Figure 2a and b, there are shown the rises of temperature measured with pyrometer and thermovision camera during twisting the samples of WT22 alloy (Figure 2a) and an austenitic steel 0H18N9 (Figure 2b) at the moment of sample fracture. Along with an increase of rotational speed a local rise of sample temperature is observed, while the temperature rise recorded by thermovision camera is by about 50% bigger than that recorded by optical pyrometer. A gradient of temperature rise ΔT is due to the fact that the point of strain imposing would not necessarily coincide with the measuring point of pyrometer. A local rise of temperature at high rotational speed of 1000 rpm can approach even 140 °C, which would require a correction of the flow stress value, since an essential diversification of temperature relates also to small strains (Figure 3a and b).

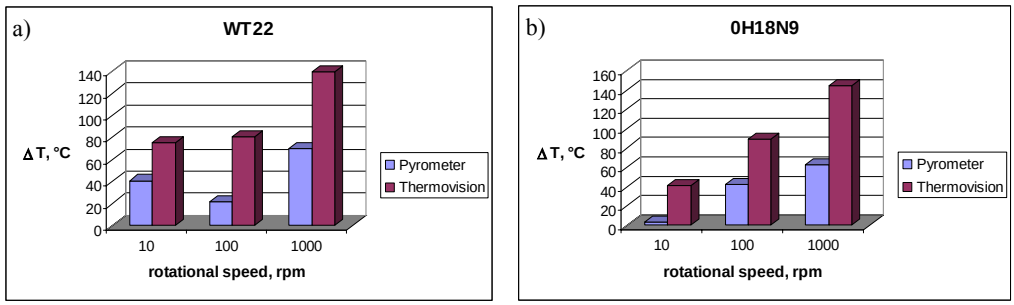

Fig. 2. Temperature rise ΔT recorded with pyrometer and thermovision camera at the moment when a sample is fractured for WT22 alloy (a) and austenitic steel 0H18N9 (b). T = 900 °C

The correction of flow stress value, accounting for diversification of temperature during torsion, was calculated from the relation:

$$\sigma' = \sigma + \Delta\sigma' , \tag{3}$$

where:

$$\Delta\sigma' = \sigma(\varepsilon, \dot{\varepsilon}, T) - \sigma(\varepsilon, \dot{\varepsilon}, T + \Delta T) , \tag{4}$$

thus:

$$\Delta\sigma' = A\varepsilon^{B}\exp(C\varepsilon)\dot{\varepsilon}^{D}\exp\left(\frac{E}{T}\right) - A\varepsilon^{B}\exp(C\varepsilon)\dot{\varepsilon}^{D}\exp\left(\frac{E}{T+\Delta T}\right), \tag{5}$$

$A = 1.699$; $B = 0.0785$; $C = -0.355$; $D = 0.203$; $E = 4005.976$ (WT22),
$A = 2.092$; $B = 0.0931$; $C = -0.077$; $D = 0.156$; $E = 4250.638$ (0H18N9).

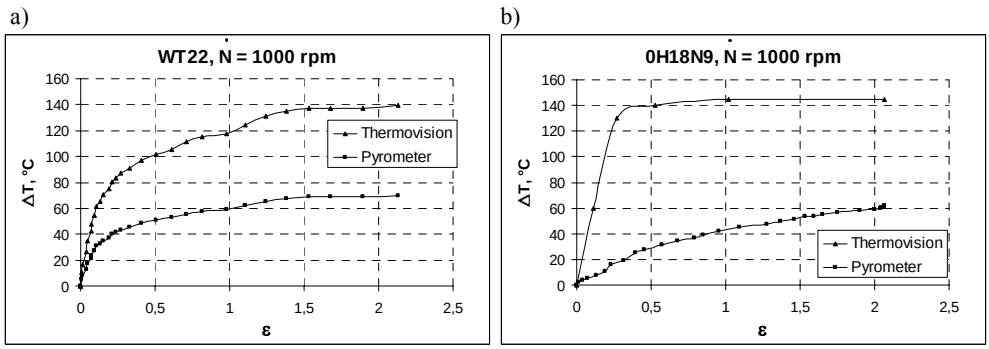

Fig. 3. Temperature rise ΔT recorded with thermovision camera and optical pyrometer during torsion of the sample of titanium alloy WT22 (a) and austenitic steel 0H18N9 (b) at the temperature of 900 °C and the a rate ▒ = 1000 rpm

The corrected and uncorrected course of flow stress relation to the strain due to differentiation of sample temperature is presented in Figure 5. At low torsion rates both the rises of temperature (Figure 2) as well as diversification of stress–strain relation (Figure 5a) are insignificant. Along with the rise of rotational speed the local temperature rises are bigger and bigger, achieving even 140 °C (Figure 3) at ▒ = 1000 rpm. Introduction of correction of the flow stress–strain relation at high torsion speeds is then indispensable (Figure 4b and c). Correction of the course of flow function produces the changes in the values of peak flow stress $\sigma_{p\max}$ shown in Figure 5a and b. The differences in $\sigma_{p\max}$ range from several up to 25% (Figure 5a).

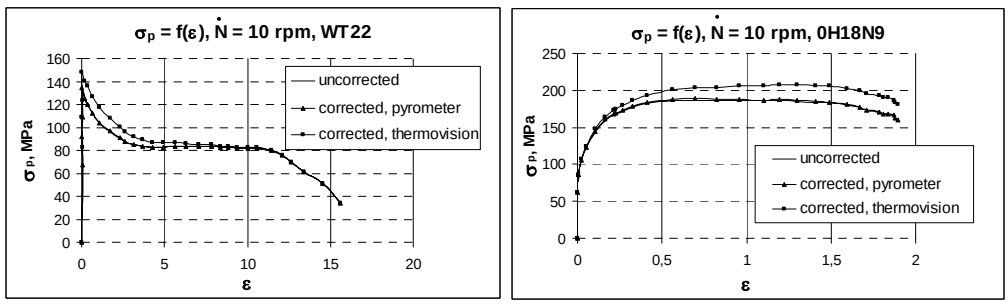

Fig. 4a. Correction in σ–ε relationship resulting from an increase of temperature for WT22 alloy and austenitic steel 0H18N9 at rotational speed ▒ = 10 rpm

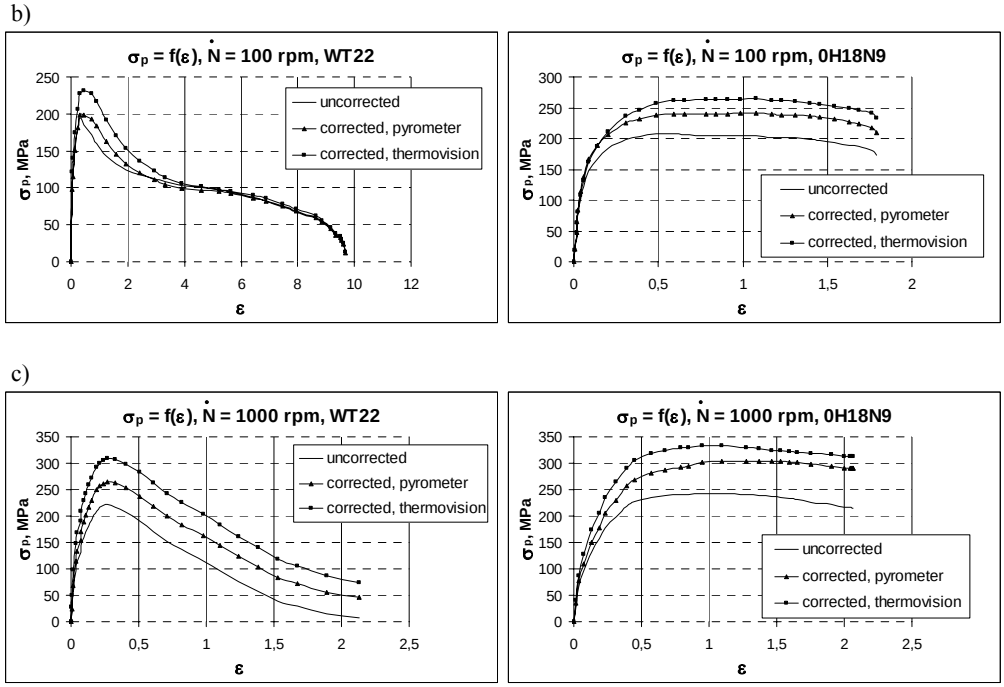

Fig. 4b,c. Correction in σ–ε relationship resulting from an increase of temperature for WT22 alloy and austenitic steel 0H18N9 at rotational speed: ▒ = 100 rpm (b), ▒ = 1000 rpm (c)

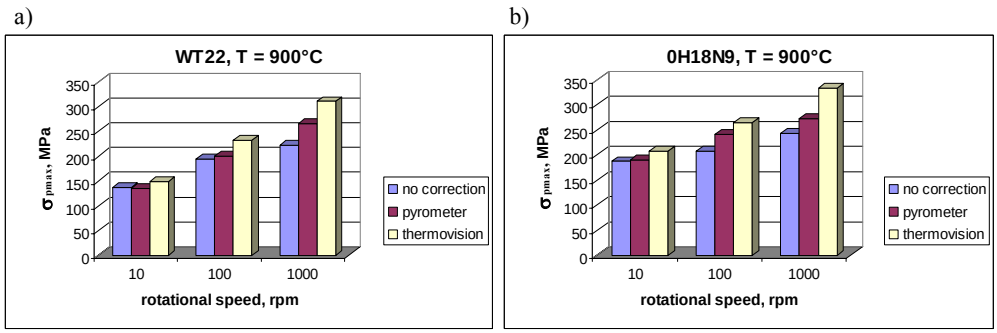

Fig. 5. Values of peak flow stress $\sigma_{p\max}$ corrected and uncorrected due to temperature differentiation for WT22 alloy (a) and 0H18N9 austenitic steel (b), depending on rotational speed

4. Summary

Measurements of temperature made by pyrometer or thermocouple depend on a point lying at the surface or inside of sample. Because of the strain diversification along the length of the twisted sample, the maximum thermal effect and related tem-

perature rise of sample are located at a point of the peak strain. As this place has no fixed location, the measurement of maximum temperature value is possible by means of thermovision equipment, which can record the temperature along the whole length of the sample. Since the values of torque and accompanying strain depend on the section of sample with the highest temperature, this (maximum) temperature will allow a univocal evaluation of flow stress value. For a correct representation of the relation $\sigma_p = f(\varepsilon)$ it is indispensable to know the local strain in the area corresponding to the area with the highest temperature. In the section of twisted sample, where a maximum temperature effect along with accompanying strain concentration occur, there appears also an increase of strain rate. Finally, besides the correction accounting for differentiation of temperature there is also required a correction accounting for strain rate. An adequate explanation of these phenomena would require further research.

References

[1] Grosman F., Hadasik E.: *Problemy zastosowania charakterystyk technologicznej plastyczności w komputerowych programach analizy i projektowania procesów przeróbki plastycznej*, Archiwum Hutnictwa, Kraków, 1994, z. 3, s. 263–276.
[2] Gronostajski Z.: *Modele konstytutywne opisujące zachowanie się wybranych stopów miedzi w zakresie dużych odkształceń plastycznych*, Oficyna Wydawnicza Politechniki Wrocławskiej, Wrocław, 2000.
[3] Grosman F., Schindler I., Hadasik E., Boruta J.: *Vyvoj metodologie plastometrickych zkousek*, Conference Formability '94, Ostrava, 24–27.10.1994, 193–203.
[4] Hadasik E.: *Metodyka wyznaczania charakterystyk plastyczności w próbie skręcania na gorąco*, Zeszyty Naukowe Politechniki Śląskiej, No. 63, Gliwice, 2002.
[5] Grosman F., Hadasik E., Sajdak Cz.: *Nowe stanowisko do badań plastometrycznych,* Conference *Plastyczność Materiałów*, *PLAST'94*, Wisła, 29–30.09.1994, 67–70.
[6] Grosman F., Hadasik E., Kurek K.: *Analiza numeryczna wpływu sposobu nagrzewania na rozkład temperatury w próbkach plastometrycznych*, Conference *FORMING'99*, Zlate Hory, 15–17.09.1999, 182–189.
[7] Rdzawski Z., Stobrawa J., Muzia G.: *Wyniki badań rozkładu temperatury na próbkach ze stopu WT22 oraz stali austenitycznej podczas próby skręcania*, IMN, Gliwice, 2002, unpublished.

This work was supported by the Polish Committee for Scientific Research under grant No. 4 T08A 02922.

Wpływ efektu cieplnego na wyniki badań plastometrycznych

Oceniono wpływ przyrostu temperatury próbki na wyznaczoną w próbie skręcania na gorąco zależność naprężenia uplastyczniającego od odkształcenia. Pomiaru temperatury dokonano dla próbek ze stali austenitycznej 0H18N9 i stopu tytanu WT22 odkształcanych w temperaturze 900 °C z prędkością skręcania 10, 100 i 1000 obr/min za pomocą pirometru częścio-

wego promieniowania oraz systemu termowizyjnego. Wykazano, że zmiany temperatury istotnie zależą od prędkości skręcania, co ma związek z reakcją systemu regulacji temperatury plastometru. Przyrost temperatury rejestrowany kamerą termowizyjną jest o ok. 50% większy od przyrostu rejestrowanego pirometrem optycznym. Przyczyną tego jest miejsce odkształcenia inne niż miejsce pomiaru pirometrem znajdujące się w połowie długości bazy pomiarowej próbki. Ponieważ różnice w lokalnych przyrostach temperatury sięgają 140 °C w porównaniu z temperaturą zadaną, wskazano na konieczność korekty naprężenia uplastyczniającego. Różnice w skorygowanych wartościach naprężenia uplastyczniającego z powodu zróżnicowania temperatury dochodzą do 25% w porównaniu do nie skorygowanych wartości naprężenia uplastyczniającego.

ARCHIVES OF CIVIL AND MECHANICAL ENGINEERING

Vol. IV 2004 No. 2

Information about PhD thesis at the Civil Engineering Faculty and the Mechanical Engineering Faculty of Wrocław University of Technology

Title: *Analytical and experimental study of padded teeth shaping for digging of argillaceous rocks* (in Polish) *Analityczno-eksperymetalne studium kształtowania zębów napawanych do urabiania skał gliniastych*

Author: Jerzy Bogdan Alenowicz
Supervisor: Professor Dionizy Dudek
Promoting Council: Council of Mechanical Faculty, Institute of Machines Design and Operation
Reviewers:
Professor Wiesław Trąpczyński
Professor Włodzimierz Dudziński
Date of PhD thesis presentation: January 28th, 2003
PhD thesis is available in Main Library and Scientific Information Centre of WUT
The monograph contains: 128 pages, 70 figs, bibliography: 75 items
Keywords: *surface mining, mine machines, bucket wheel excavator (bucket teeth), construction, production technology*

Abstract: Based on theoretical analysis of argillaceous rock digging process by bucket wheel excavator, results of laboratory research and former tests, which were carried out in foreign and domestic research centers, the new type of exchangeable padded teeth for buckets of wheel excavators was developed. These teeth are especially fitted for digging of overburden in open cast mines with dominant hard diggable, highly abrasive formations (boulder clay with stones, quartz sands, silts). The experimental verification of the developed teeth construction was carried out under the field operation conditions. The above construction has many advantages, the most important being its durability by 102% higher compared to formerly used padded teeth, by 26% higher compared to casting teeth (which are also more expensive) and reduction of digging resistance. The construction has been introduced to production in Konin Open Cast Lignite Mine. After implementation, considerable economic effect has been obtained.

Title: ***The influence grease and wall material on rheological properties of boundary layer*** **(in Polish)**
Wpływ rodzaju smaru plastycznego i materiału ścianki na wybrane właściwości reologiczne warstwy przyściennej

Author: Krzysztof Ludwik Biernacki
Supervisor: Professor Ryszard Czarny
Promoting Council: Council of the Mechanical Faculty, Institute of Machines Design and Operation
Reviewers:
Professor Andrzej Kulczycki
Professor Stanisław Krawiec
Date of PhD thesis presentation: July 11th, 2003
PhD thesis is available in Main Library and Scientific Information Centre of WUT
The monograph contains: 133 pages, 79 figs, bibliography: 90 items
Keywords: *grease, boundary layer*

Abstract: The research presents the influence of material of the wall in a lubrication conduit on the resistance of flow of greases in the boundary layer. The greases that were tested in all experiments showed considerable changes in the shear stress of the greases near the boundary layer, which has been proved for different types of materials.

Title: *Numerical method of predicting the characteristics of the large-size air springs* (in Polish)
Numeryczna metoda prognozowania charakterystyk wielkogabarytowych sprężyn pneumatycznych

Author: Zbigniew Kazimierz Chabraś
Supervisor: Professor Eugeniusz Rusiński
Promoting Council: Council of the Mechanical Faculty, Institute of Machines Design and Operation
Reviewers:
Professor Tomasz Łodygowski
Professor Dionizy Dudek
Date of PhD thesis presentation: March 4th, 2003
PhD thesis is available in Main Library and Scientific Information Centre of WUT
The monograph contains: 163 pages, 157 figs, bibliography: 115 items
Keywords: *air spring, finite elements method, suspension system*

Abstract: The hypothesis of three-dimensional air spring performance is presented. It does not include a diagonal of rigidity matrix only. An important effect of it on the response of transverse force of air spring is shown as well. Diagonal can be calculated only experimentally because of a complicated character of the co-operation between coat of spring and its edges. During design step it is necessary to use, e.g. FEM (Finite Elements Method), but in this case, many difficult numeric problems should be solved as is shown by a simple example.

Title: *Numerical and experimental modelling of the load-carrying structures under the action of thermal loads* (in Polish) *Numeryczno-doświadczalne modelowanie ustrojów nośnych poddanych obciążeniom cieplnym*

Author: Artur Jan Górski
Supervisor: Professor Eugeniusz Rusiński
Promoting Council: Council of the Mechanical Faculty, Institute of Machines Design and Operation
Reviewers:
Professor Jerzy Okrajni
Professor Dionizy Dudek
Date of PhD thesis presentation: June 10th, 2003
PhD thesis is available in Main Library and Scientific Information Centre of WUT
The monograph contains: 148 pages, 123 figs, bibliography: 88 items
Keywords: *construction, thermal loads, finite elements method, temperature, stresses, load-carrying structure*

Abstract: The purpose of the dissertation was to estimate the object effort state under the action of thermal loads. Nowadays there are a lot of methods which give the possibility of estimating the effort state of the objects working at high temperatures. There exists a great need to verify the correct strength of the new type of constructions, as well as of the objects that are still running. Therefore a broad aim of the dissertation was to develop an original method for state of stress determination in the objects at high temperatures.

Such integral experimental methods as the numerical methods and measurement were used. They were based on computer systems that used the finite elements method. The well-known measurement methods, i.e. thermovision and extensometers, were applied.

Achievements of modern computer technology and the advanced calculation methods in the professional CAD systems made it possible to develop this kind of methods. The big advantage of this method is the possibility of using it for the object with small geometrical dimensions; for instance: for the part of the coating of generator's turbine, as well as for the object with developed geometrical form, i.e. power boiler or power boiler supporting structure. The calculation models of the real objects that work under thermal load conditions were carried out in order to verify the efficiency of the method application. The sequence of numerical calculation and the experimental research were carried out as well.

Title: A*ssessment of the effect of machines and appliances on environment* (in Polish)
Zagadnienia oceny wpływu maszyn i urządzeń na środowisko

Author: Anna Izabela Jurek
Supervisor: Professor Zbigniew Kłos
Promoting Council: Council of Mechanical Faculty, Institute of Machines Design and Operation
Reviewers:
Professor Jerzy Markisz
Professor Franciszek Przystupa
Date of PhD thesis presentation: February 25th, 2003
PhD thesis is available in Main Library and Scientific Information Centre of WUT
The monograph contains: 167 pages, 51 figs, bibliography: 106 items
Keywords: *appliance, environment, assessment, describing*

Abstract: The monograph deals with the problem of quantitative evaluation of the impact of mechanical objects in their life cycle on environment. The dissertation appears as a contribution to the enrichment and the dissemination of knowledge about transformation consequences in a technosphere. Its main purpose originates from the desire to create quantitative determinant of the relation between the machine and the environment. The first part of dissertation, which refers to the background of the problems shown, emphasizes the importance of scientific world perception integrity. Hitherto existing ways of describing machines and appliances have been analysed. Among other things some types of classification, quantitative and qualitative characteristics and specification of life cycle stages have been highlighted. The attention has been paid to the necessity of including the environmental life cycle aspect in mechanical object characteristics. The next section contains the identification of the environmental influences typical of life cycle stages, which is based on system formulation of machine as an element taking part in the matter, energy and information circulation. The legal regulations and technical norms connected with environmental impact of mechanical objects have been gathered. In this way, the basis for the environmental feature of machines and appliances statement has been created. In order to bring useful features of dissertation into relief, the application possibilities of environmental feature of mechanical objects have been revealed. Also, the attempt to generate the environmental classification of machines and appliances has been undertaken. To conclude the research results, the guidelines for the further studies have been suggested.

Title: *The method of forming of damping properties of air spring filled with porous elastomer* (in Polish)
Metoda kształtowania właściwości tłumiących sprężyny pneumatycznej wypełnionej elastomerem porowatym

Author: Krzysztof Paweł Lewandowski
Supervisor: Professor Tomasz Nowakowski
Promoting Council: Council of Mechanical Faculty, Institute of Machines Design and Operation
Reviewers:
Professor Jerzy Kwaśnikowski
Professor Piotr Dudziński
Date of PhD thesis presentation: October 14th, 2003
PhD thesis is available in Main Library and Scientific Information Centre of WUT
The monograph contains: 245 pages, 204 figs, bibliography: 52 items
Keywords: *air spring, pneumatic cascade, elastic chamber, porous material*

Abstract: General task of the work was to derive the reciprocal relationships between the damping properties of hybrid air spring, i.e. air spring filled with porous material, and the properties of conventional system, i.e. air spring without or with external rigid reservoir, and also mechanical properties of filling porous material.

Final results are as follows:

- Porous filler in air spring increases dynamic stiffness and the coefficient of dissipation of energy of air spring in its two configurations: with an external rigid reservoir or without it.
- Porous filler in air spring has effect on the changes in dynamic stiffness and the coefficient of dissipation of energy, depending on type of the filler, air spring configuration and the changes of pressure.
- The structure of the filling porous material decides on an increase in the coefficient of dissipation of energy in air spring configuration without external rigid reservoir.
- In air spring configuration with external rigid reservoir, the structure of filling porous material decides on an increase in the coefficient of dissipation of energy.
- In the research, an original method of selecting the foams for air spring filling was developed.
- This method of foam selection can be extensively used in practice, i.e. in vehicle industry.

Title: *Numerical and experimental method for prediction of fatigue life of load-carrying structures* (in Polish) *Numeryczno-doświadczalne metoda prognozowania trwałości elementów ustrojów nośnych*

Author: Przemysław Jan Moczko
Supervisor: Professor Eugeniusz Rusiński
Promoting Council: Council of Mechanical Faculty, Institute of Machines Design and Operation
Reviewers:
Professor Grzegorz Gasiak
Professor Tomasz Smolnicki
Date of PhD thesis presentation: July 8th, 2003
PhD thesis is available in Main Library and Scientific Information Centre of WUT
The monograph contains: 141 pages, 99 figs, bibliography: 121 items
Keywords: *numerical analysis, finite element method*

Abstract: There are numerous methods for prediction of fatigue life of load-carrying structures of machines and vehicles. However, many fatigue failures of those machines show that we still need to develop the methods for evaluating fatigue life during design process. The most important reason for appearing fatigue cracks problem with estimating stress or strain state in the elements investigated and the load to which they are subjected. It is also important that 3-dimensional residual stresses are neglected. The utility aim of PhD is to work out a new method for prediction of fatigue life of load-carrying structures of machines and vehicles based on advanced numerical methods (finite element method) and experimental tests.

Title: *Influence of stabilization system on bone structure displacements in human cervical spine* (in Polish)
Wpływ systemów stabilizacji na przemieszczenia struktur kostnych odcinka szyjnego kręgosłupa człowieka

Author: Sylwia Szotek
Supervisor: Professor Romuald Będziński
Promoting Council: Council of Mechanical Faculty, Institute of Machines Design and Operation
Reviewers:
Professor Włodzimierz Jarmundowicz
Professor Mieczysław Szata
Date of PhD thesis presentation: November 18th, 2003
PhD thesis is available in Main Library and Scientific Information Centre of WUT
The monograph contains: 213 pages, 172 figs, bibliography: 147 items
Keywords: *biomechanics, physical models, cervical stabilization, fixators, experimental methods in mechanics*

Abstract: The aim of the research was to analyse biomechanical conditions for different cervical spine stabilization used in operation treatment. The tests were performed in order to compare the changes of the displacement nature in cervical vertebrae in the case of their stabilization with bone graft only and with the bone graft with stabilizing on plate implanted from frontal access. A relatively wider range of the displacement of the vertebrae in the area of the stabilized movement segment of the spine after the implantation of the implant was shown. The tests were carried out with use of both animal and human specimens under different load conditions that simulated physiological situations. Peak values of forces and load moments, global displacement values for the whole tested spine section and their angular displacements were taken as measuring parameters. A separate testing task, very important in the meaning of cognitive and application aspects, was an analysis of the method of occipito-cervical stabilization made from a surgical back access. Innovative solutions of occipito-cervical stabilizers of Polish production were tested. In these tests, the following laser methods were employed: electronic speckle pattern interferometry (ESPI) and holographic interferometry. The results of these tests allowed assessing the influence of geometric and resistance parameters of the tested occipital bone specimens on a displacement distribution under different load conditions applied to the implanted stabilizer. Based on a CT an importance of the choice of a proper implantation place and accuracy of the implantation of the occipital bone-stabiliser connector was indicated.

Title: *Influence of moisture on the strength properties of filter cakes* (in Polish) *Wpływ wilgotności na własności wytrzymałościowe osadów filtracyjnych*

Author: Janusz Stanisław Szymków
Supervisor: Professor Kazimierz Pieczonka
Promoting Council: Council of Mechanical Faculty, Institute of Machines Design and Operation
Reviewers:
Professor Józef Jonak
Professor Piotr Dudziński
Date of PhD thesis presentation: January 14th, 2003
PhD thesis is available in Main Library and Scientific Information Centre of WUT
The monograph contains: 177 pages, 212 figs, bibliography: 36 items
Keywords: *filtration, filtration cake, unsaturated granular material, shear strength, tensile strength*

Abstract: The main aim of the paper was to determine a relationship between shear strength of filter cakes and saturation. A new apparatus (direct shear cell) was designed and implemented for this purpose. The experiments were carried out with the apparatus using limestone powder and sphere glasses as a material tested. Results were obtained for real filter cakes of different saturation and showed the influence of saturation on shear stress at failure and tensile strength. This relationship was represented by a mathematical model, which was tested.

Title: *Dynamic properties of the air spring–pipe–auxiliary reservoir system* (in Polish)
Właściwości dynamiczne układu: sprężyna pneumatyczna–długi przewód–zbiornik dodatkowy

Author: Piotr Sebastian Wolko
Supervisor: Professor Tomasz Nowakowski
Promoting Council: Council of Mechanical Faculty, Institute of Machines Design and Operation
Reviewers:
Professor Włodzimierz Gąsowski
Professor Dionizy Dudek
Date of PhD thesis presentation: October 7th, 2003
PhD thesis is available in Main Library and Scientific Information Centre of WUT
The monograph contains: 135 pages, 144 figs, bibliography: 62 items
Keywords: *railway transport, pneumatic suspensions, air spring*

Abstract: Dynamic properties of the air spring–pipe–auxiliary reservoir system have been studied. Pipe is used in order to connect the air spring to auxiliary reservoir if there is no space to mount the reservoir close to the air spring or sometimes in order to connect two air springs in the bogie which increases rolling damping. Models of different complexity describing the pneumatic suspension systems and their dynamic characteristics have been presented. The thesis: "Modelling the pipe as a lumped system allows describing the dynamic properties of the system: air spring–pipe–auxiliary reservoir" have been taken. The model proposed is based on the Krettek–Grajnert thermodynamic model of the air spring. Model of the pipe divided between chambers with differential equation describing the mass flow was added. To verify the model an experiment was carried out. FD 40-10 Continental air spring connected to auxiliary reservoir by pipe was the system tested. Pipe diameter and length, reservoir volume and nominal pressure were changed. The tests showed that the model presented describes better the dynamic properties of system studied than the known models.

Title: *Nonlinear modeling of structures prestressed with tendons* (in Polish) Nieliniowe modelowanie konstrukcji wstępnie napiętymi cięgnami

Author: Daniel Antoniak
Supervisor: Professor Piotr Konderla
Promoting Council:
Reviewers:
Professor Jan Biliszczuk
Professor Jan Kubik
Date of PhD thesis presentation: May 20th, 2002
PhD thesis is available in Main Library and Scientific Information Centre of WUT
The monograph contains: 100 pages, 33 figs, bibliography: 65 items
Keywords: *tendon prestressing, bond slip, friction, finite element method, shell*

Abstract: Physical and finite element models of a general shell structure prestressed with tendons are constructed. Friction between tendons and ducts as well as the tendon slip are taken into account. Geometrical linearity is presumed but nonlinear constitutive relations are allowed. The contact problem due to friction accounts for additional non-linearity.

In the present formulation, contrary to the commonly used load-equivalent concept, the prestressing force is introduced in accordance with the real phenomenon, i.e. either by loading the end of a tendon or by elongating the tendon or by inducing initial axial forces in the tendon. The equilibrium equations are derived from the principle of virtual work in which the energy dissipated by friction is accounted for.

The embedded approach is used to formulate the discrete model of a prestressed shell. The concept of a hybrid element is introduced which stands for a parent element together with all embedded tendon elements. A shell-tendon hybrid element is described in detail. Other types of hybrid elements such as beam-tendon and volume-tendon elements are briefly discussed. The embedded tendon element presented in the paper can be used as a model of all types of reinforcement including pretensioned, and posttensioned, bonded, and unbonded as well regular one.

For the numerical solution of the discrete model equations, an algorithm, which handles nonlinearity and variation of boundary conditions caused by friction, is presented. The correctness of the algorithm has been thoroughly validated. Three numerical examples are presented in the paper. Some of the results are compared to analytical solution. Good agreement in the case of the tested types of hybrid elements is observed proving the usefulness and versatility of the hybrid element concept.

Title: *Adjustment of the mixture proportions of HPFRC to fibers parameters using rheological methods* (in Polish)
Dostosowanie składu wysokowartościowej matrycy do parametrów niskomodułowych włókien węglowych z wykorzystaniem metody badań reologicznych

Author: Dominik Logoń
Supervisor: Professor Leokadia Kucharska
Promoting Council: Professor Antoni Biegus
Reviewers:
Professor Andrzej Brandt
Professor Lech Rudziński
Date of PhD thesis presentation: June 26th, 2002
The monograph contains: 140 pages, 91 figs, bibliography: 100 items
Keywords: *carbon fibres, cement composite, rheology, multiple cracking*

Abstract: The influence of different admixtures and pitch-based fibres on rheological and mechanical behaviour of HPFRC was investigated. There are presented test results concerning the effect of "pitch" carbon fibre reinforcement (V_f = 0−2.5%) of cement pastes and mortars with water/binder ratio *w/b* = 0.3. For mortars three kinds of sand were used: with grain <1, <0.5 and <0.25 mm in such a proportion to maintain similar contact surface between the sand grains and the paste. In all compositions, 10% of cement mass was replaced with silica fume and additionally 30% with fly ash.

It was confirmed that the addition of fly ash and silica fume enable obtaining a homogeneous distribution and orientation of fibres. The maximum fibre volume that can be correctly dispersed is related to the initial rheological properties of the mortar. It may be determined by the rheological tests. A rapid increase of yield value (g) after exceeding that characteristic fibre content has been explained by an interaction between fibres witch corresponds which V_{fcr}.

The influence of the matrix composition was analysed based on the curves obtained from four-point bending test. It has been found that when an important reinforcing effect was obtained due to multiple cracking, the crack propagation was only slightly controlled by the fibres. Moreover, it has been proved that reinforcing effect is considerably reduced by small amount of sand, and enhanced by addition of fly ash. In the mortars, the reinforcing effect was smaller than in the pastes and various causes of reduced influence of the fibres on crack propagation in these two kinds of composites are discussed.

Information for Authors

Send to: *Archives of Civil and Mechanical Engineering*
Polish Academy of Sciences, Wrocław Branch
Podwale 75, 50-414 Wrocław, Poland

Archives of Civil and Mechanical Engineering (ACME) publishes both theoretical and experimental papers which explore or exploit new ideas and techniques in the following areas: structural engineering (structures, machines and mechanical systems), mechanics of materials (elasticity, plasticity, rheology, fatigue, fracture mechanics), materials science (metals, composites, ceramics, plastics, wood, concrete, etc., their structures and properties, methods of evaluation), manufacturing engineering (process design, simulation, diagnostics, maintenance, durability, reliability). In addition to research papers, the Editorial Board welcome: state-of-the-art reviews of specialized topics, letters to the Editor for quick publication, brief work-in-progress reports, brief accounts of completed doctoral thesis (one page is maximum), and bibliographical note on habilitation theses (maximum 250 words). All papers are subject to a referee procedure, except for letters, work-in-progress reports and doctoral and habilitation theses, which are briefly reviewed by the Editorial Board.

The papers submitted have to be unpublished works and should not be considered for publication elsewhere.

The Editorial Board would be grateful for all comments on the idea of the journal.

Submit three copies, each complete with abstract, tables, and figures.
Detailed information about the Journal on web:

http://www.pan.wroc.pl
www.ib.pwr.wroc.pl/wydzial/czasopismoACME.html
http://www.wmech.pwr.wroc.pl

Price 12 zł
(0% VAT)